Electronic Supplementary Material (ESI) for Materials Chemistry Frontiers.

SUPPLEMENTARY INFORMATION

Tuning the charge stabilization and transport in naphthalimide-based semiconductors *via* fused-ring and core-engineering strategy

Raúl González-Núñez, [a,†] Matías J. Alonso-Navarro, [b,c,†] Fátima Suárez-Blas, [b,c,†] Elena Gala, [b,c] M. Mar Ramos, [c] José L. Segura, [b,*] and Rocío Ponce Ortiz. [a,*]

[a] *Department of Physical Chemistry, University of Málaga, Málaga, 29071, Spain.*

[b] *Department of Organic Chemistry, Complutense University of Madrid, Faculty of Chemistry, Madrid 28040, Spain.*

[c] *Chemical and Environmental Technology Department. Univ. Rey Juan Carlos, Móstoles, 28933, Spain.*

[†]These authors contributed equally to this work.

General contents

1. General Information

All reagents were purchased from commercial suppliers and used without further purification. Compounds **NID**,[1] **NIA**,[2] **1**,[3] **2**[4] and **3**[3] were prepared according previously published procedures. Solvents were dried distillation over sodium or benzophenone under argon before use. TLC analyses were performed using silica gel (Kieselgel 60 F254, Macherey–Nagel) and spots were visualized under UV light. Column chromatography was carried out with silica gel 60 (0.04-0.06 mm, Scharlau) columns, using the eluent reported in each case.

^{1}H and ^{13}C NMR spectra were recorded using Bruker DPX 300MHz or Bruker AVIIII 300MHz BACS-60 systems at room temperature. Chemical shifts are given in ppm (δ) and referenced to the residual nondeuterated solvent frequencies ($CDCl_3$: δ 7.26 ppm for ^{1}H, δ 77 ppm for ^{13}C). Coupling constants (*J*) are in Hertz [Hz] and signals are described as follows: s, singlet; d, doublet; t, triplet; quint, quintuplet; m, multiplet; br, broad; app, apparent. IR spectra are reported in wavenumbers (cm^{-1}) and were carried out in a Shimadzu FTIR 8300 spectrophotometer. Mass spectra were recorded by means of Matrix-Assisted Laser Desorption/Ionization-Time Of Flight (MALDI-TOF). UV–vis absorption spectra of the compounds in HPLC chloroform solutions at 20 °C were recorded on a Varian Cary 50 UV–vis spectrophotometer. Cyclic voltammetry experiments were performed with a computed controlled potentiostat in a three-electrode single-compartment cell (5 mL). The platinum working electrode consisted of a platinum wire with a surface of A = 0.785 mm^2, which was polished down to 0.5 µm with polishing paste prior to use in order to obtain reproducible surfaces. The counter electrode consisted of a platinum wire, and the reference electrode was a Ag/AgCl secondary electrode. An electrolyte solution of 0.1 M $TBAPF_6$ in freshly distilled and degassed CH_2Cl_2 (HPLC) was used in all experiments.

2. Synthesis of compounds and characterization

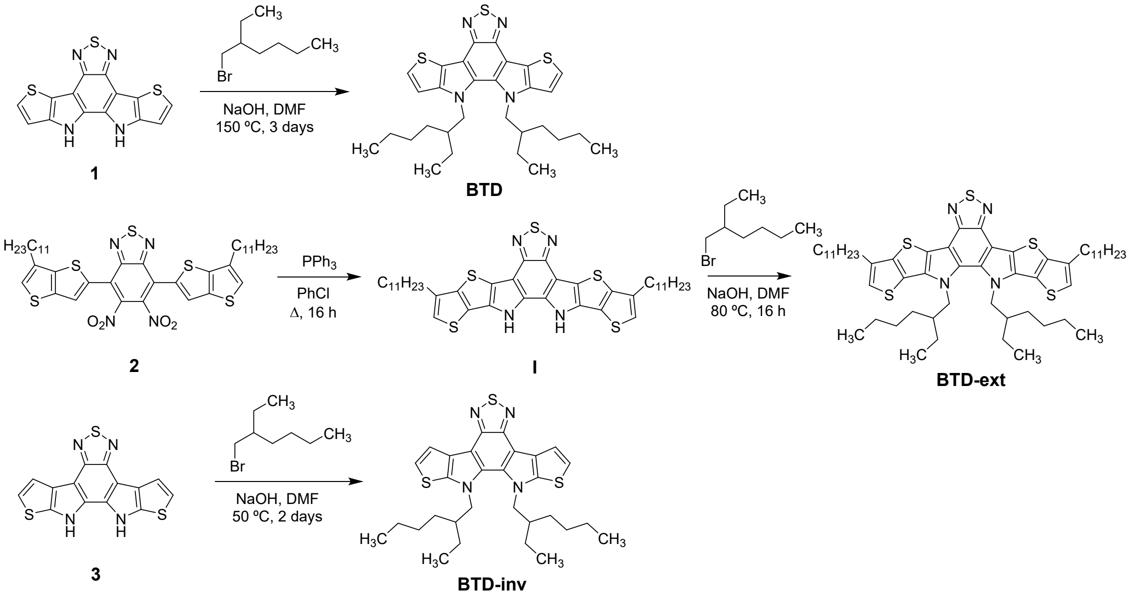

Scheme S1: Synthesis of **BTD**, **BTD-ext** and **BTD-inv.**

10,11-Bis(2-ethylhexyl)-10,11-dihydro-[1,2,5]thiadiazolo[3,4-*e*]thieno[2',3':4,5]pyrrolo[3,2-*g*]thieno[3,2-*b*]indole (BTD)[3]

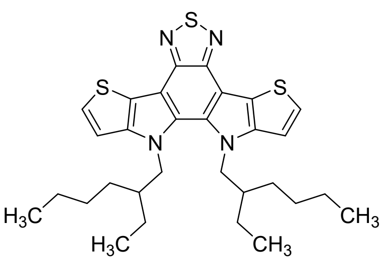

Compound **1** (350 mg, 1.07 mmol) and NaOH (343 mg, 8.58 mmol) were placed in a round bottom flask under argon atmosphere. Then, 31 mL of anhydrous DMF were added and the mixture was heated at 150 °C. Once this temperature was reached and the reagents were complete dissolved, 2-ethyl-1-hexylbromide (1.3 mL, 7.18 mmol) was added dropwise and the mixture was allowed to react at 150 °C for 3 days. The reaction crude was verted over HCl 0.5 M (100 mL) and extracted with CH_2Cl_2 (3 x 25 mL). The combined organic phases were washed with brine and dried over $MgSO_4$ and the solvent was removed under reduced pressure. The crude obtained was purified by column chromatography (Hexane:Ethyl acetate 10:1), obtaining **BTD** as an amber oil (305 mg, 52 %). ^{1}H NMR (300 MHz, $CDCl_3$): δ (ppm) = 7.42 (2H, d, *J* = 5.2 Hz), 7.16 (2H, d, *J* = 5.2 Hz), 4.50 (4H, m), 1.96 (2H, m), 1.08 – 0.98 (4H, m), 0.93 – 0.81 (12H, m), 0.64 (12H, m). ^{13}C NMR (75 MHz, $CDCl_3$): δ (ppm) = 147.9, 145.4, 132.9, 127.0, 120.7, 112.1, 110.9, 54.3, 39.3, 29.9, 28.4, 23.3, 22.1, 14.3, 10.1 (some aliphatic carbon signals overlap). FTIR (ATR, CH_2Cl_2): $\nu_{\text{máx}}$ (cm^{-1}) = 3104, 3088, 2960, 2927, 2856, 1728, 1558, 1460, 1353, 1295, 1182, 1155, 1092, 962, 870, 849, 810, 723, 660. HRMS (MALDI-TOF) calculated for $C_{30}H_{38}N_4S_3$ $[M^{+\cdot}]$ 550.2259, found 550.2260.

12,13-bis(2-ethylhexyl)-3,9-diundecyl-12,13-dihydro-[1,2,5]thiadiazolo[3,4-*e*]thieno-[2'',3'':4',5']thieno[2',3':4,5]pyrrolo[3,2-*g*]thieno[2',3':4,5]thieno[3,2-*b*]indole (BTD-ext)[4,5]

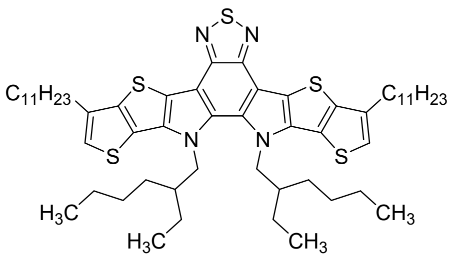

To a solution of compound **2** (953.3 mg, 1.18 mmol) in chlorobenzene (23 mL) in a pressure reaction vessel, triphenylphosfine (3.08 g, 11.75 mmol) was added. The mixture was refluxed overnight and, then, cooled to room temperature. The solution obtained was purified by column chromatography (hexane/CH_2Cl_2 1:1 → CH_2Cl_2). The resulting product, intermediate **I**, was employed in the following step without further purification as follows: Compound **I**, 1-bromo-2-ethylhexane (1.94 mL, 10.7 mmol) and potassium carbonate (1.63 g, 11.8 mmol) were placed in a round bottom flask under argon atmosphere. Anhydrous DMF (50 mL) was added, and the mixture was deoxygenated by bubbling argon for 15 minutes. The reaction was stirred at 80 °C overnight. Once the reaction was complete, it was cooled to room temperature and the residue was extracted with ethyl acetate (3x30 mL) and the combined organic phases were washed with water and dried over $MgSO_4$. After removing the solvent under reduced pressure, the desired product was purified employing column chromatography (Hexane/CH_2Cl_2 10:1) and, finally, **BTD-ext** was obtained as a red solid (493 mg, 43 %, two steps). ^1H NMR (300 MHz, $CDCl_3$): δ (ppm) = 7.01 (2H, s), 4.60 (4H, br d, *J* = 7.6 Hz), 2.83 (4H, t, *J* = 7.6 Hz), 2.04 (2H, m), 1.86 (4H, m), 1.35 – 1.22 (36H, m), 0.91 – 0.81 (18 H, m), 0.66 – 0.57 (12 H, m). ^{13}C NMR (75 MHz, $CDCl_3$): δ (ppm) = 147.7, 142.0, 137.0, 136.8, 131.4, 123.6, 122.5, 119.2, 111.4, 54.9, 39.9, 31.9, 29.7, 29.6, 29.5, 29.4, 29.3, 28.8, 27.7, 14.1, 13.7, 10.1, 10.0 (some aliphatic carbon signals overlap). FTIR (ATR, CH_2Cl_2): $\nu_{\text{máx}}$ (cm^{-1}) = 2955, 2921, 2856, 1471, 1682, 1553, 1459, 1376, 1296, 814, 722. HRMS (MALDI-TOF) calculated for $C_{56}H_{82}N_4S_5$ $[M^{+\cdot}]$ 970.5143, found 970,5158.

10,11-Bis(2-ethylhexyl)-10,11-dihydro-[1,2,5]thiadiazolo[3,4-*e*]thieno[3',2':4,5]pyrrolo[3,2-*g*]thieno[2,3-*b*]indole (BTD-inv)[3]

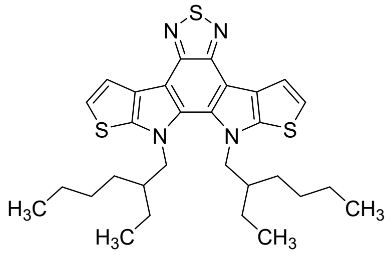

Product **3** (273 mg, 0.84 mmol) and NaOH (266 mg, 6.65 mmol) were placed in a round bottom flask under argon atmosphere. Then, 27 mL of anhydrous DMF were added and the mixture was heated at 50 °C. Once this temperature was reached and the reagents were complete dissolved, 2-ethyl-1-hexylbromide (1.0 mL, 5.6 mmol) was added dropwise and the mixture was allowed to react at 50 °C for 2 days. The reaction crude was verted over HCl 0.5 M (90 mL) and extracted with CH_2Cl_2 (3 x 25 mL). The combined organic phases were washed with brine and dried over $MgSO_4$ and the solvent was removed under reduced pressure. The crude obtained was purified by column chromatography (Hexane:Ethyl acetate 9:1), obtaining **BTP-inv** as an amber oil (203.9 mg, 61 %). ^1H NMR (300 MHz, $CDCl_3$): δ (ppm) = 7.77 (2H, d, *J* = 5.2 Hz), 7.15 (2H, d, *J* = 5.2 Hz), 4.41 (4H, m), 2.18 (2H, m), 1.15 – 1.04 (4H, m), 1.01 – 0.83 (12H, m), 0.68 (12H, m). ^{13}C NMR (75 MHz, $CDCl_3$): δ (ppm) = 148.2, 142.8, 133.3, 127.3, 120.3, 118.6, 110.0, 55.7, 38.4, 29.7, 23.1, 22.7, 13.8, 10.1. FTIR

(ATR, CH_2Cl_2): $\nu_{\text{máx}}$ (cm^{-1}) = 2961, 2963, 2854, 1559, 1459, 1400, 1294, 1112, 870, 833, 812, 760, 727, 678, 628. HRMS (MALDI-TOF) calculated for $C_{30}H_{38}N_4S_3$ [$M^{+\cdot}$] 550.2259, found 550,2234.

4,5,13-Tris(2-ethylhexyl)-4,5-dihydro-12H-pyrido[3',4',5':5,6]acenaphtho[1,2-*b*]thieno[2',3':4,5]-pyrrolo[3,2-*f*]thieno[2',3':4,5]pyrrolo[2,3-*h*]quinoxaline-12,14(13*H*)-dione (NIP)

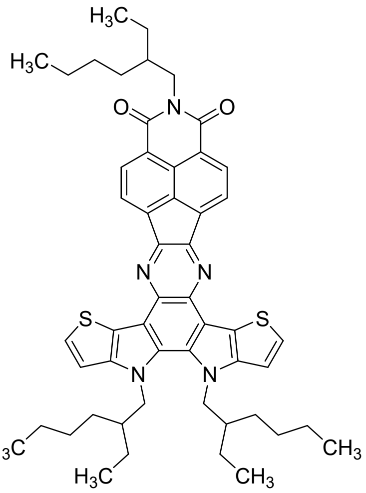

Benzothiadiazole derivative **BTD** (60 mg, 0.11 mmol) was suspended, under argon atmosphere, into 4 mL of glacial acetic acid and heated to 80 °C until its complete dissolution. Then, zinc powder (93 mg, 1.42 mmol) was added and the reaction mixture was warmed to 140 °C, allowed to react during 30 minutes and cooled to room temperature. After that, this solution was added to another solution containing **NID** (44 mg, 0.12 mmol) and a catalytic amount of *p*-toluenesulfonic acid in anhydrous chloroform (4 mL) under argon atmosphere, observing an instant colour change. The reaction mixture was heated to 50 °C and stirred at this temperature during 24 h. Solvent was removed under reduced pressure and the resulting crude dissolved in the minimum amount as possible of CH_2Cl_2, precipitating a solid which was isolated by filtration. After washing with cold and hot methanol, **NIP** was obtained as a dark green solid (35 mg, 38 %). ^1H NMR (300 MHz, $CDCl_3$): δ (ppm) = 8.61 (2H, d, *J* = 7.3 Hz), 8.46 (2H, d, *J* = 7.3 Hz), 7.53 (2H, d, *J* = 5.2 Hz), 7.22 (2H, d, *J* = 5.2 Hz), 4.62 – 4.53 (4H, m), 4.14 (2H, m), 2.12 – 2.04 (2H, m), 1.96 (1H, m), 1.51 – 1.27 (8H, m), 1.13 – 0.85 (16H, m), 0.67 (12H, m). ^{13}C NMR (75 MHz, $CDCl_3$): δ (ppm) = 164.4, 151.1, 146.4, 139.1, 133.9, 132.7, 132.3, 128.0, 125.4, 123.7, 122.1, 120.3, 118.4, 112.1, 54.4, 44.5, 39.6, 38.4, 31.0, 29.9, 28.9, 28.0, 24.2, 23.3, 22.9, 14.3, 13.9, 10.8, 10.3, 10.2 (some aliphatic carbon signals overlap). FTIR (ATR, CH_2Cl_2): $\nu_{\text{máx}}$ (cm^{-1}) = 3086, 2957, 2923, 2859, 1700, 1666, 1640, 1570, 1456, 1381, 1364, 1328, 1236, 1165, 1128, 1097, 1019, 941, 855, 752, 663. HRMS (MALDI-TOF) calculated for $C_{52}H_{59}N_5O_2S_2$ [$M^{+\cdot}$] 849.4110, found 849.4125.

4,5,13-Tris(2-ethylhexyl)-4,5-dihydrobenzo[*lmn*]thieno[2''',3''':4'',5'']pyrrolo[3'',2'':6',7']-thieno[3'',2'':2',3']indolo[4',5':4,5]imidazo[2,1-*b*][3,8]phenanthroline-12,14,17(13H)-trione (NDI)

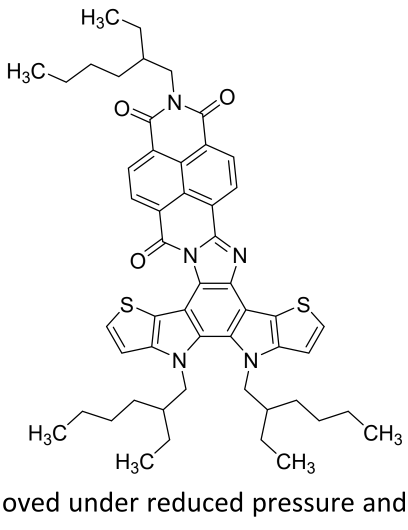

Benzothiadiazole derivative **BTD** (144 mg, 0.26 mmol) was suspended, under argon atmosphere, into 4 mL of glacial acetic acid and heated to 80 °C until its complete dissolution. Then, zinc powder (93 mg, 1.42 mmol) was added and the reaction mixture was warmed to 140 °C, allowed to react for 30 minutes and cooled to room temperature. After that, this solution was added to another solution containing **NIA** (109 mg, 0.29 mmol) in acetic acid (10 mL) under argon atmosphere, observing an instant colour change. The reaction mixture was heated to 100 °C and stirred at this temperature during 24 h. Solvent was removed under reduced pressure and the resulting crude dissolved in the minimum amount as possible of CH_2Cl_2, precipitating a solid which was isolated by filtration. After washing with cold and hot methanol, **NDI** was obtained as a dark green solid (73 mg, 32 %). ^{1}H NMR (300 MHz, $CDCl_3$): δ (ppm) = 9.04 (1H, d, *J* = 7.7 Hz), 9.02 (1H, d, *J* = 7.8 Hz), 8.81 (1H, d, *J* = 7.7 Hz), 8.77 (1H, d, *J* = 7.8 Hz), 7.51 (2H, app d, *J* = 5.3 Hz), 7.20 (1H, d, *J* = 5.2 Hz), 7.15 (1H, d, *J* = 5.4 Hz), 4.49 (4H, m), 4.15 (2H, m), 1.98 (1H, m), 1.85 (2H, m), 1.45 – 1.25 (8H, m), 1.05 – 0.85 (14H, m), 0.82 – 0.68 (8H, m), 0.67 – 0.52 (12H, m). ^{13}C NMR (75 MHz, $CDCl_3$): δ (ppm) = 163.8, 163.6, 159.7, 147.8, 146.4, 145.3, 133.6, 133.4, 132.1, 131.9, 131.2, 130.9, 129.5, 128.1, 127.6, 127.4, 126.8, 125.5, 123.0, 121.7, 120.1, 119.2, 113.8, 113.2, 112.7, 112.0, 110.0, 109.1, 54.2, 53.9, 44.6, 39.2, 38.9, 38.2, 30.9, 29.9, 29.8, 29.8, 28.8, 28.0, 27.8, 27.7, 24.19, 23.4, 23.3, 23.2, 22.8, 14.3, 13.9, 10.8, 10.2 (some aliphatic carbon signals overlap). FTIR (ATR, CH_2Cl_2): $\nu_{máx}$ (cm^{-1}) = 3116, 3078, 2961, 2927, 2861, 1702, 1663, 1598, 1578, 1543, 1512, 1464, 1441, 1405, 1376, 1337, 1303, 1241, 1087, 989, 865, 764, 726, 654. HRMS (MALDI-TOF) calculated for $C_{52}H_{59}N_5O_3S_2$ [M$^{+\cdot}$] 865.4059, found 865.4053.

2,11,12-Tris(2-ethylhexyl)-8,15-diundecyl-11,12-dihydro-1*H*-pyrido[3',4',5':5,6]acenaphtho-[1,2-b]thieno[2'',3'':4',5']thieno[2',3':4,5]pyrrolo[3,2-*f*]thieno[2'',3'':4',5']thieno[2',3':4,5]-pyrrolo[2,3-*h*]quinoxaline-1,3(2*H*)-dione (NIP-ext)

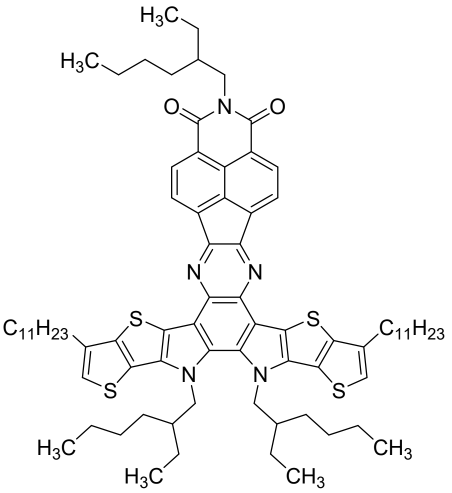

Benzothiadiazole derivative **BTD-ext** (106.8 mg, 0.11 mmol) was suspended, under argon atmosphere, into 4 mL of glacial acetic acid and heated to 80 °C until its complete dissolution. Then, zinc powder (93 mg, 1.42 mmol) was added and the reaction mixture was warmed to 140 °C, allowed to react during 30 minutes and cooled to room temperature. After that, this solution was added to another solution containing **NID** (44 mg, 0.12 mmol) and a catalytic amount of *p*-toluenesulfonic acid in anhydrous chloroform (4 mL) under argon atmosphere, observing an instant colour change. The reaction mixture was heated to 50 °C and stirred at this temperature during 24 h. Solvent was removed under reduced pressure and the resulting crude dissolved in the minimum amount as possible of CH_2Cl_2, precipitating a solid which was isolated by filtration. After washing with cold and hot methanol, **NIP-ext** was obtained as a dark green solid (86.7 mg, 62 %). ^{1}H NMR (300 MHz, $CDCl_3$): δ (ppm) = 8.64 (2H, d, *J* = 7.3 Hz), 8.53 (2H, d, *J* = 7.3 Hz), 7.06 (2H, s), 4.68 (4H, m), 4.14 (2H, m), 2.88 (4H, t, *J* = 7.7 Hz), 2.14 (2H, m), 1.91 (1H, m), 1.57 – 1.25 (44H, m), 1.12 – 0.86 (28H, m), 0.65 (12H, m). ^{13}C NMR (75 MHz, $CDCl_3$): δ (ppm) = 164.2, 151.1, 143.1, 138.1, 131.0, 123.7, 122.0, 119.4, 119.0, 55.0, 39.9, 38.3, 31.9, 30.8, 29.7, 29.6, 29.5, 29.4, 28.9, 27.7, 23.1, 22.8, 22.7, 14.1, 13.8, 10.7, 10.1. FTIR (ATR, CH_2Cl_2): $\nu_{máx}$ (cm^{-1}) = 2957, 2923, 2846, 1698, 1663, 1459, 1321, 1161, 1087, 1012, 800. HRMS (MALDI-TOF) calculated for $C_{78}H_{103}N_5O_2S_4$ [M$^{+\cdot}$] 1269.6995, found 1269.6941.

2,11,12-Tris(2-ethylhexyl)-8,15-diundecyl-11,12-dihydrobenzo[*lmn*]thieno[2'''',3'''':4''',5''']-thieno[2''',3''':4'',5'']pyrrolo[3'',2'':6',7']thieno[2''',3''':4'',5'']thieno[3'',2'':2',3']indolo[4',5':4,5]imidazo[2,1-*b*][3,8]phenanthroline-1,3,18(2*H*)-trione (NDI-ext)

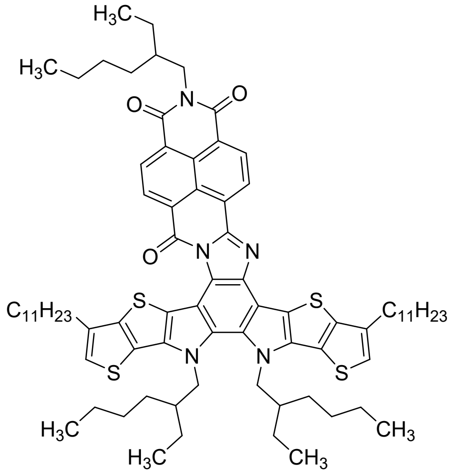

Benzothiadiazole derivative **BTD-ext** (252,5 mg, 0.26 mmol) was suspended, under argon atmosphere, into 4 mL of glacial acetic acid and heated to 80 °C until its complete dissolution. Then, zinc powder (93 mg, 1.42 mmol) was added and the reaction mixture was warmed to 140 °C, allowed to react for 30 minutes and cooled to room temperature. After that, this solution was added to another solution containing **NIA** (109 mg, 0.29 mmol) in acetic acid (10 mL) under argon atmosphere, observing an instant colour change. The reaction mixture was heated to 100 °C and stirred at this temperature during 24 h. Solvent was removed under reduced pressure and the resulting crude dissolved in the minimum amount as possible of CH_2Cl_2, precipitating a solid which was isolated by filtration. After washing with cold and hot methanol, **NDI-ext** was obtained as a dark blue solid (130.4 mg, 39 %). ^1H NMR (300 MHz, $CDCl_3$): δ (ppm) = 9.09 (1H, d, *J* = 7.6 Hz), 9.02 (1H, d, *J* = 7.8 Hz), 8.81 (1H, d, *J* = 7.6 Hz), 8.77 (1H, d, *J* = 7.8 Hz), 7.06 (1H, s), 7.02 (1H, s), 4.59 (4H, m), 4.17 (2H, m), 2.86 (4H, m), 2.01 – 1.85 (6H, m), 1,46 – 1.26 (39H, m), 1.08 – 0.73 (30H, m), 0.62 – 0.50 (12H, m). ^{13}C NMR (75 MHz, $CDCl_3$): δ (ppm) = 170.49, 164.21, 151.13, 143.63, 138.83, 138.17, 136.95, 133.94, 132.52, 130.97, 123.71, 123.55, 122.06, 121.64, 119.41, 119.00, 109.00, 55.0, 39.9, 38.3, 31.9, 30.8, 29.7, 29.6, 29.5, 29.4, 28.9, 27.7, 23.1, 22.8, 22.7, 14.1, 13.8, 10.7, 10.1. FTIR (ATR, CH_2Cl_2): $\nu_{máx}$ (cm^{-1}) = 2959, 2920, 2848, 1705, 1660, 1461, 1374, 1337, 1299, 756, 714. HRMS (MALDI-TOF) calculated for $C_{78}H_{103}N_5O_3S_4$ [$M^{+\cdot}$] 1285.6944, found 1285.6969.

2,10,11-Tris(2-ethylhexyl)-10,11-dihydro-1*H*-pyrido[3',4',5':5,6]acenaphtho[1,2-*b*]thieno-[3',2':4,5]pyrrolo[3,2-*f*]thieno[3',2':4,5]pyrrolo[2,3-*h*]quinoxaline-1,3(2*H*)-dione (NIP-inv)

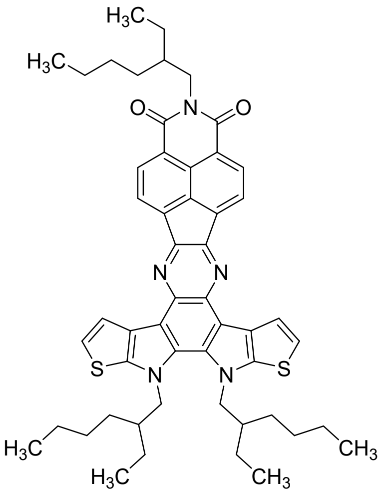

Benzothiadiazole derivative **BTD-inv** (60 mg, 0.11 mmol) was suspended, under argon atmosphere, into 4 mL of glacial acetic acid and heated to 80 °C until its complete dissolution. Then, zinc powder (93 mg, 1.42 mmol) was added and the reaction mixture was warmed to 140 °C, allowed to react during 30 minutes and cooled to room temperature. After that, this solution was added to another solution containing **NID** (44 mg, 0.12 mmol) and a catalytic amount of *p*-toluenesulfonic acid in anhydrous chloroform (4 mL) under argon atmosphere, observing an instant colour change. The reaction mixture was heated to 70 °C and stirred at this temperature during 24 h. Solvent was removed under reduced pressure and the resulting crude dissolved in the minimum amount as possible of CH_2Cl_2, precipitating a solid which was isolated by filtration. The solid was purified by column chromatography (hexane/ethyl acetate 9:1) and **NIP-inv** was obtained as a brown solid (28 mg, 30 %). ^1H NMR (300 MHz, $CDCl_3$): δ (ppm) = 8.65 (2H, d, *J* = 7.3 Hz), 8.46 (2H, d, *J* = 7.3 Hz), 8.15 (2H, d, *J* = 5.2 Hz), 7.21 (2H, d, *J* = 5.2 Hz), 4.48 (4H, m), 4.16 (2H, m), 2.25 (2H, m), 1.97 (1H, m), 1.46 – 1.29 (12H, m), 1.16 – 0.85 (21H, m), 0.70 (9H, m). ^{13}C NMR (75 MHz, $CDCl_3$): δ (ppm) = 164.1, 150.9, 144.5, 138.9, 134.1, 132.8, 132.4, 129.8, 127.1, 125.1, 124.4, 123.5, 121.4, 120.3, 119.7, 117.5, 55.8, 44.1, 38.6, 38.2, 30.8, 29.8, 29.70, 28.8, 28.0, 28.0, 24.1, 23.2, 23.1, 22.8, 14.1, 13.8, 10.7, 10.3, 10.2 (some aliphatic carbon signals overlap). FTIR (ATR, $CHCl_3$): $\nu_{\text{máx}}$ (cm^{-1}) = 2955, 2924, 2856, 1699, 1665, 1638, 1456, 1316, 1233, 1105, 752, 605. HRMS (MALDI-TOF) calculated for $C_{52}H_{59}N_5O_2S_2$ [$M^{+\cdot}$] 849.4110, found 849.4094.

2,11,12-Tris(2-ethylhexyl)-11,12-dihydrobenzo[*lmn*]thieno[3''',2''':4'',5'']pyrrolo[3'',2'':6',7']-thieno[2'',3'':2',3']indolo[4',5':4,5]imidazo[2,1-*b*][3,8]phenanthroline-1,3,6(2*H*)-trione (NDI-inv)

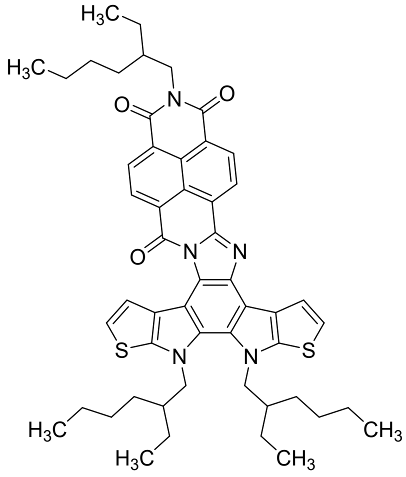

Benzothiadiazole derivative **BTD-inv** (144 mg, 0.26 mmol) was suspended, under argon atmosphere, into 4 mL of glacial acetic acid and heated to 80 °C until its complete dissolution. Then, zinc powder (93 mg, 1.42 mmol) was added and the reaction mixture was warmed to 140 °C, allowed to react for 30 minutes and cooled to room temperature. After that, this solution was added to another solution containing **NIA** (109 mg, 0.29 mmol) in acetic acid (10 mL) under argon atmosphere, observing an instant colour change. The reaction mixture was heated to 100 °C and stirred at this temperature during 24 h. Solvent was removed under reduced pressure and the resulting crude dissolved in the minimum amount as possible of CH_2Cl_2, precipitating a solid which was isolated by filtration. The solid was purified by column chromatography (hexane/ethyl acetate 9:1) and **NDI-inv** was obtained as a dark blue solid (55 mg, 24 %). ^1H NMR (300 MHz, $CDCl_3$): δ (ppm) = 8.83 (2H, m), 8.66 (1H, d, *J* = 7.7 Hz), 8.62 (1H, dd, *J* = 7.6 and 1.0 Hz), 8.02 (1H, d, *J* = 7.7 Hz), 7.81 (1H, *J* = 5.2 Hz), 7.14 (1H, d, *J* = 5.2 Hz), 7.07 (1H, d, *J* = 5.4 Hz), 4.43 (2H, m), 4.36 (2H, m), 4.07 (2H, m), 2.17 (2H, m), 1.94 (1H, m), 1.43 – 1.24 (8H, m), 1.15 – 0.88 (22H, m), 0.76 – 0.62 (12H, m). ^{13}C NMR (75 MHz, $CDCl_3$): δ (ppm) = 163.5, 163.3, 159.2, 146.0, 145.6, 145.3, 134.1, 133.9, 132.2, 131.8, 130.6, 130.6, 128.4, 127.3, 127.1, 126.8, 126.5, 125.8, 125.2, 125.0, 124.1, 122.8, 120.3, 119.4, 119.0, 117.3, 112.8, 109.2, 55.7, 55.5, 44.4, 38.2, 38.0, 37.9, 31.9, 30.8, 30.0, 29.7, 29.4, 28.7, 28.2, 28.1, 28.1, 27.9, 24.1, 23.4, 23.1, 22.8, 22.7, 14.1, 13.9, 13.8, 10.6, 10.4, 10.3, 10.3, 10.2. FTIR (ATR, $CHCl_3$): $\nu_{\text{máx}}$ (cm^{-1}) = 2965, 2924, 2861, 1708, 1667, 1479, 1417, 1389, 1285, 1083, 757, 729. HRMS (MALDI-TOF) calculated for $C_{52}H_{59}N_5O_3S_2$ [$M^{+\cdot}$] 865.4059, found 865.4095.

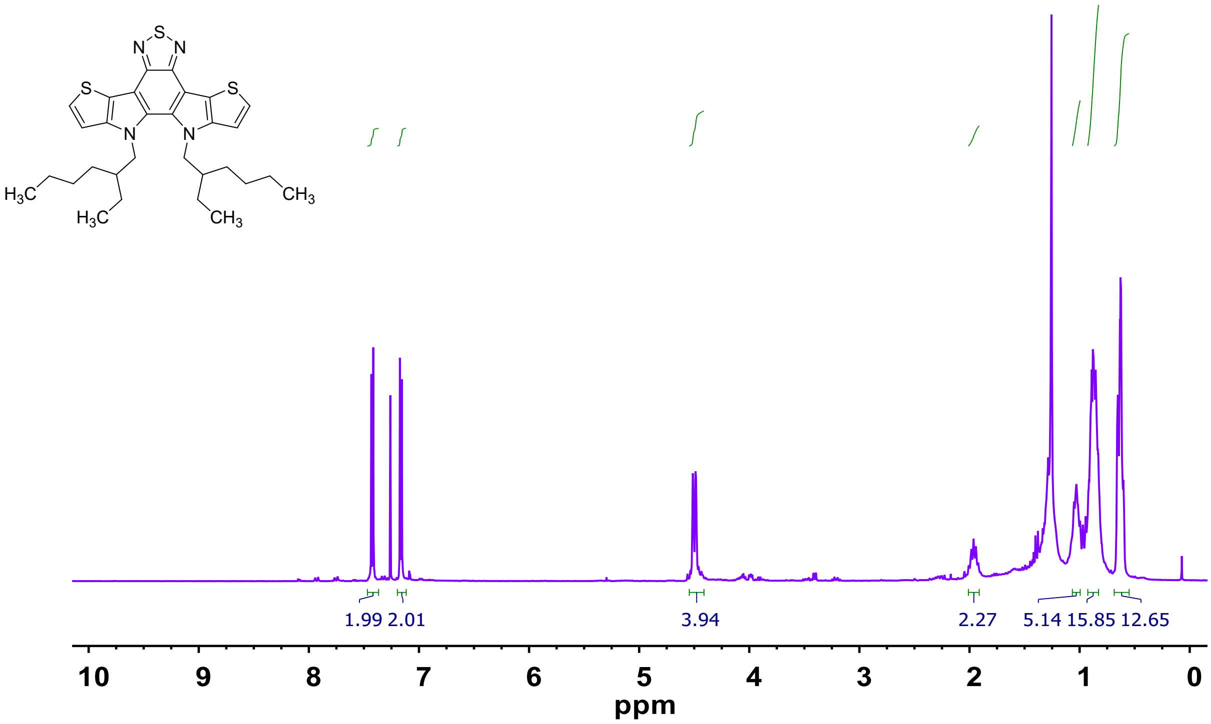

Figure S1. ^{1}H-NMR spectrum of **BTD** in CDCl$_3$.

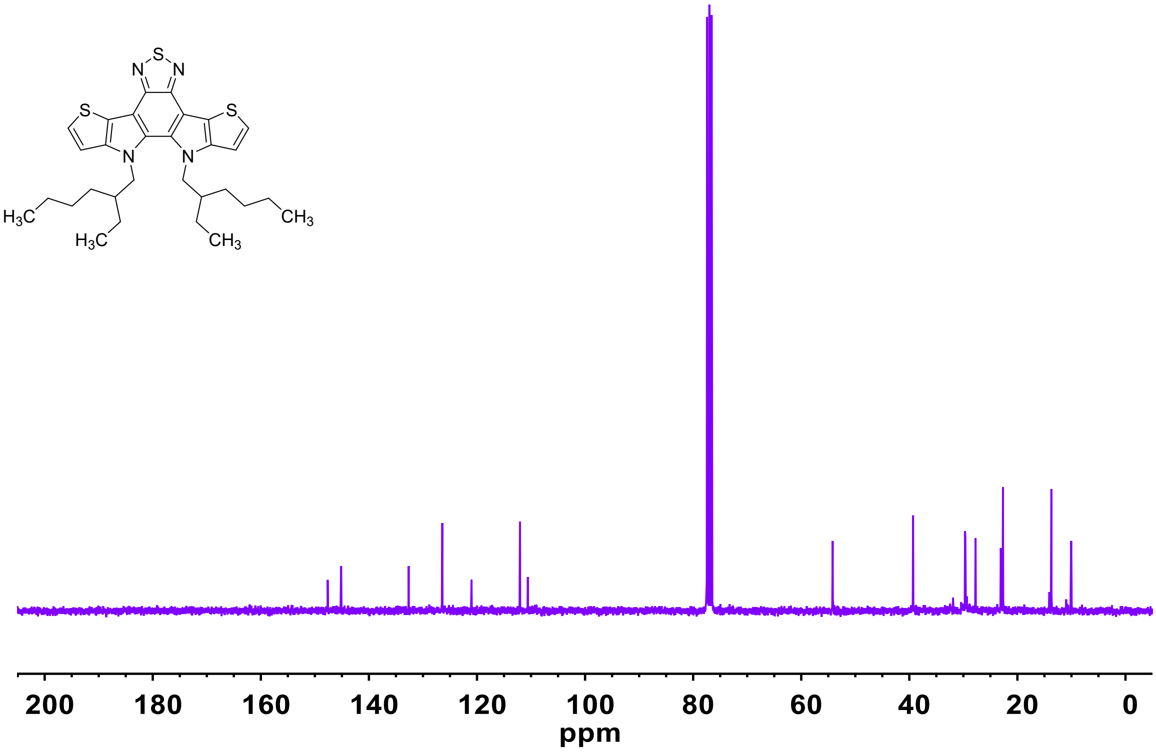

Figure S2. ^{13}C-NMR spectrum of **BTD** in CDCl$_3$.

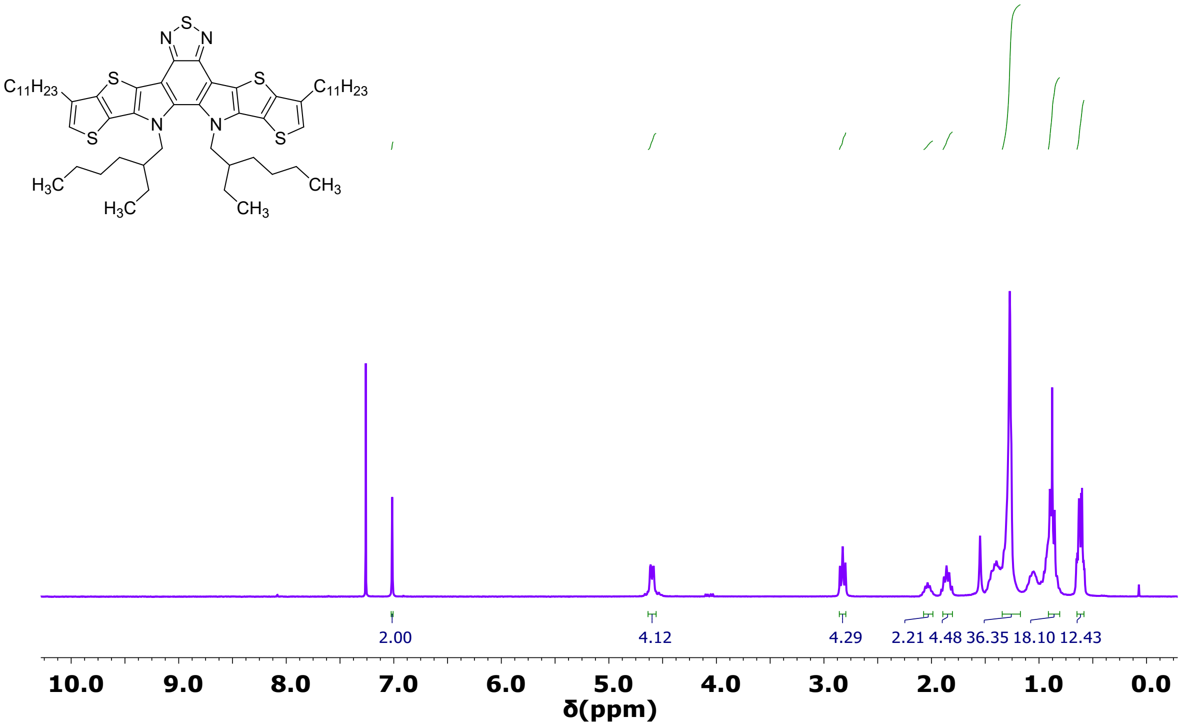

Figure S3. ^{1}H-NMR spectrum of **BTD-ext** in $CDCl_3$.

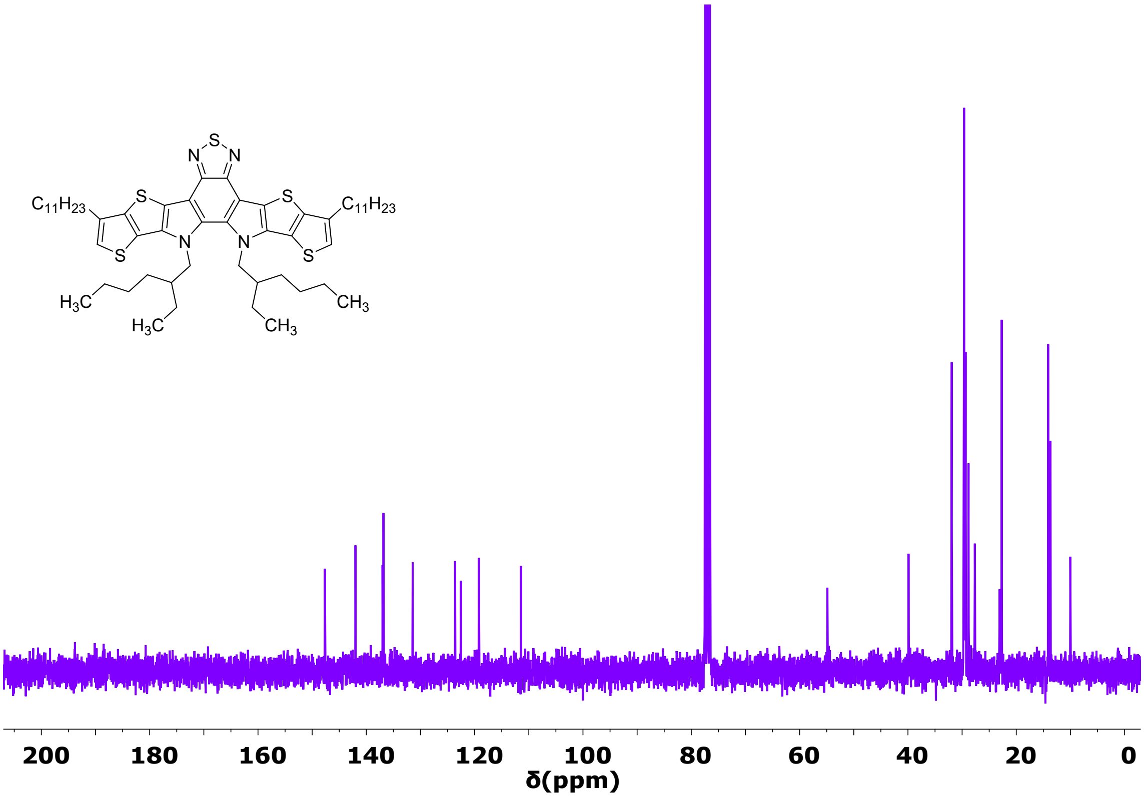

Figure S4. ^{13}C-NMR spectrum of **BTD-ext** in CDCl$_3$.

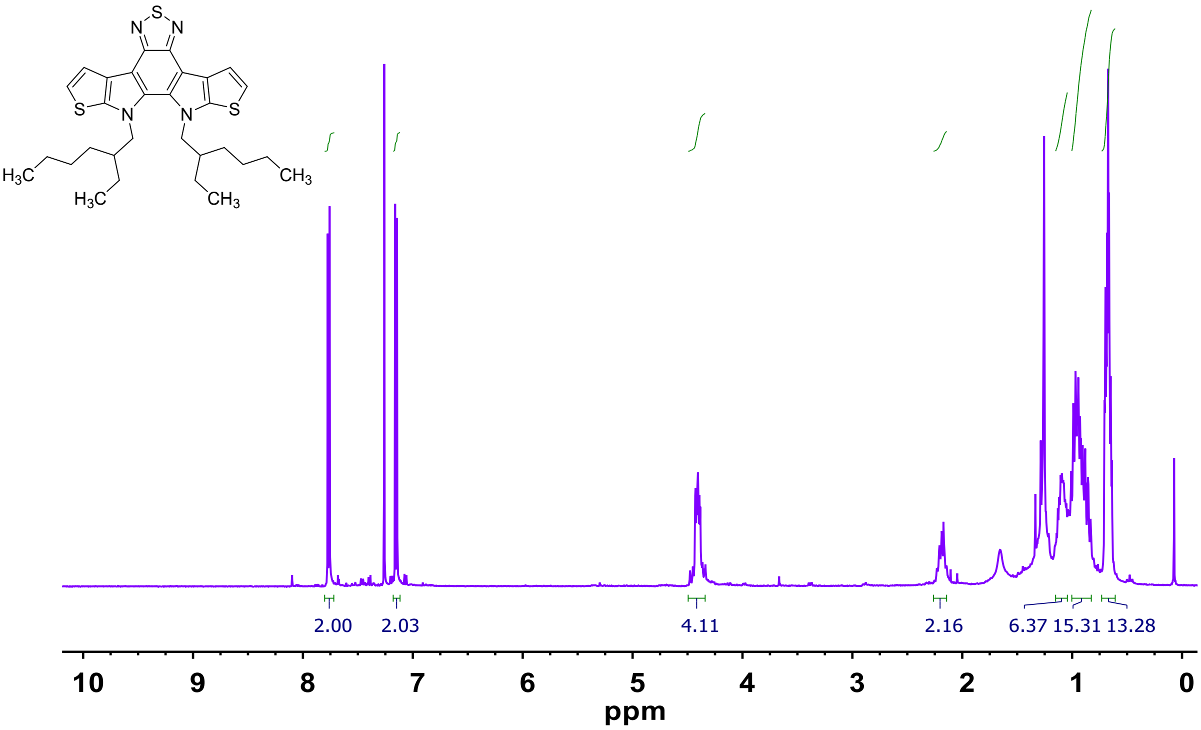

Figure S5. ^{1}H-NMR spectrum of **BTD-inv** in CDCl$_3$.

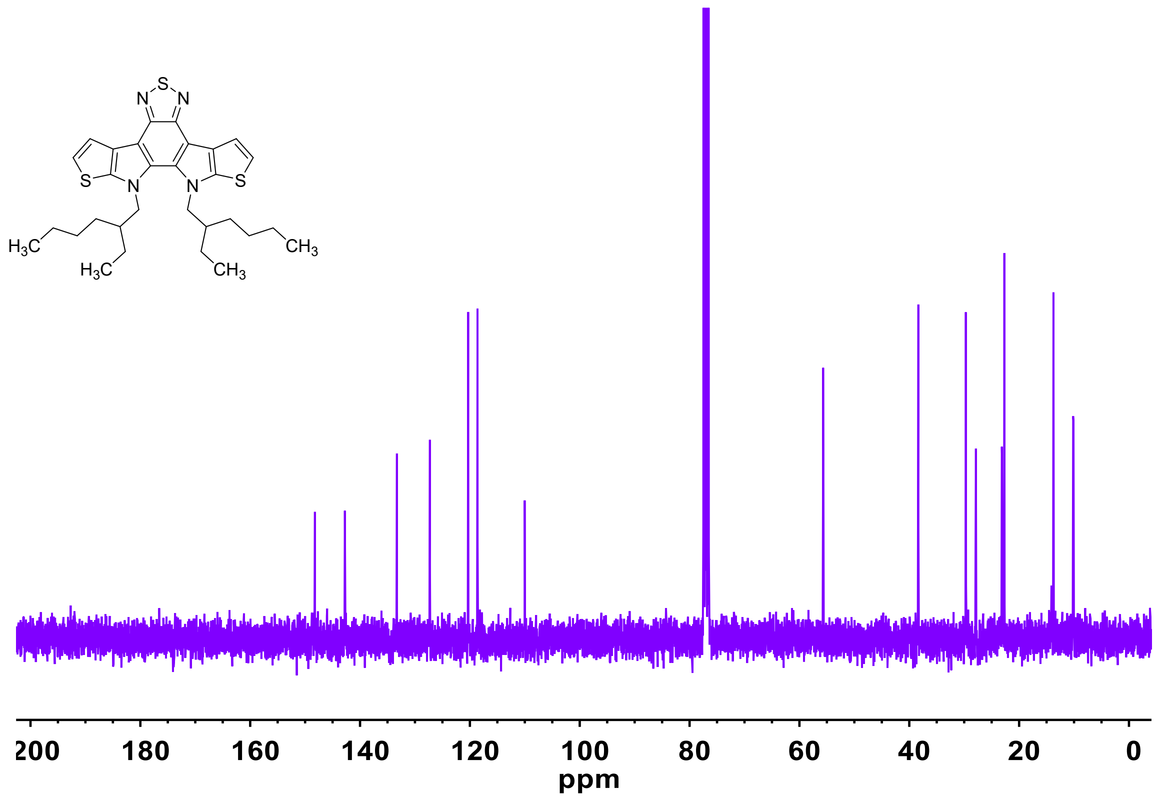

Figure S6. ^{13}C-NMR spectrum of **BTD-inv** in CDCl$_3$.

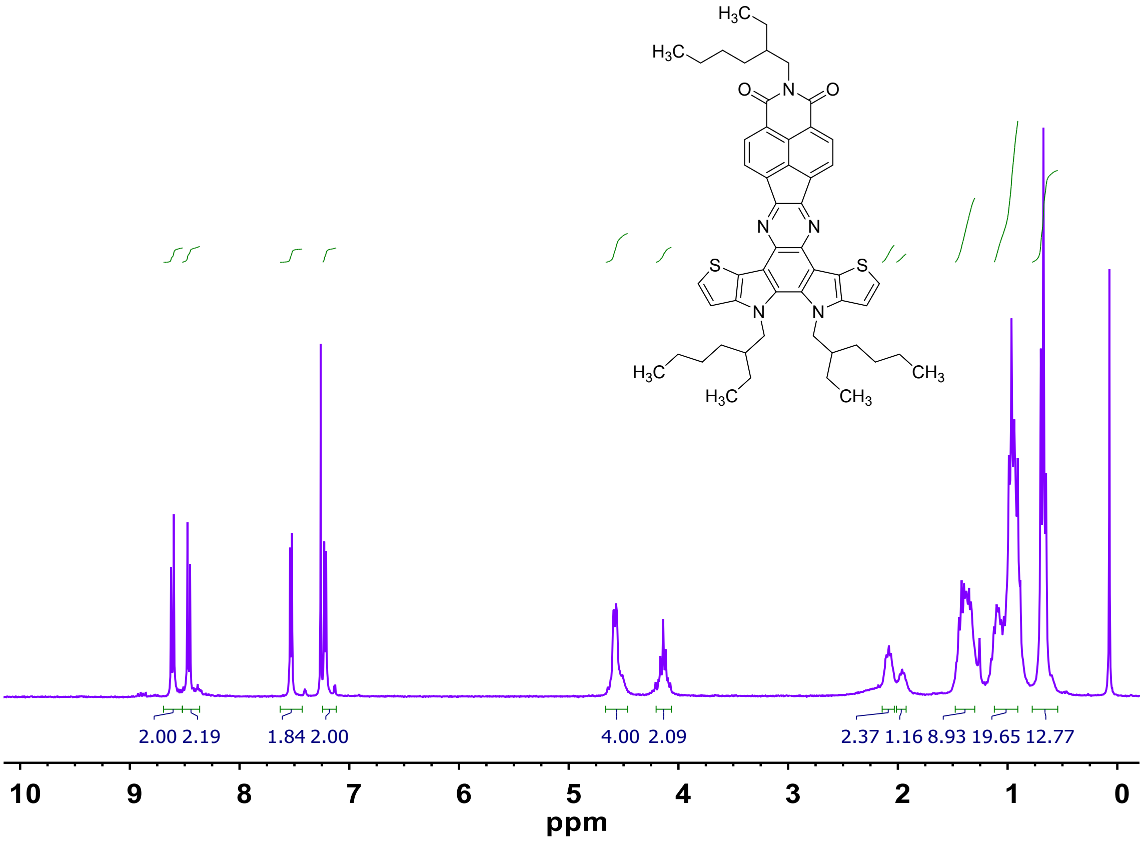

Figure S7. ^{1}H-NMR spectrum of **NIP** in $CDCl_3$.

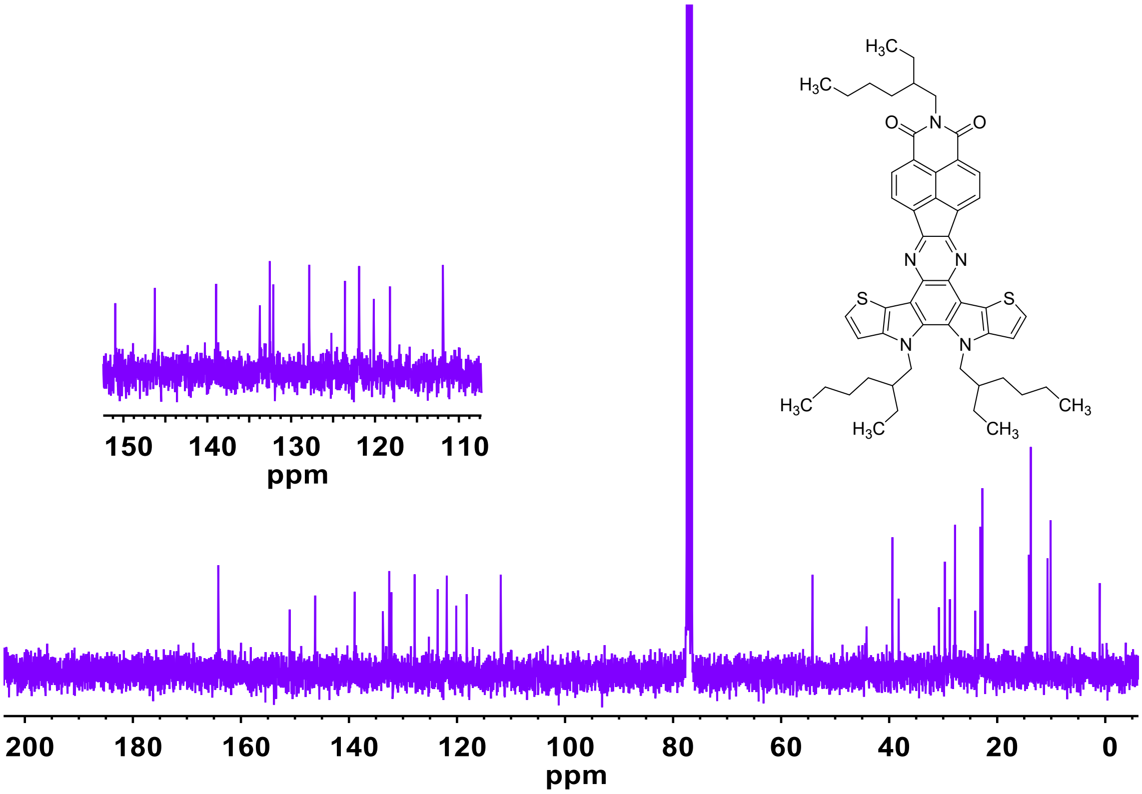

Figure S8. ^{13}C-NMR spectrum of **NIP** in $CDCl_3$.

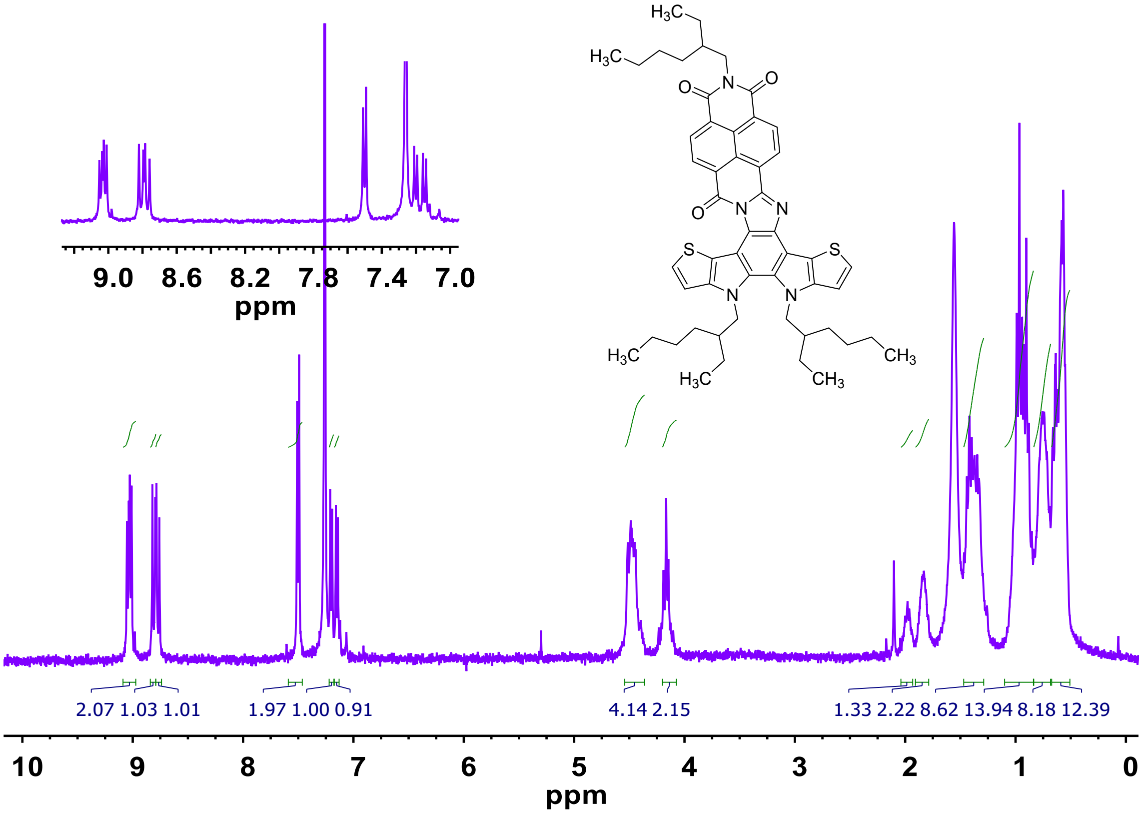

Figure S9. ^{1}H-NMR spectrum of **NDI** in CDCl$_3$.

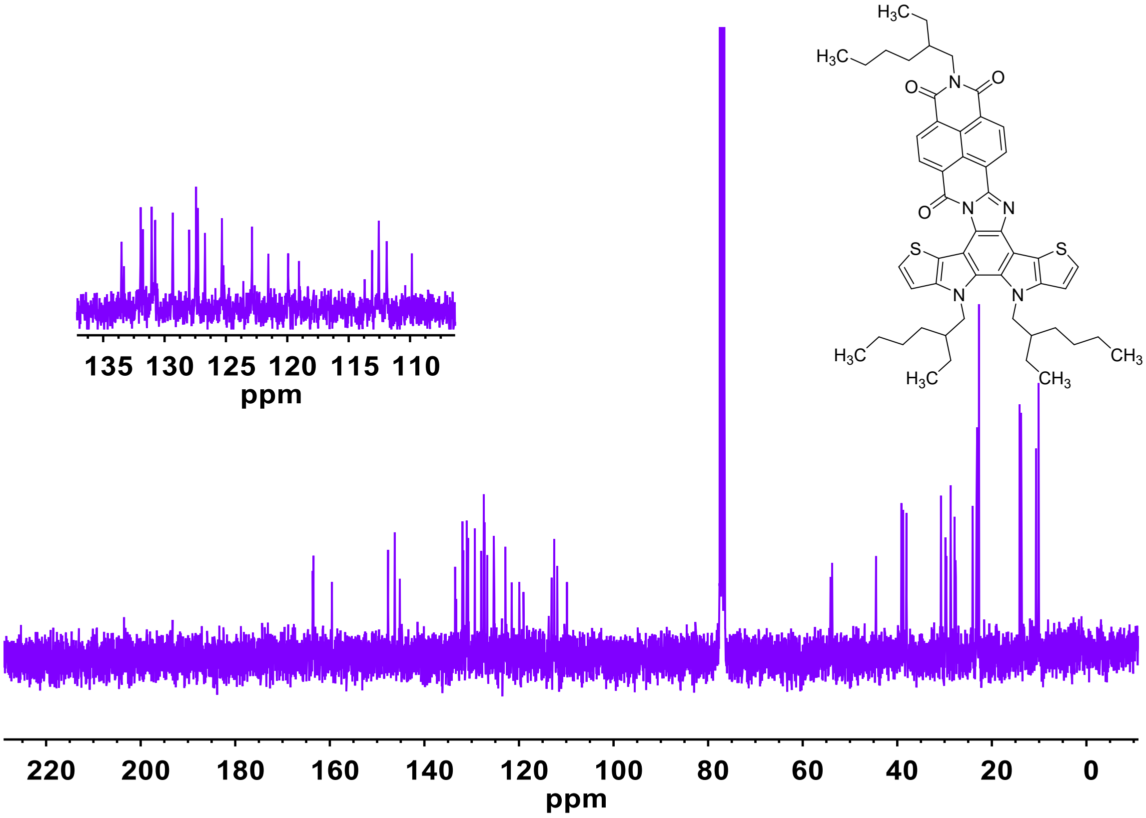

Figure S10. ^{13}C-NMR spectrum of **NDI** in CDCl$_3$.

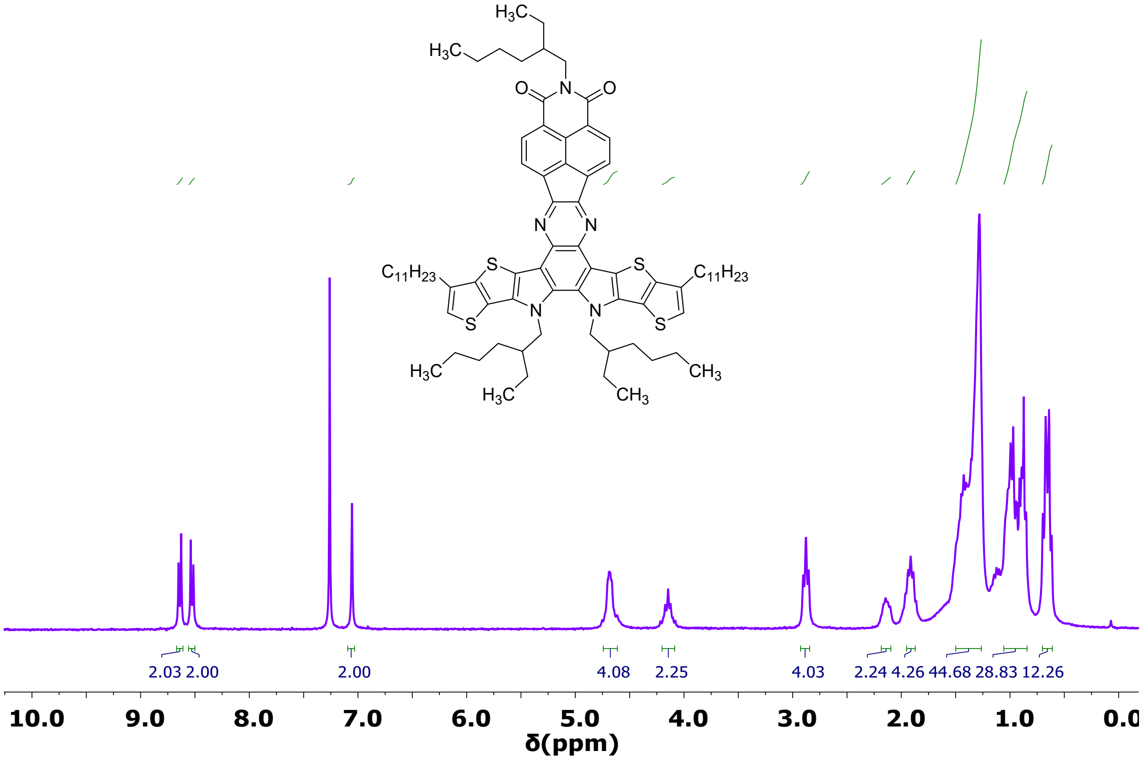

Figure S11. ^{1}H-NMR spectrum of **NIP-ext** in $CDCl_3$.

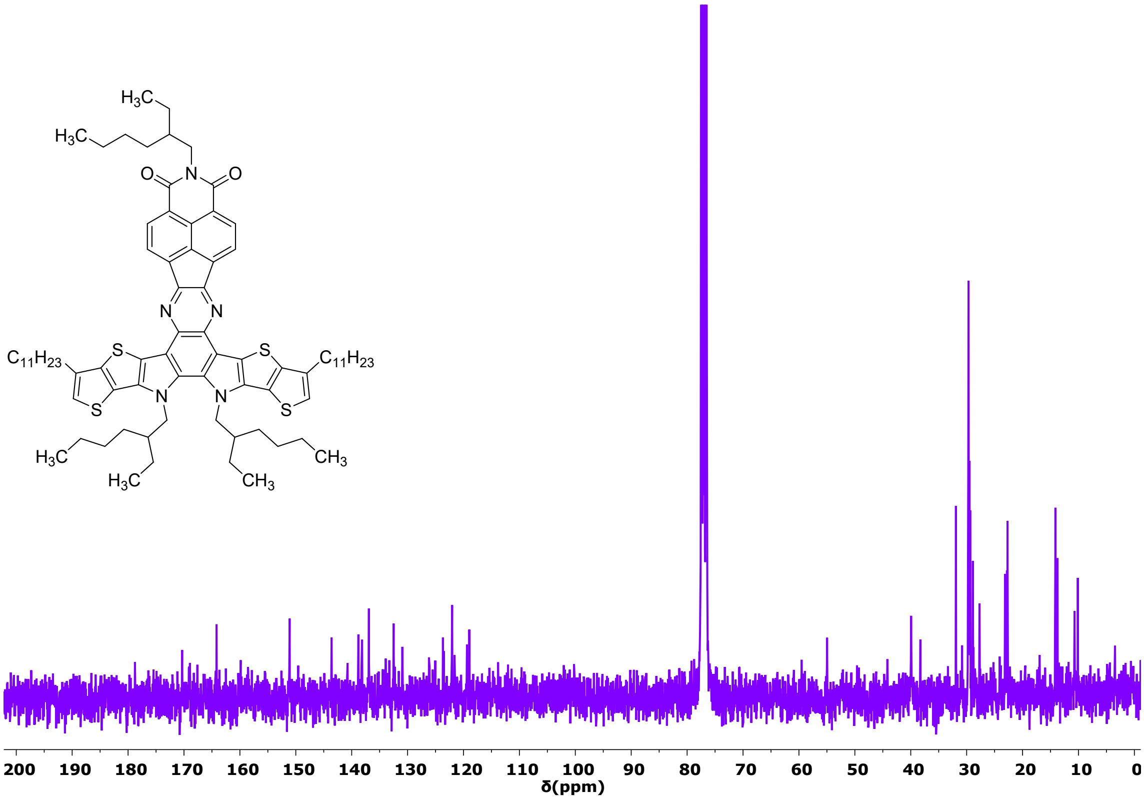

Figure S12. ^{13}C-NMR spectrum of **NIP-ext** in $CDCl_3$.

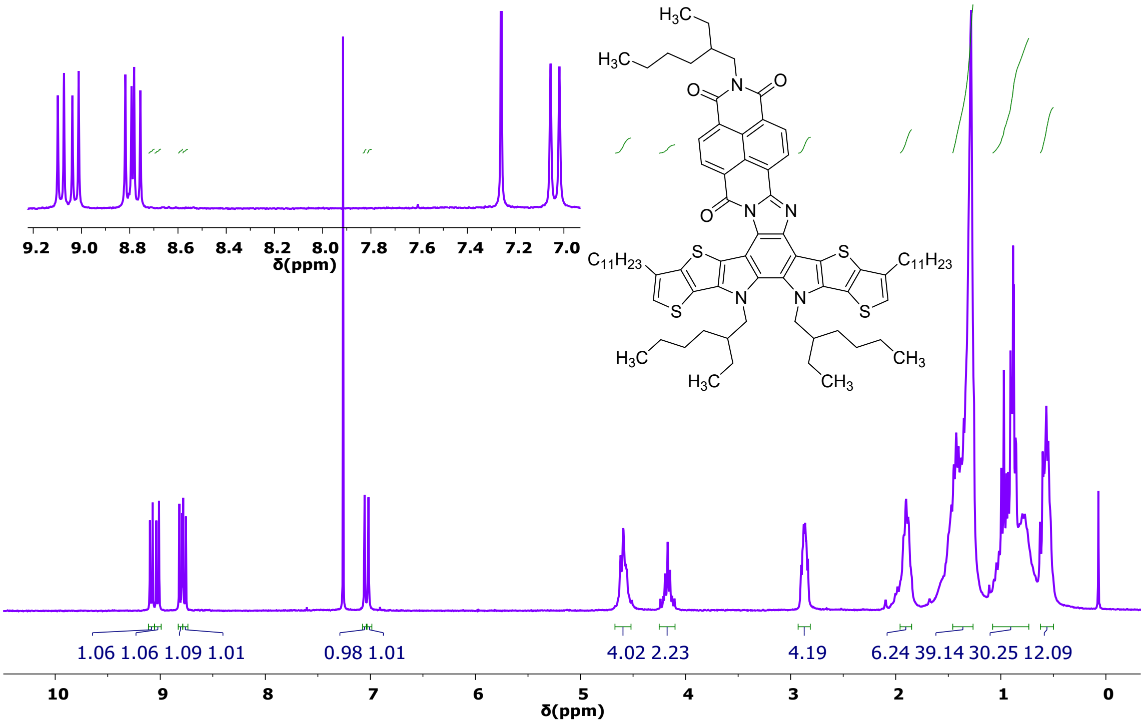

Figure S13. ^{1}H-NMR spectrum of **NDI-ext** in $CDCl_3$.

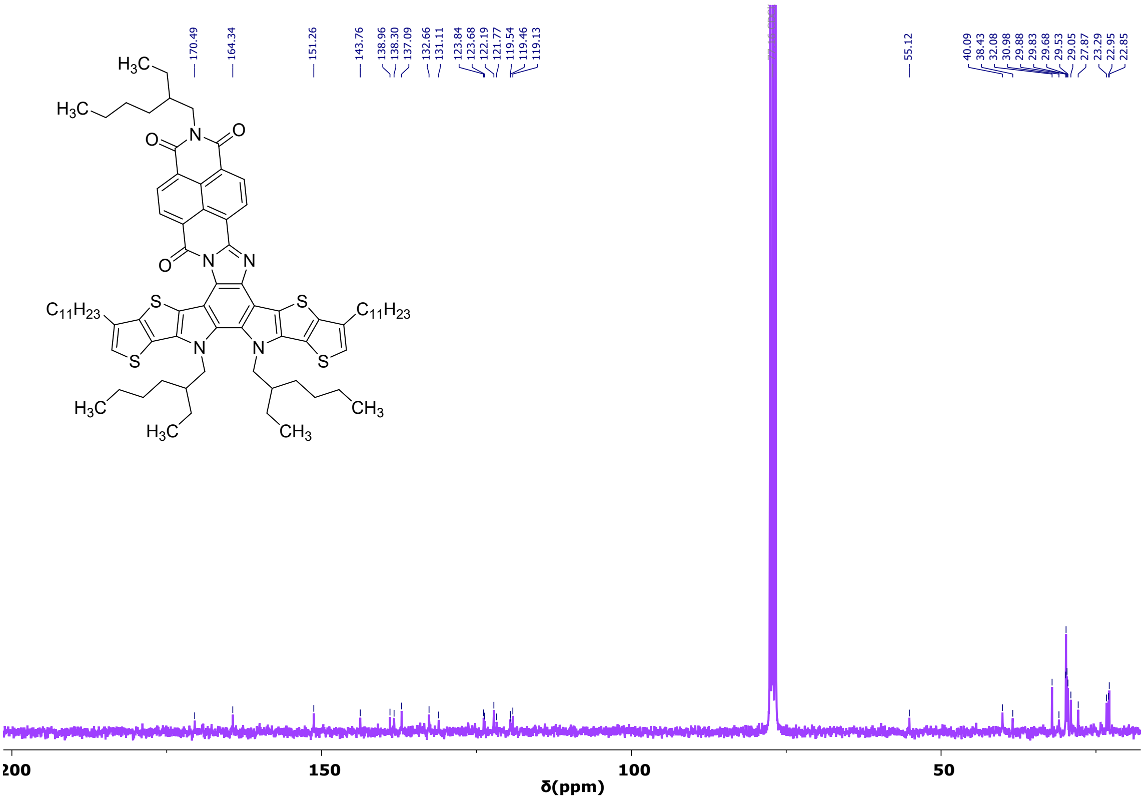

Figure S14. ^{13}C-NMR spectrum of **NDI-ext** in $CDCl_3$.

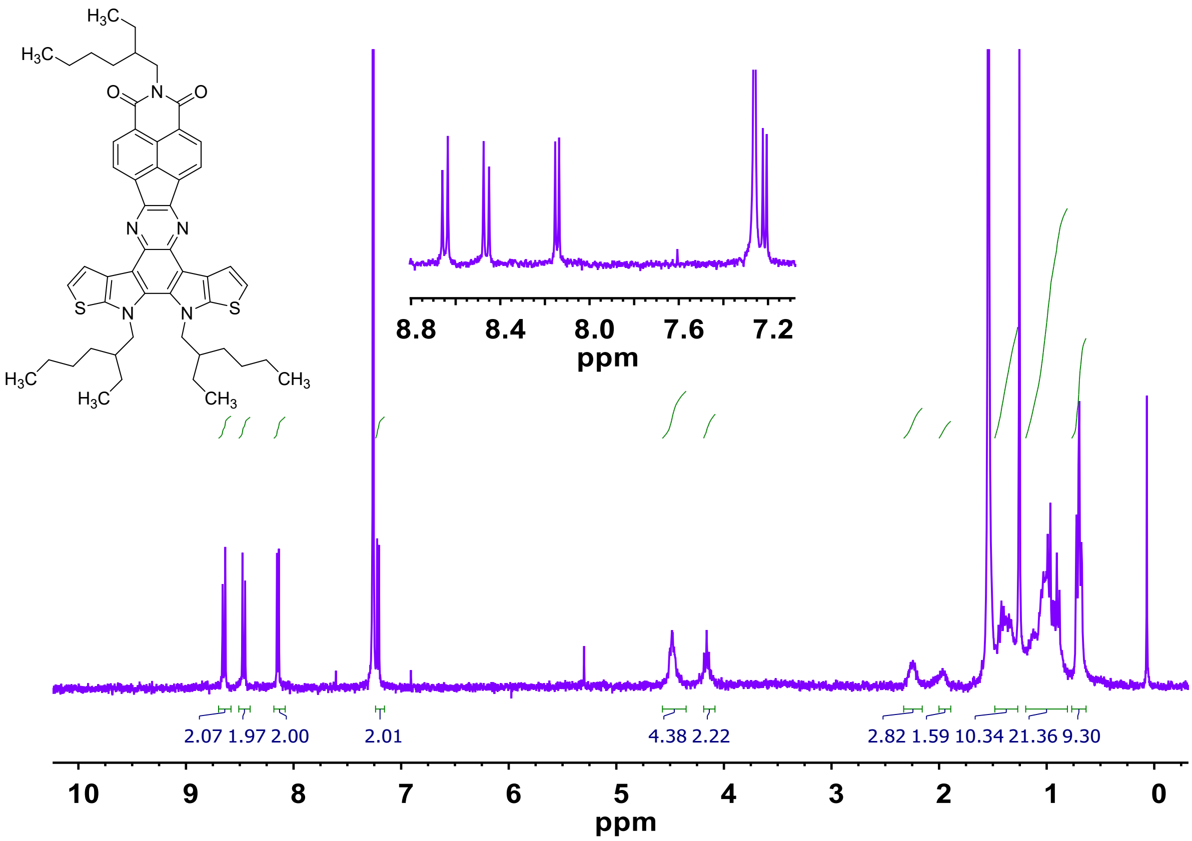

Figure S15. ^{1}H-NMR spectrum of **NIP-inv** in $CDCl_3$.

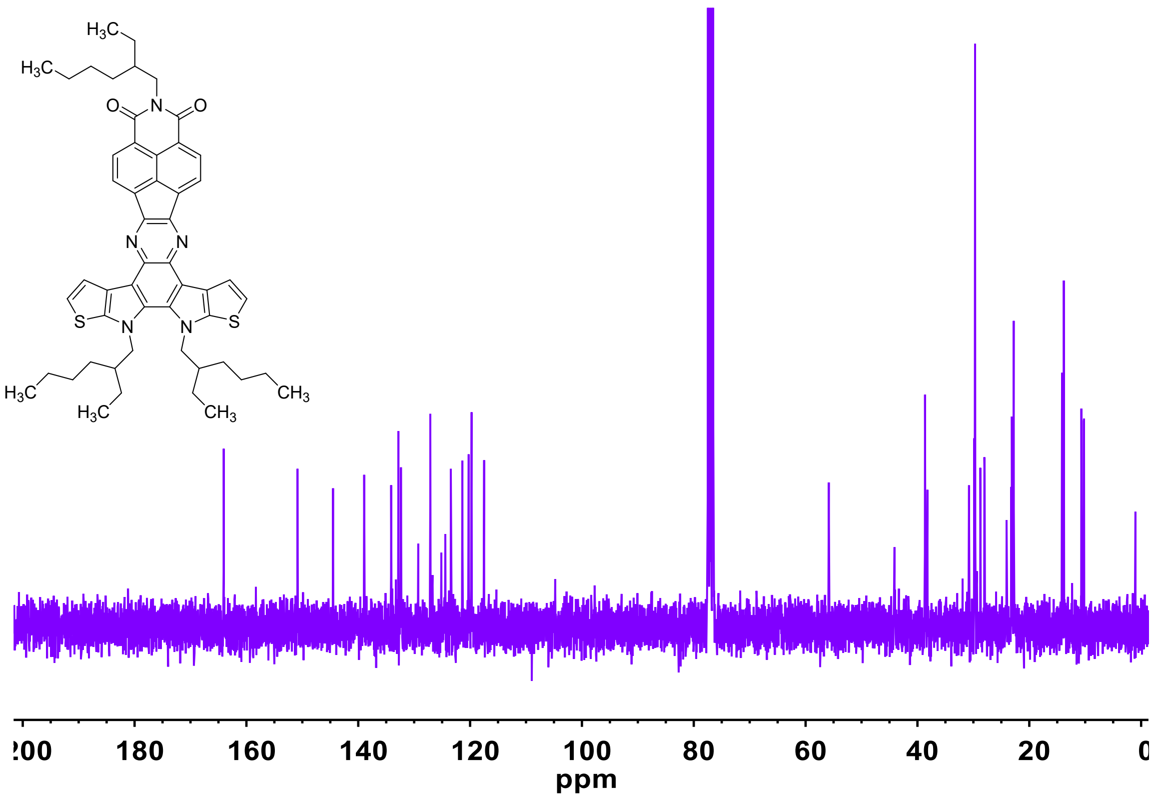

Figure S16. ^{13}C-NMR spectrum of **NIP-inv** in CDCl$_3$.

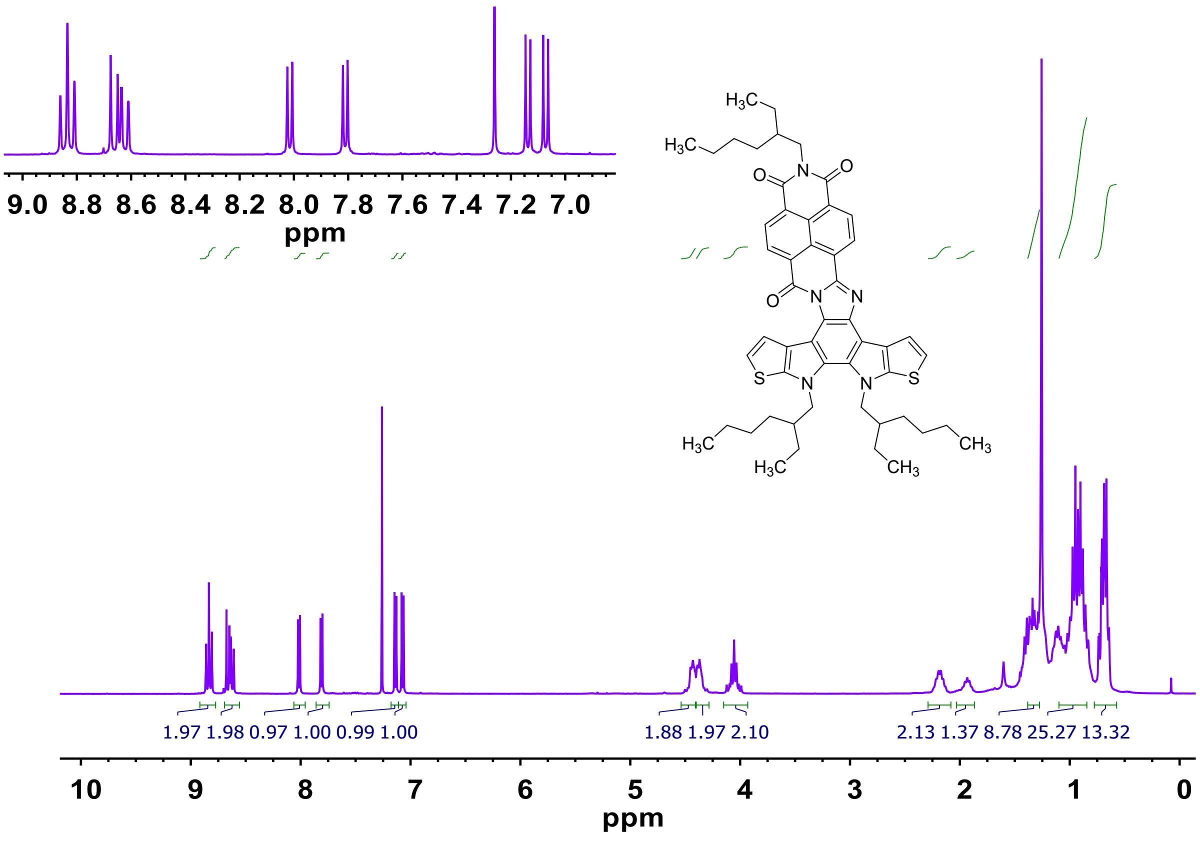

Figure S17. ^{1}H-NMR spectrum of **NDI-inv** in CDCl$_3$.

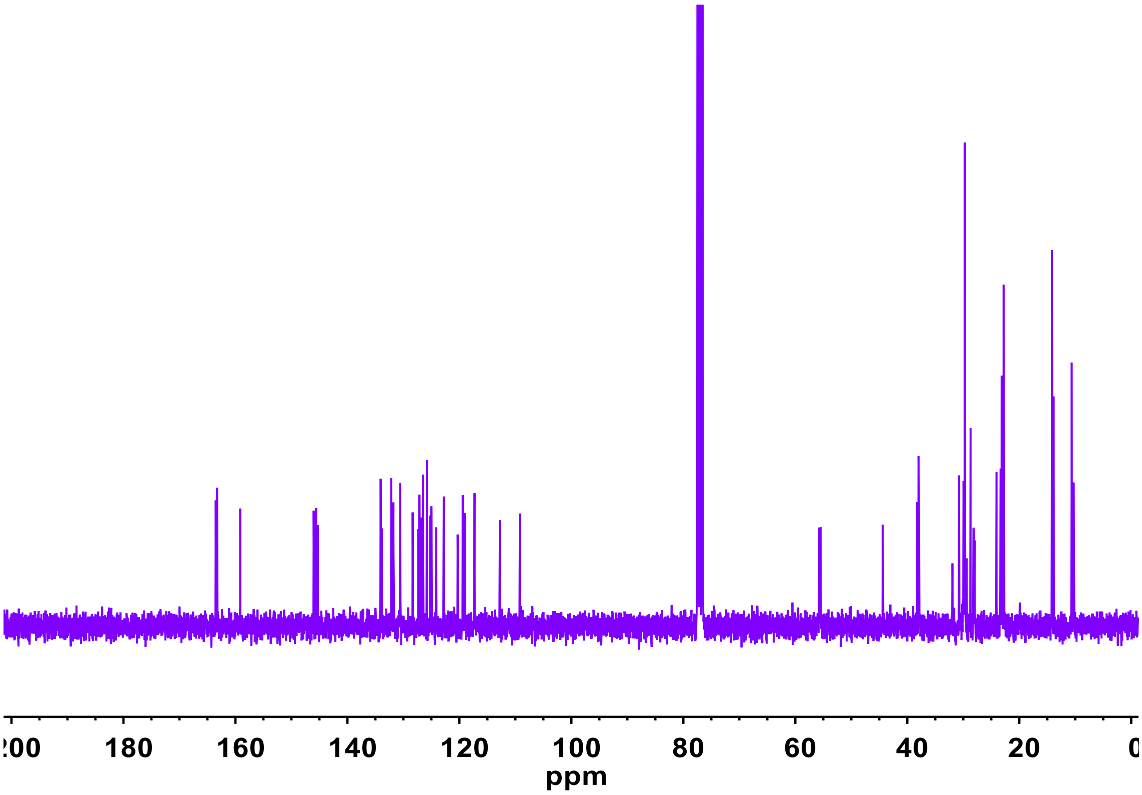

Figure S18. ^{13}C-NMR spectrum of **NDI-inv** in $CDCl_3$.

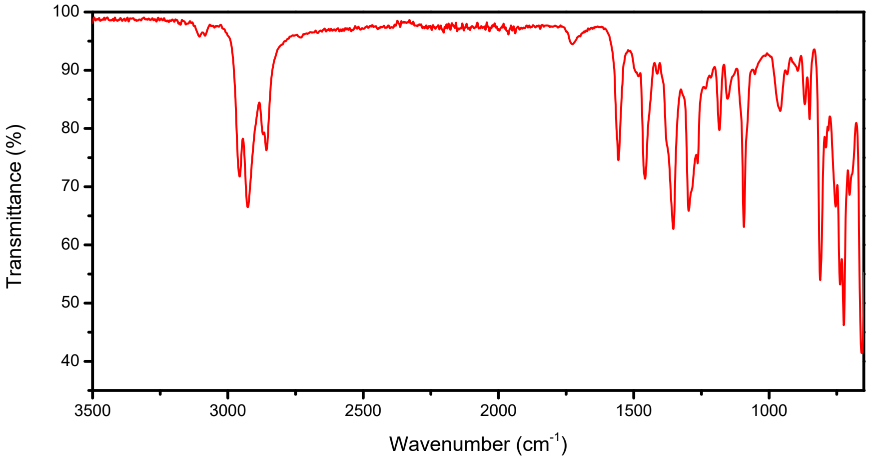

Figure S19. FTIR spectrum of **BTD**.

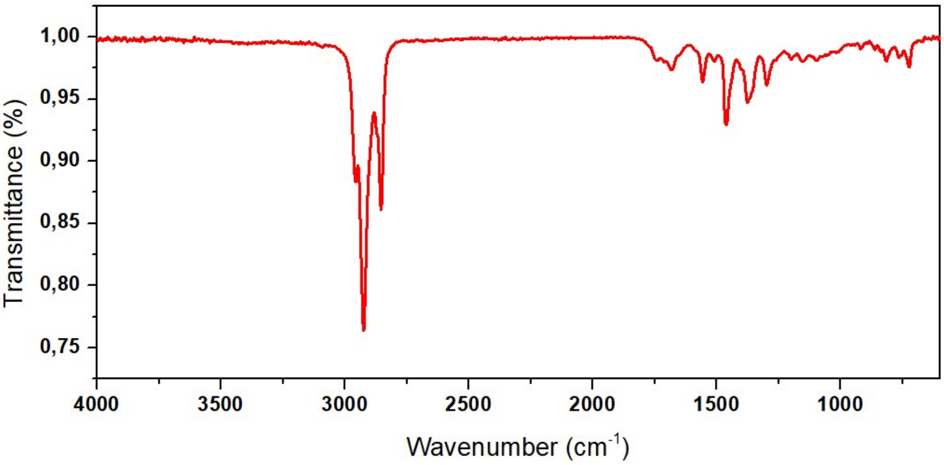

Figure S20. FTIR spectrum of **BTD-ext.**

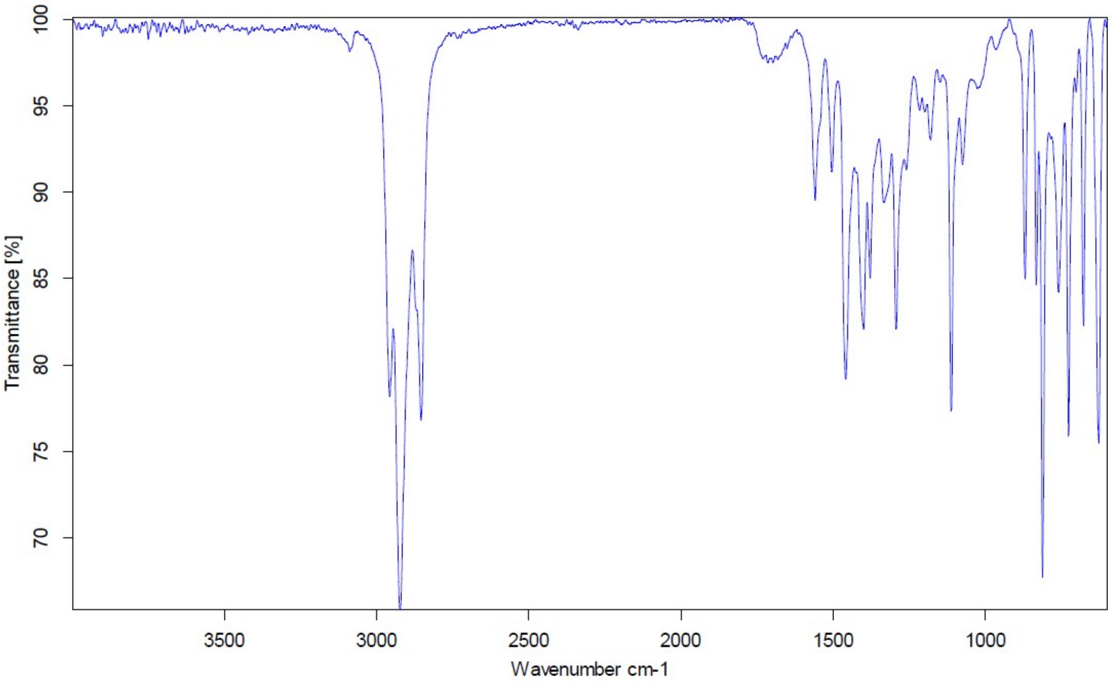

Figure S21. FTIR spectrum of **BTD-inv.**

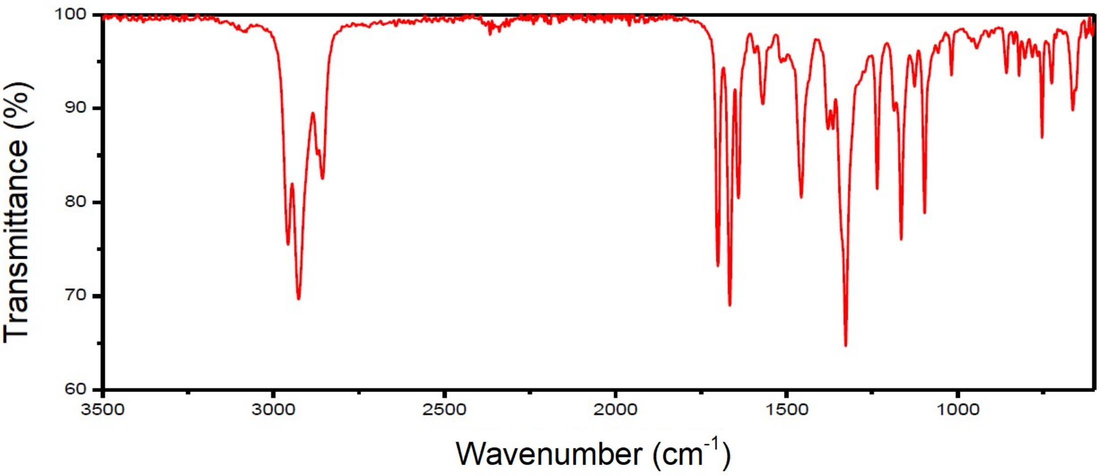

Figure S22. FTIR mass spectrum of **NIP**.

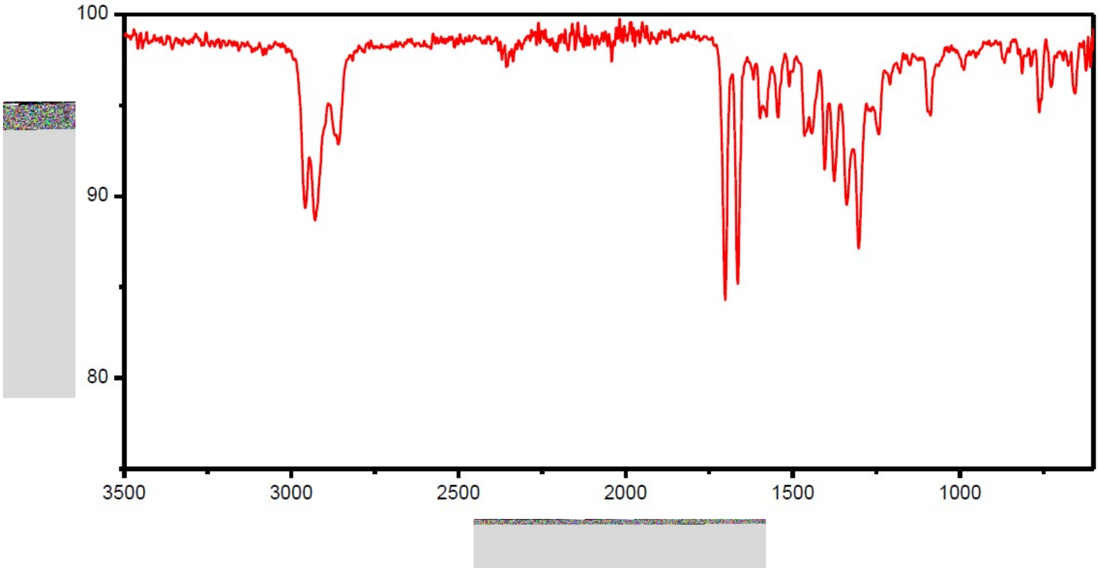

Figure S23. FTIR mass spectrum of **NDI**.

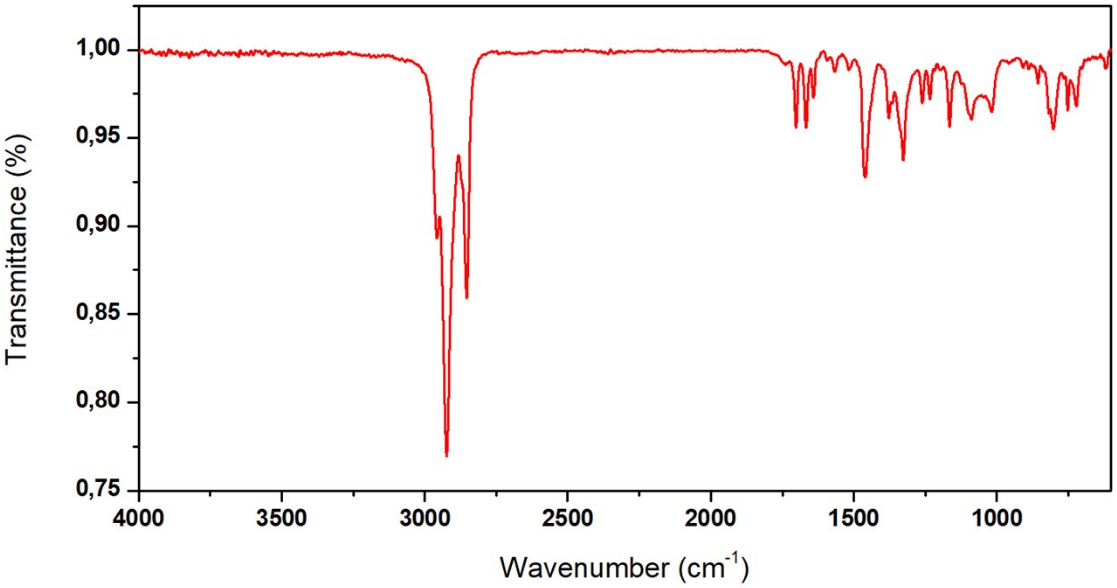

Figure S24. FTIR mass spectrum of **NIP-ext.**

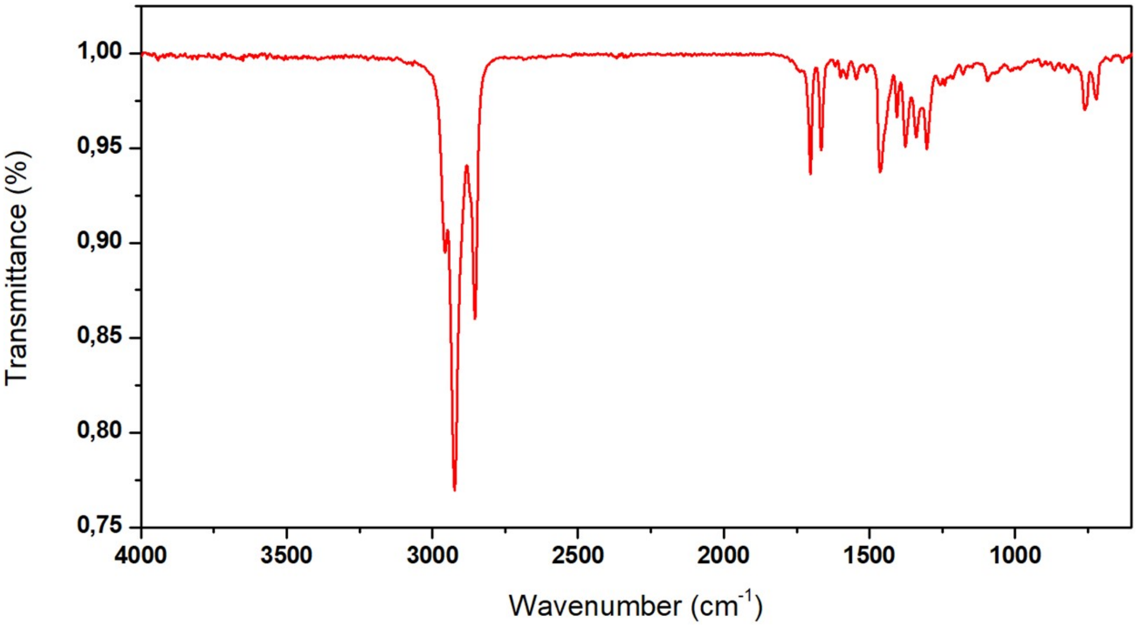

Figure S25. FTIR mass spectrum of **NDI-ext.**

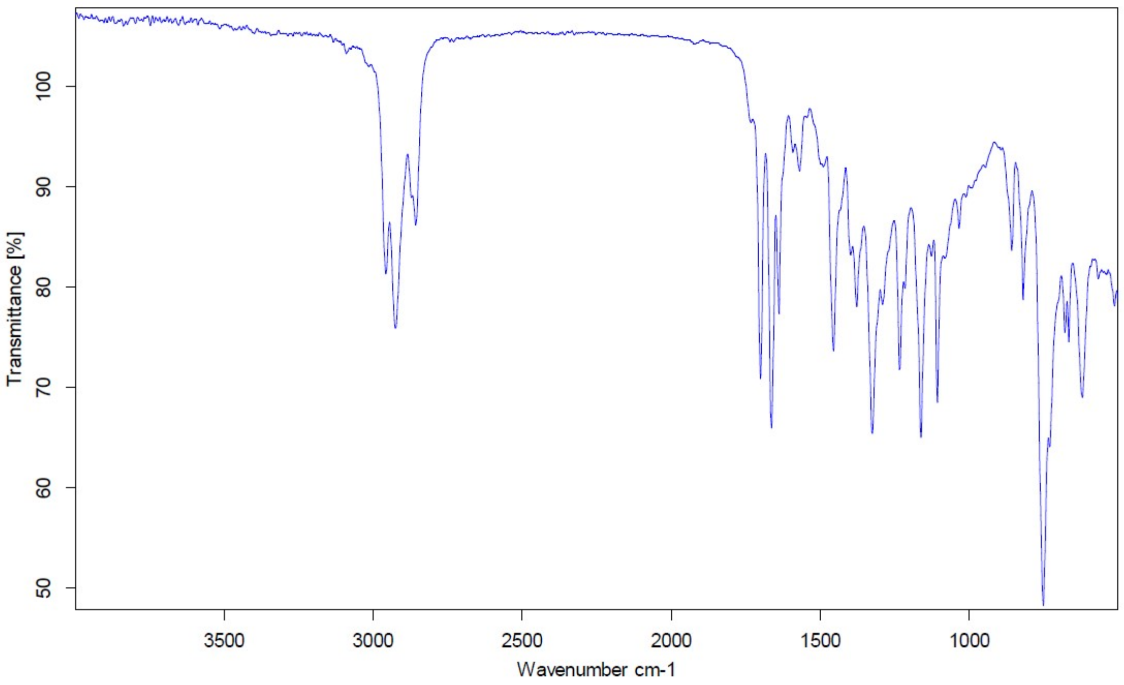

Figure S26. FTIR mass spectrum of **NIP-inv.**

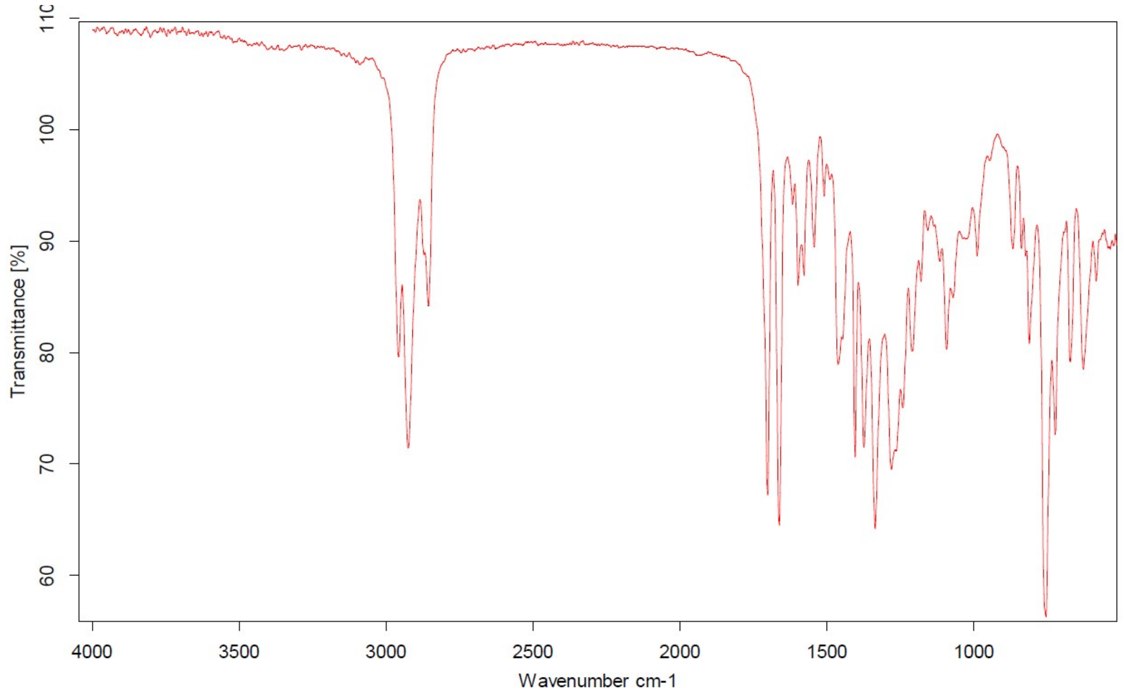

Figure S27. FTIR mass spectrum of **NDI-inv.**

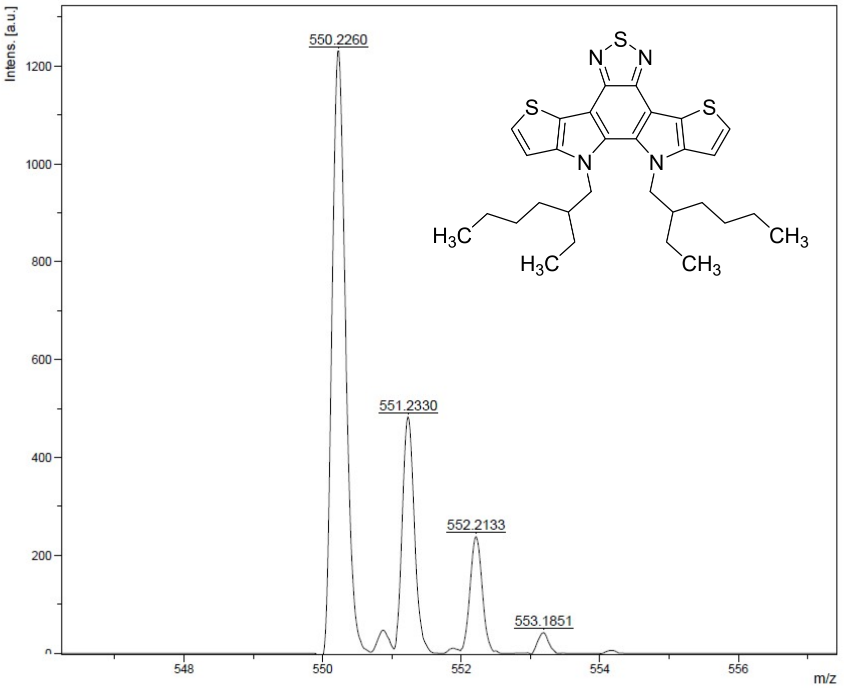

Figure S28. MALDI-HRMS (m/z) mass spectrum of **BTD**.

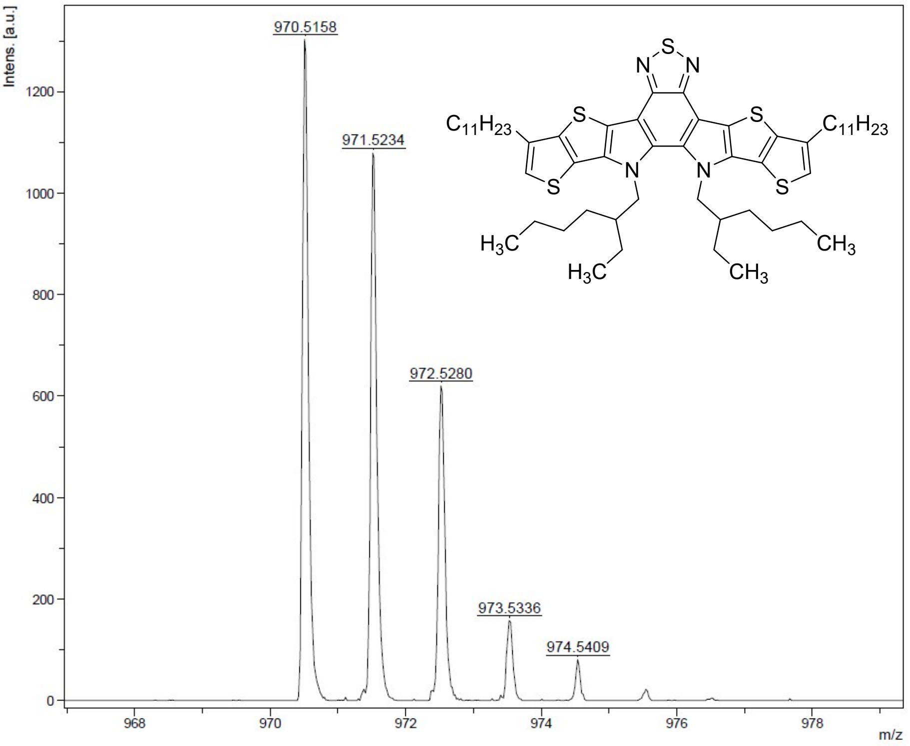

Figure S29. MALDI-HRMS (m/z) mass spectrum of **BTD-ext.**

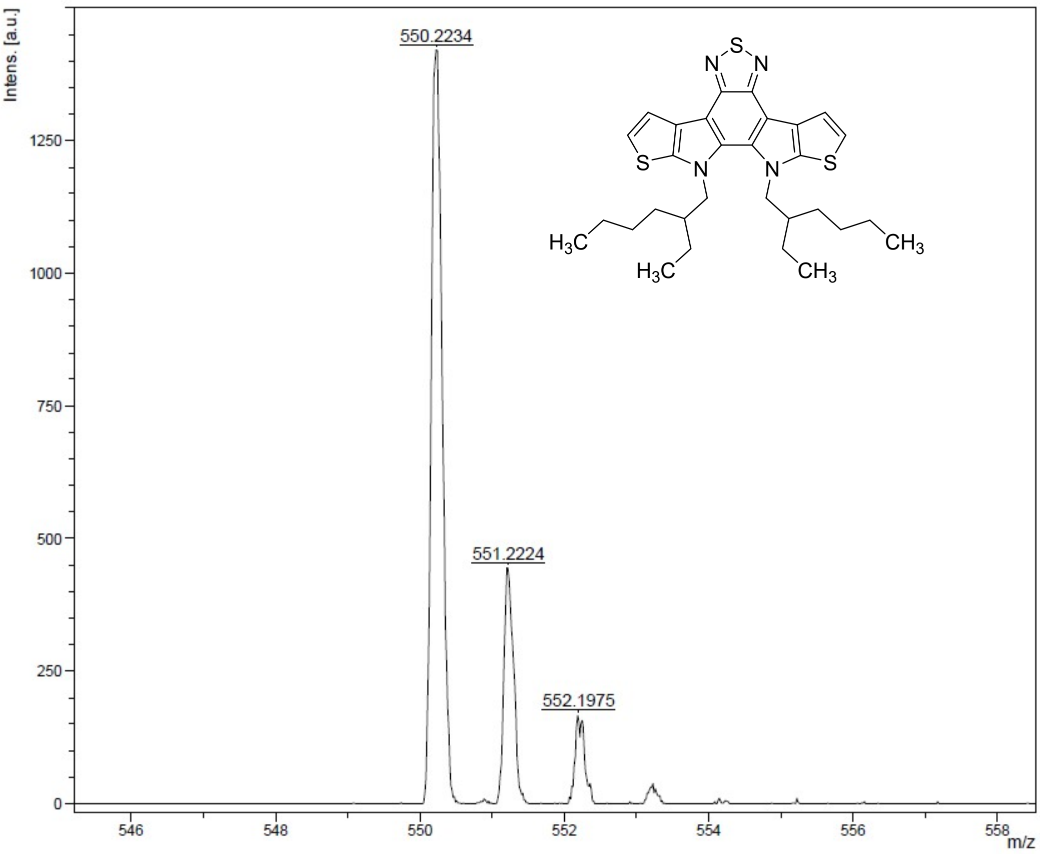

Figure S30. MALDI-HRMS (m/z) mass spectrum of **BTD-inv.**

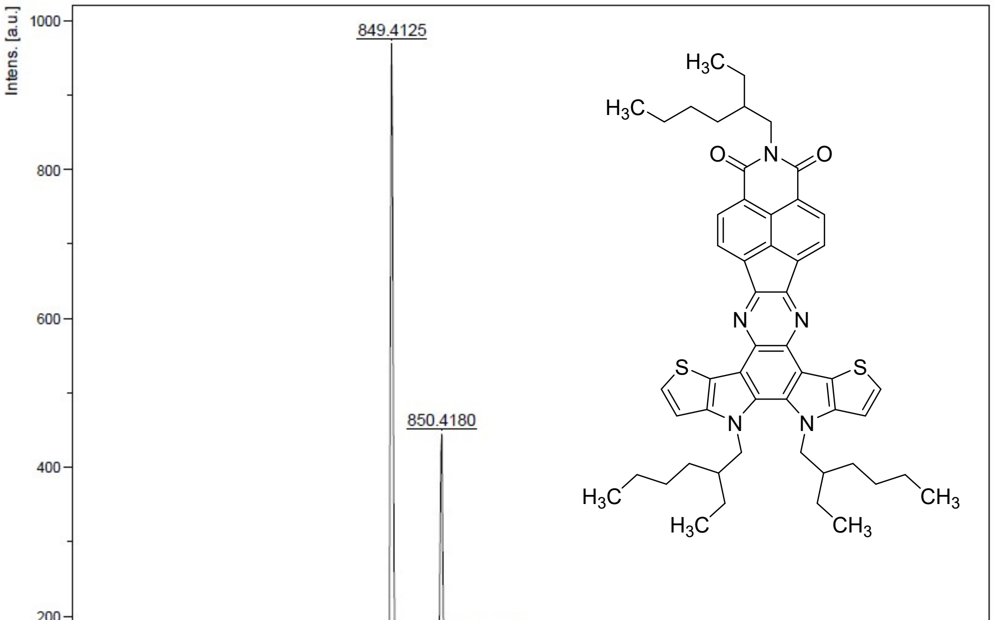

Figure S31. MALDI-HRMS (m/z) mass spectrum of **NIP**.

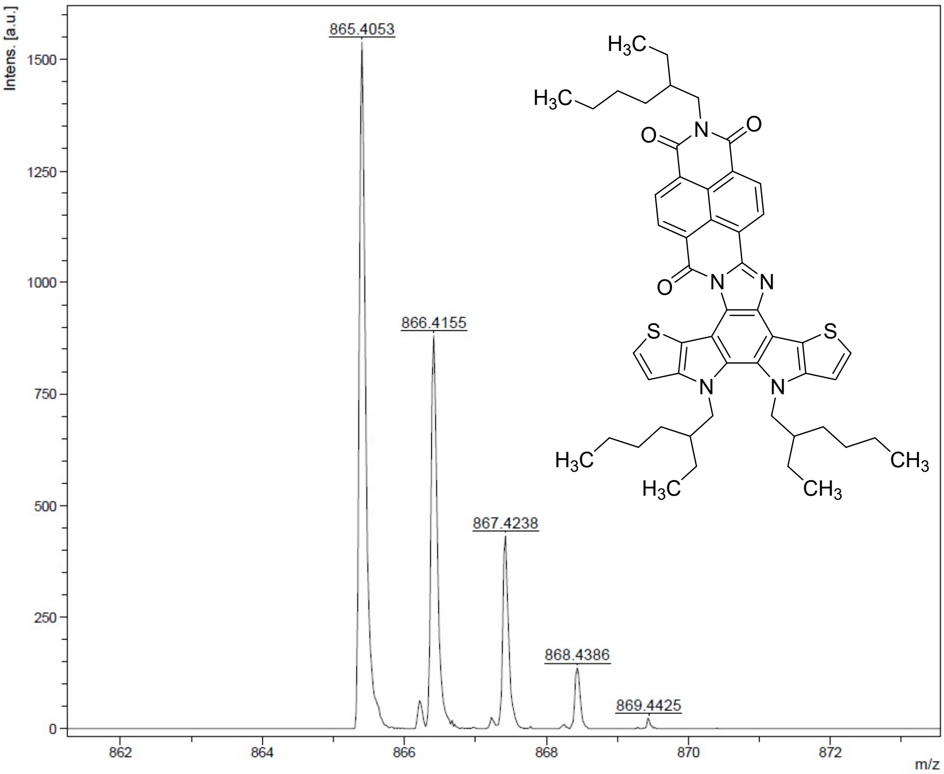

Figure S32. MALDI-HRMS (m/z) mass spectrum of **NDI**.

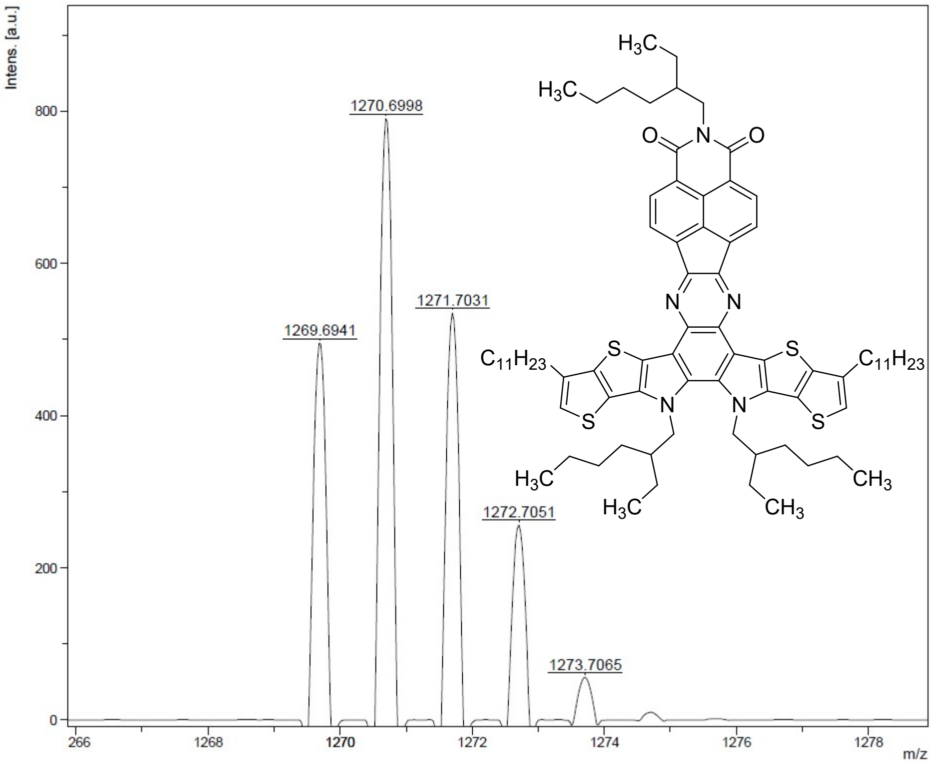

Figure S33. MALDI-HRMS (m/z) mass spectrum of **NIP-ext.**

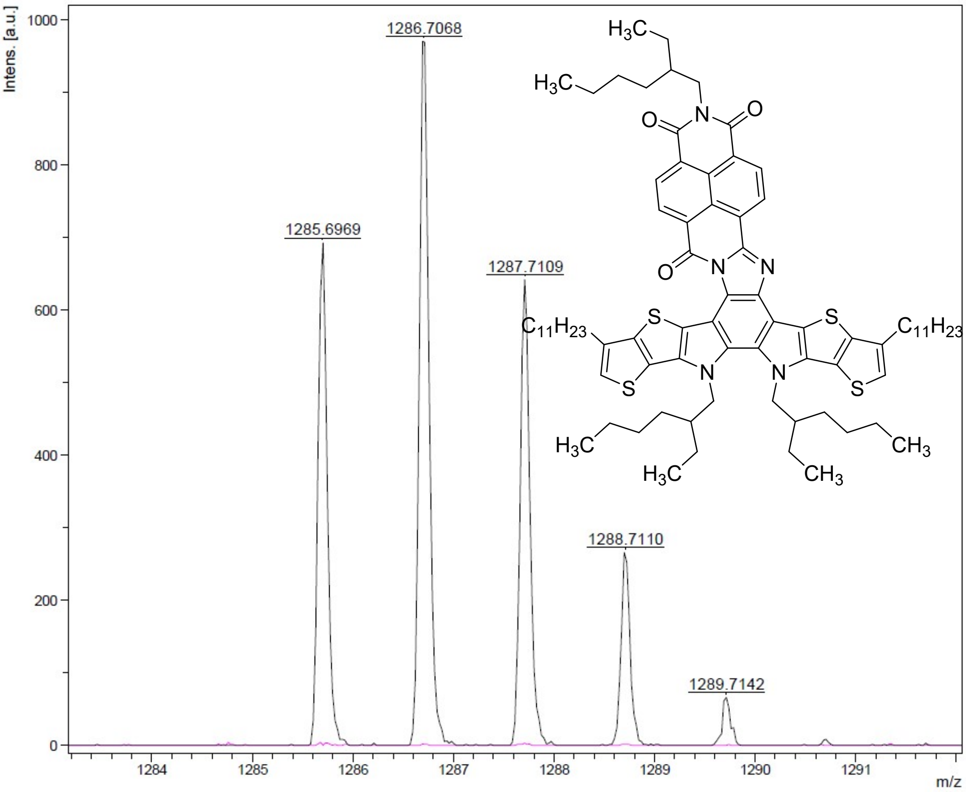

Figure S34. MALDI-HRMS (m/z) mass spectrum of **NDI-ext.**

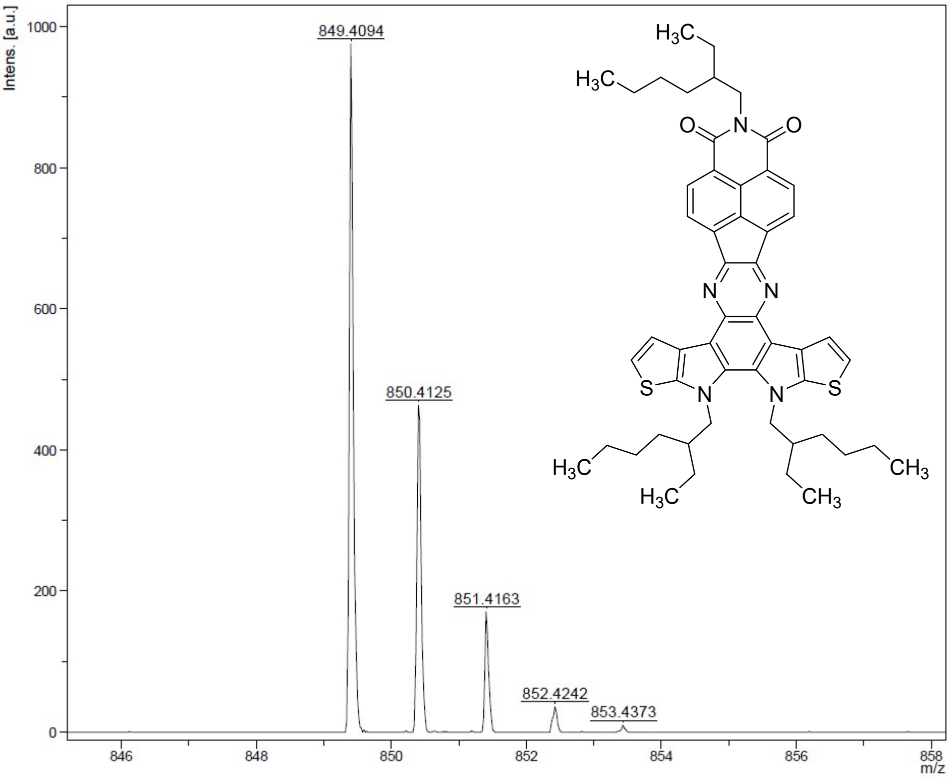

Figure S35. MALDI-HRMS (m/z) mass spectrum of **NIP-inv.**

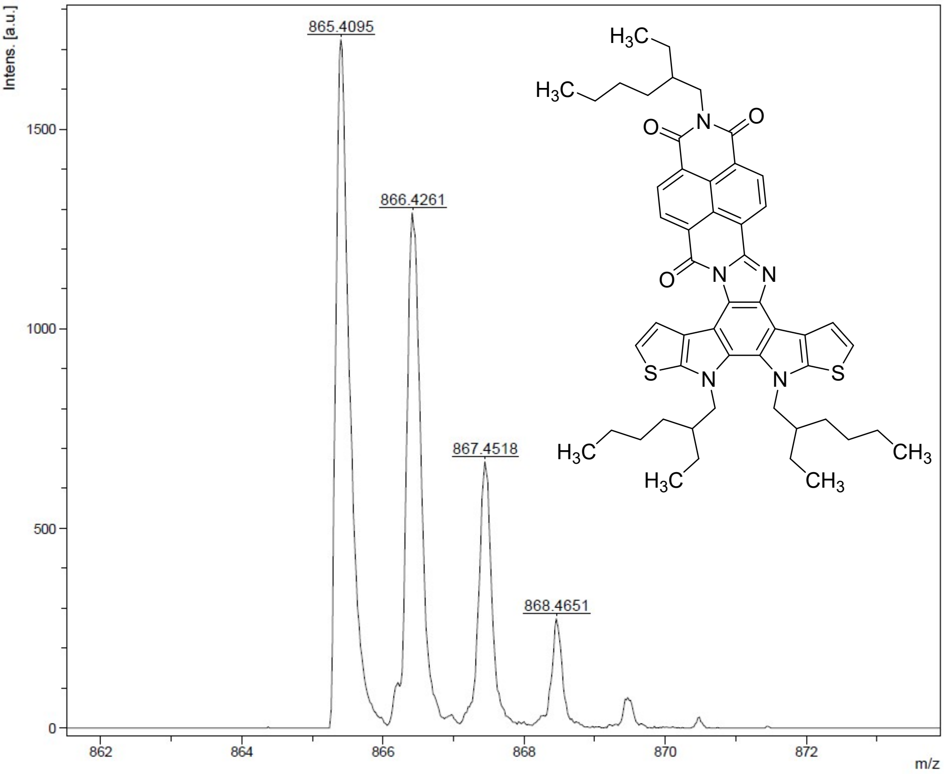

Figure S36. MALDI-HRMS (m/z) mass spectrum of **NDI-inv.**

3. DFT and TD-DFT calculations

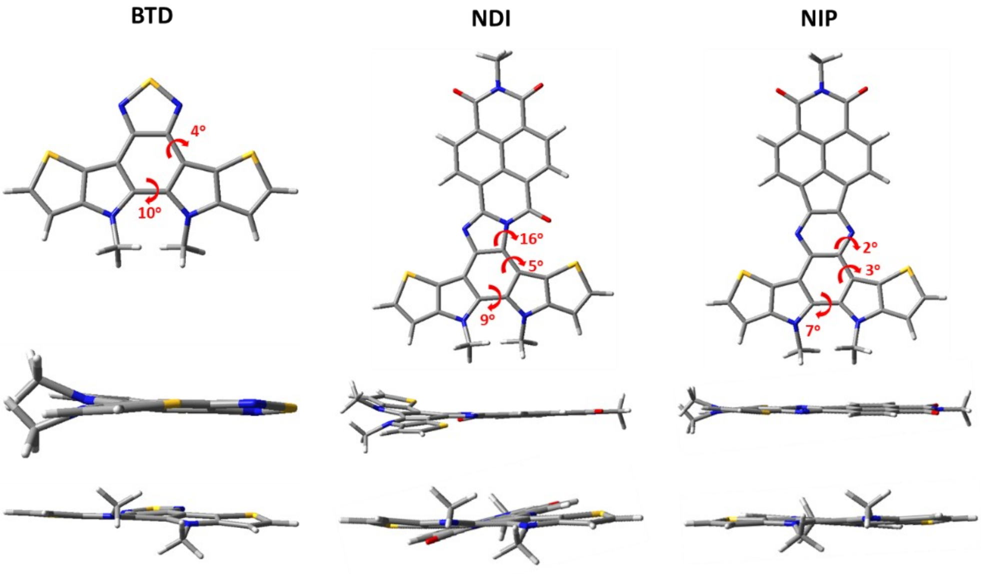

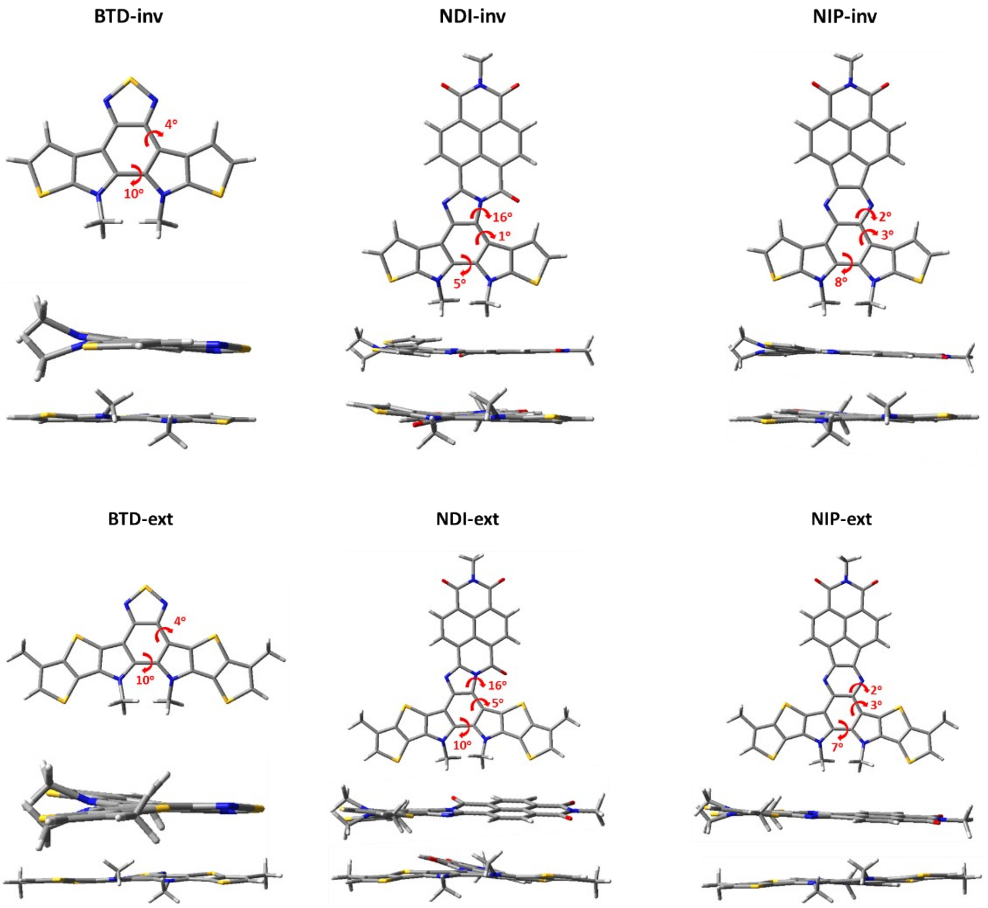

Figure S37. Optimized structures obtained at the B3LYP/6-31G** level for the different units studied.

Table S1. Calculated (B3LYP/6-31G**) HOMO and LUMO energy levels and reorganization energies.

	Theoretical results				
	LUMO (eV)	**HOMO (eV)**	**E_{gap} (eV)**	**λ_e (meV)**	**λ_h (meV)**
BTD	**-1.71**	**-4.95**	**3.24**	**472**	**289**
NDI	**-3.14**	**-5.01**	**1.87**	**343**	**287**
NIP	**-2.77**	**-5.08**	**2.31**	**320**	**283**
BTD-ext	**-1.79**	**-4.80**	**3.01**	**441**	**259**
NDI-ext	**-3.18**	**-4.85**	**1.67**	**347**	**260**
NIP-ext	**-2.82**	**-4.91**	**2.09**	**319**	**253**

BTD-inv	**-1.69**	**-5.06**	**3.37**	**485**	**310**
NDI-inv	**-3.17**	**-5.13**	**1.96**	**343**	**277**
NIP-inv	**-2.81**	**-5.20**	**2.39**	**324**	**295**

Table S2. Electronic transitions obtained by TD-DFT B3LYP/6-31G** level of theory for **BTD** Compound.

Electronic transitions	Description	E_{max} (λ_{max})	f
$S_0 \rightarrow S_1$	H→L (97%)	2.8 eV (450 nm)	0.136
$S_0 \rightarrow S_2$	H-1→L (93%)	3.6 eV (343 nm)	0.200
$S_0 \rightarrow S_3$	H-2→L (58%) H→L (40%)	3.8 eV (324 nm)	0.117
$S_0 \rightarrow S_4$	H-2→L (41%) H→L+1 (56%)	4.0 eV (308 nm)	0.527
$S_0 \rightarrow S_{16}$	H-3→L+1 (30%) H→L+4 (20%) H→L+5 (37%)	5.3 eV (234 nm)	0.125
$S_0 \rightarrow S_{25}$	H-5→L+1 (13%) H-1→L+4 (27%) H-1→L+5 (38%) H→L+7 (15%)	5.8 eV (212 nm)	0.270

Table S3. Electronic transitions obtained by TD-DFT B3LYP/6-31G** level of theory for **NDI** Compound.

Electronic transitions	Description	E_{max} (λ_{max})	f
$S_0 \rightarrow S_1$	H→L (91%)	1.5 eV (810 nm)	0.10

$S_0\rightarrow S_2$	**H-1→L (91%)**	**1.7 eV (733 nm)**	**0.14**
$S_0\rightarrow S_9$	**H-5→L (59%) H-1→L+1 (31%)**	**3.5 eV (358 nm)**	**0.52**
$S_0\rightarrow S_{18}$	**H-9→L (17%) H-1→L+2 (31%) H→L+4 (28%)**	**4.0 eV (312 nm)**	**0.19**
$S_0\rightarrow S_{19}$	**H-1→L+3 (13%) H-1→L+4 (50%) H→L+4 (20%)**	**4.0 eV (312 nm)**	**0.18**
$S_0\rightarrow S_{20}$	**H-9→L (38%) H-1→L+3 (19%) H-1→L+4 (25%)**	**4.0 eV (307 nm)**	**0.18**
$S_0\rightarrow S_{26}$	**H-1→L+5 (87%)**	**4.7 eV (266 nm)**	**0.11**

Table S4. Electronic transitions obtained by TD-DFT B3LYP/6-31G** level of theory for **NIP** Compound.

Electronic transitions	**Description**	**E_{max} (λ_{max})**	**f**
$S_0\rightarrow S_1$	**H→L (98%)**	**2.0 eV (629 nm)**	**0.11**
$S_0\rightarrow S_6$	**H-2→L (14%) H-1→L+1 (80%)**	**3.3 eV (381 nm)**	**0.83**
$S_0\rightarrow S_9$	**H-3→L (94%)**	**3.4 eV (360 nm)**	**0.25**
$S_0\rightarrow S_{15}$	**H-9→L (18%) H→L+2 (59%)**	**3.9 eV (316 nm)**	**0.29**
$S_0\rightarrow S_{16}$	**H-9→L (24%)**	**4.0 eV (311 nm)**	**0.25**

	H-3→L+1 (41%) H→L+2 (20%)		
$S_0 \rightarrow S_{24}$	H-11→L (21%) H-6→L+1 (16%) H-1→L+3 (47%)	4.4 eV (279 nm)	0.16
$S_0 \rightarrow S_{25}$	H-12→L (17%) H-1→L+4 (73%)	4.5 eV (275 nm)	0.24

Table S5. Electronic transitions obtained by TD-DFT B3LYP/6-31G** level of theory for **BTD-inv** Compound.

Electronic transitions	Description	E_{max} (λ_{max})	f
$S_0 \rightarrow S_1$	H→L (99%)	2.8 eV (435 nm)	0.12
$S_0 \rightarrow S_2$	H-1→L (95%)	3.6 eV (347 nm)	0.17
$S_0 \rightarrow S_{10}$	H-1→L+1 (21%) H→L+3 (68%)	4.8 eV (259 nm)	0.10
$S_0 \rightarrow S_{14}$	H-5→L (65%) H-1→L+1 (26%)	5.1 eV (242 nm)	0.18
$S_0 \rightarrow S_{15}$	H-5→L (31%) H-1→L+1 (47%) H→L+3 (13%)	5.1 eV (242 nm)	0.56
$S_0 \rightarrow S_{21}$	H-8→L (40%) H-2→L+2 (52%)	5.5 eV (226 nm)	0.15
$S_0 \rightarrow S_{23}$	H-2→L+1 (56%) H→L+7 (26%)	5.5 eV (225 nm)	0.13

Table S6. Electronic transitions obtained by TD-DFT B3LYP/6-31G** level of theory for **NDI-inv** Compound.

Electronic transitions	Description	E_{max} (λ_{max})	f
$S_0 \rightarrow S_1$	H-1→L (36%) H→L (64%)	1.6 eV (771 nm)	0.04
$S_0 \rightarrow S_2$	H-1→L (64%) H→L (36%)	1.7 eV (733 nm)	0.19
$S_0 \rightarrow S_8$	H-5→L (16%) H-1→L+1 (74%)	3.4 eV (365 nm)	0.16
$S_0 \rightarrow S_9$	H-5→L (67%) H-1→L+1 (18%)	3.5 eV (358 nm)	0.42
$S_0 \rightarrow S_{27}$	H-1→L+5 (56%) H→L+4 (12%)	4.7 eV (263 nm)	0.26

Table S7. Electronic transitions obtained by TD-DFT B3LYP/6-31G** level of theory for **NIP-inv** Compound.

Electronic transitions	Description	E_{max} (λ_{max})	f
$S_0 \rightarrow S_1$	H→L (98%)	2.0 eV (606 nm)	0.10
$S_0 \rightarrow S_6$	H-2→L (11%) H-1→L+1 (85%)	3.2 eV (387 nm)	0.82
$S_0 \rightarrow S_9$	H-3→L (94%)	3.5 eV (357 nm)	0.18
$S_0 \rightarrow S_{19}$	H-11→L (13%) H-4→L+1 (51%) H→L+3 (22%)	4.2 eV (292 nm)	0.36
$S_0 \rightarrow S_{23}$	H-11→L (66%)	4.5 eV (276 nm)	0.26

	H-6→L+1 (22%)		
$S_0 \rightarrow S_{27}$	H-1→L+3 (16%) H→L+4 (42%) H→L+5 (30%)	4.7 eV (266 nm)	0.25
$S_0 \rightarrow S_{29}$	H→L+4 (19%) H→L+5 (52%)	4.7 eV (263 nm)	0.12

Table S8. Electronic transitions obtained by TD-DFT B3LYP/6-31G** level of theory for **BTD-ext** Compound.

Electronic transitions	Description	E_{max} (λ_{max})	f
$S_0 \rightarrow S_1$	H→L (97%)	2.6 eV (484 nm)	0.26
$S_0 \rightarrow S_2$	H-1→L (86%)	3.5 eV (358 nm)	0.16
$S_0 \rightarrow S_3$	H-2→L (10%) H→L+1 (83%)	3.5 eV (358 nm)	0.64
$S_0 \rightarrow S_4$	H-2→L (89%) H→L+1 (10%)	3.6 eV (341 nm)	0.21
$S_0 \rightarrow S_6$	H-3→L (14%) H→L+2 (80%)	4.0 eV (310 nm)	0.12
$S_0 \rightarrow S_{13}$	H-3→L+1 (91%)	4.7 eV (266 nm)	0.14

Table S9. Electronic transitions obtained by TD-DFT B3LYP/6-31G** level of theory for **NDI-ext** Compound.

Electronic transitions	Description	E_{max} (λ_{max})	f
$S_0 \rightarrow S_1$	H→L (97%)	1.3 eV (920 nm)	0.10
$S_0 \rightarrow S_2$	H-1→L (91%)	1.7 eV (741 nm)	0.14
$S_0 \rightarrow S_6$	H→L+1 (96%)	3.0 eV (413 nm)	0.18

$S_0 \rightarrow S_9$	H-5→L (21%) H-1→L+1 (57%) H→L+3 (11%)	3.4 eV (369 nm)	0.47
$S_0 \rightarrow S_{10}$	H-1→L+1 (10%) H→L+2 (80%)	3.4 eV (362 nm)	0.52
$S_0 \rightarrow S_{11}$	H-6→L (55%) H→L+3 (30%)	3.5 eV (359 nm)	0.15
$S_0 \rightarrow S_{12}$	H-6→L (35%) H→L+3 (46%)	3.5 eV (356 nm)	0.20
$S_0 \rightarrow S_{23}$	H-11→L (41%) H-1→L+4 (33%) H→L+5 (10%)	4.0 eV (309 nm)	0.14

Table S10. Electronic transitions obtained by TD-DFT B3LYP/6-31G** level of theory for **NIP-ext** Compound.

Electronic transitions	**Description**	**E_{max} (λ_{max})**	**f**
$S_0 \rightarrow S_1$	H→L (99%)	1.8 eV (698 nm)	0.12
$S_0 \rightarrow S_3$	H→L+1 (92%)	2.4 eV (507 nm)	0.12
$S_0 \rightarrow S_9$	H-1→L+1 (88%)	3.3 eV (371 nm)	0.53
$S_0 \rightarrow S_{10}$	H-5→L (92%)	3.3 eV (369 nm)	0.50
$S_0 \rightarrow S_{11}$	H-2→L+1 (23%) H→L+2 (75%)	3.4 eV (361 nm)	0.55
$S_0 \rightarrow S_{12}$	H-2→L+1 (75%) H→L+2 (22%)	3.5 eV (352 nm)	0.35

$S_0 \rightarrow S_{16}$	**H-1→L+2 (13%)** **H→L+3 (77%)**	**3.8 eV (330 nm)**	**0.14**
$S_0 \rightarrow S_{21}$	**H-8→L (10%)** **H-4→L+1 (70%)**	**4.0 eV (314 nm)**	**0.25**
$S_0 \rightarrow S_{27}$	**H-1→L+3 (87%)**	**4.3 eV (286 nm)**	**0.20**

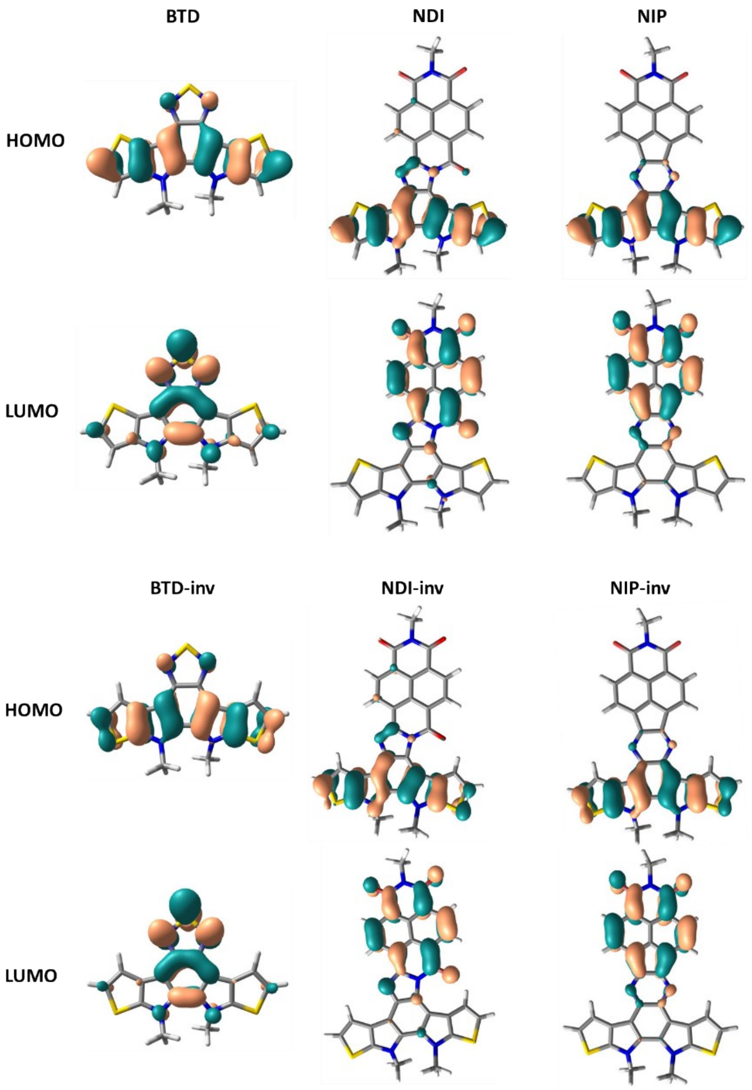

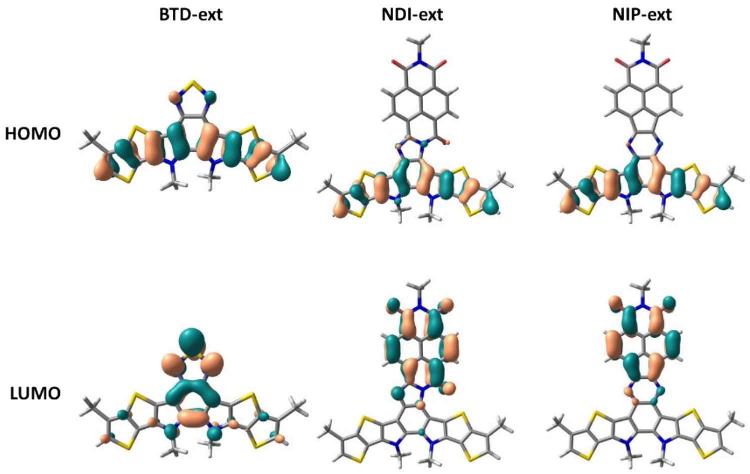

Figure S38. DFT/B3LYP/6-31G** molecular orbital topologies of all compounds under study. Isovalue=0.035.

4. UV-Vis and Electrochemical data

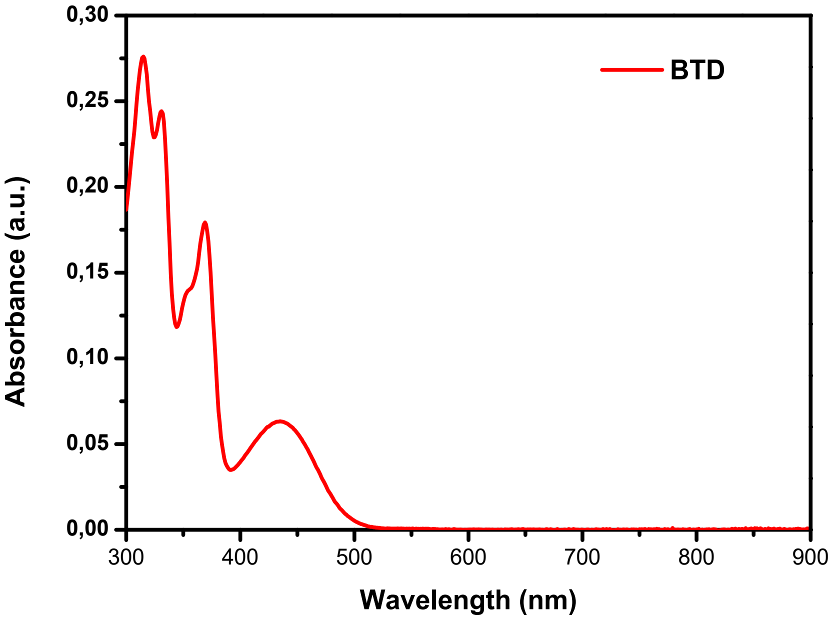

Figure S39. UV-Vis spectra of 5·10^{-6} M solution in chloroform of **BTD**.

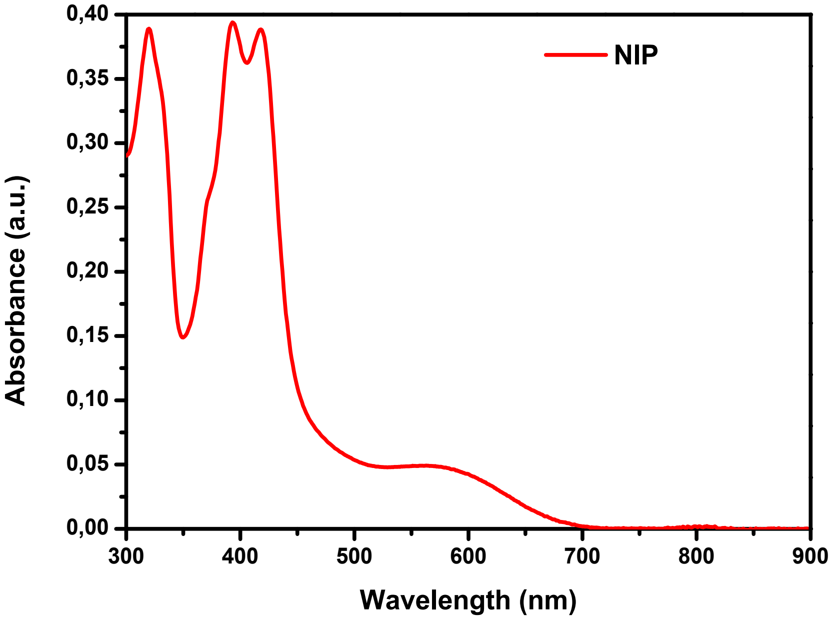

Figure S40. UV-Vis spectra of $5 \cdot 10^{-6}$ M solution in chloroform of **NIP**.

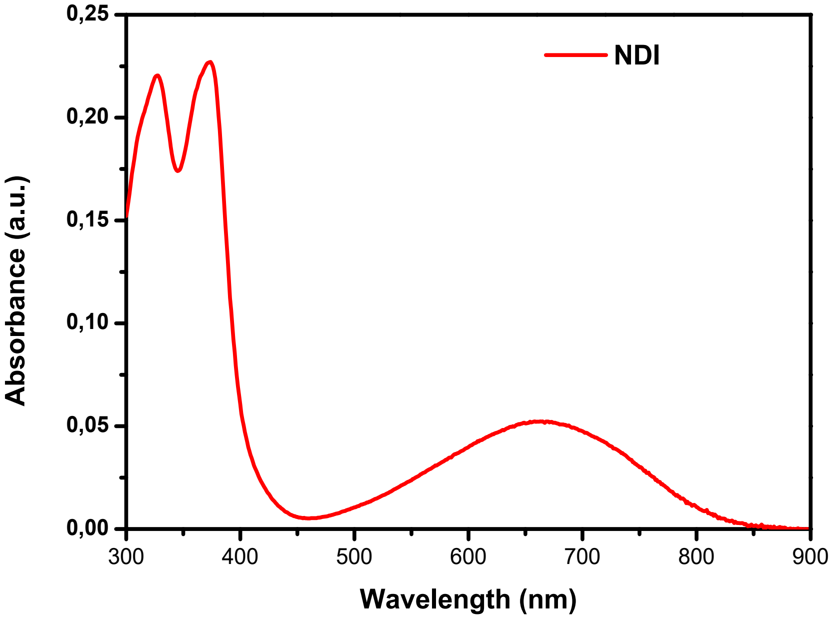

Figure S41. UV-Vis spectra of $5 \cdot 10^{-6}$ M solution in chloroform of **NDI**.

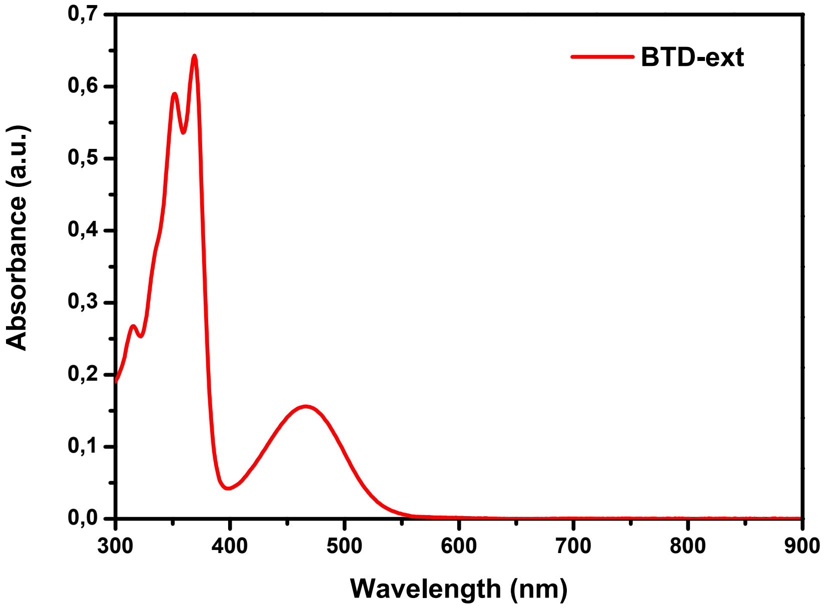

Figure S42. UV-Vis spectra of 5·10^{-6} M solution in chloroform of **BTD-ext.**

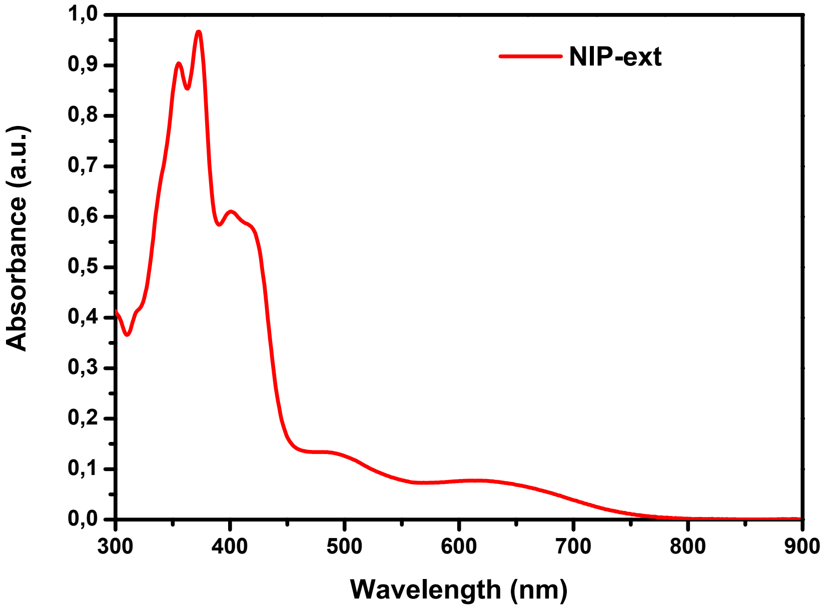

Figure S43. UV-Vis spectra of 5·10^{-6} M solution in chloroform of **NIP-ext.**

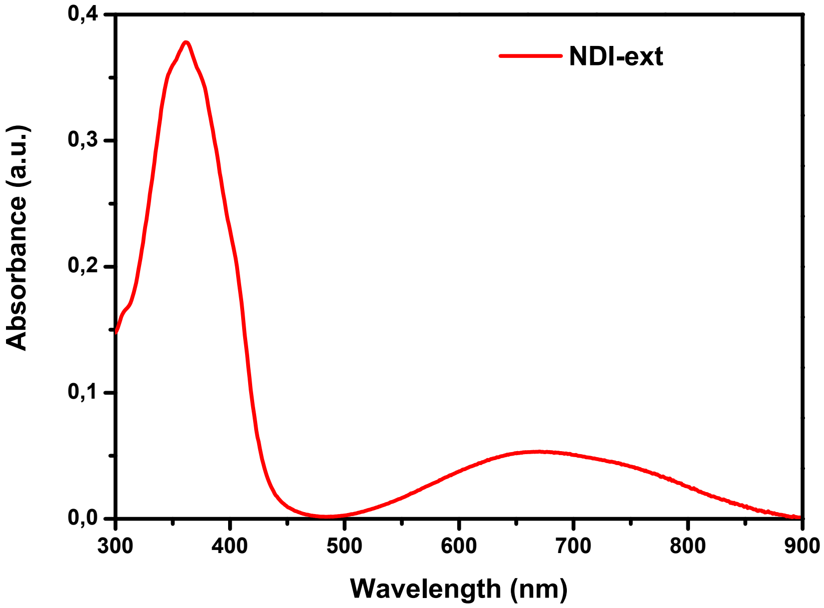

Figure S44. UV-Vis spectra of 5·10^{-6} M solution in chloroform of **NDI-ext.**

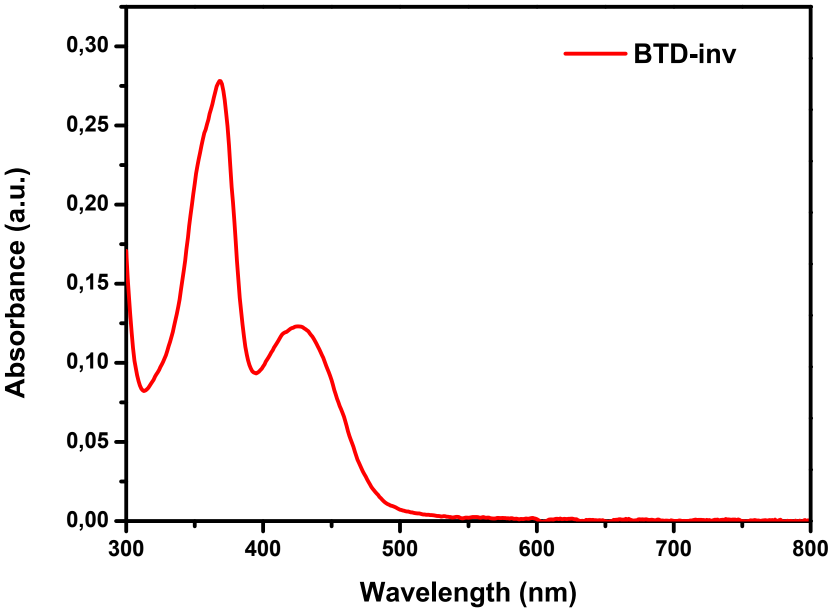

Figure S45. UV-Vis spectra of 5·10^{-6} M solution in chloroform of **BTD-inv.**

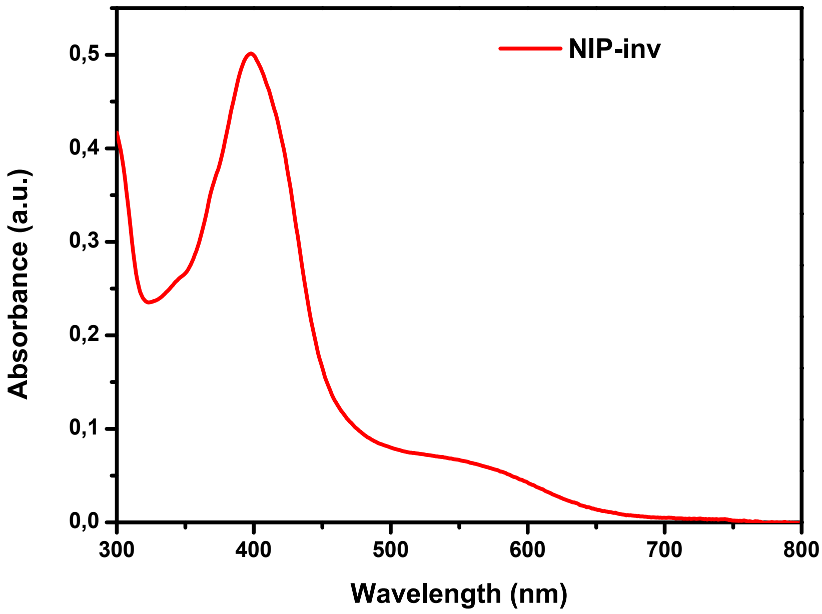

Figure S46. UV-Vis spectra of 5·10^{-6} M solution in chloroform of **NIP-inv.**

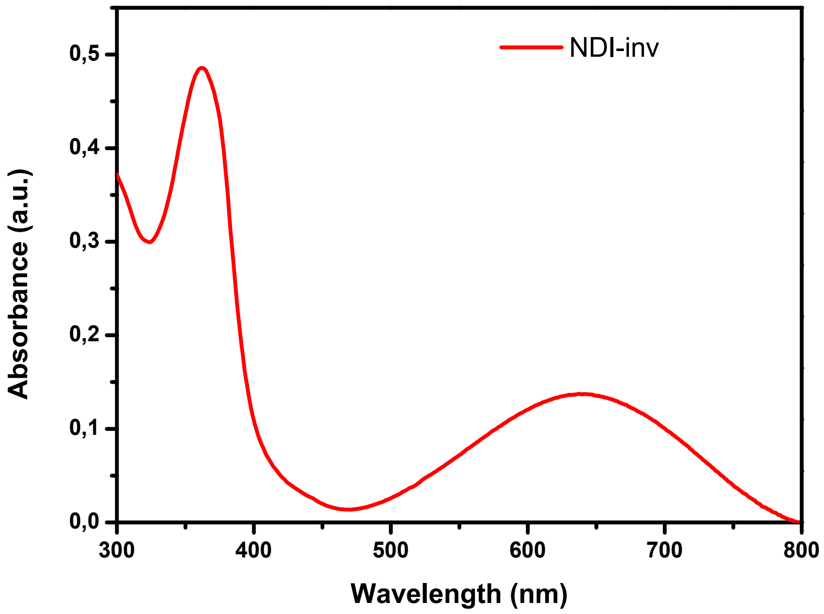

Figure S47. UV-Vis spectra of 5·10^{-6} M solution in chloroform of **NDI-inv.**

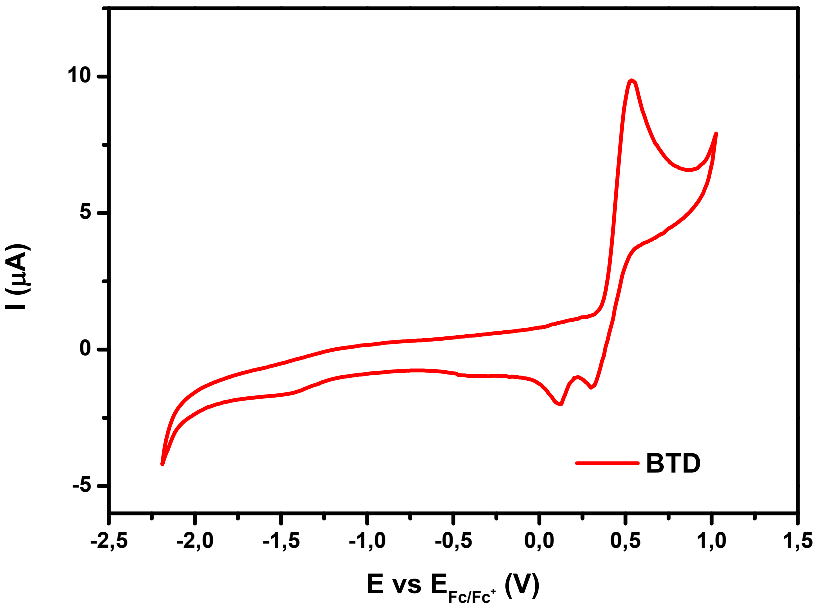

Figure S48. Cyclic voltammetry of **BTD** and 0.1 TBAPF$_6$ in dichloromethane solution.

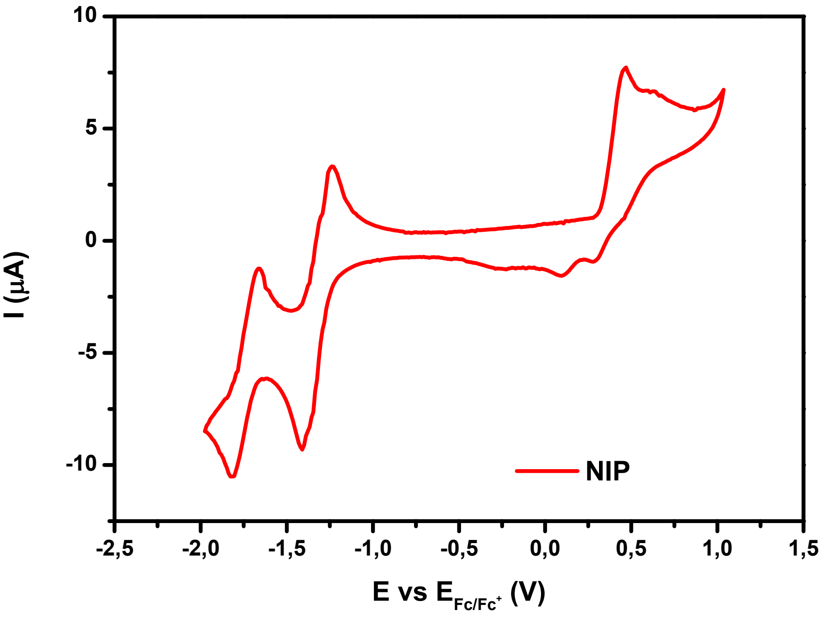

Figure S49. Cyclic voltammetry of **NIP** and 0.1 TBAPF$_6$ in dichloromethane solution.

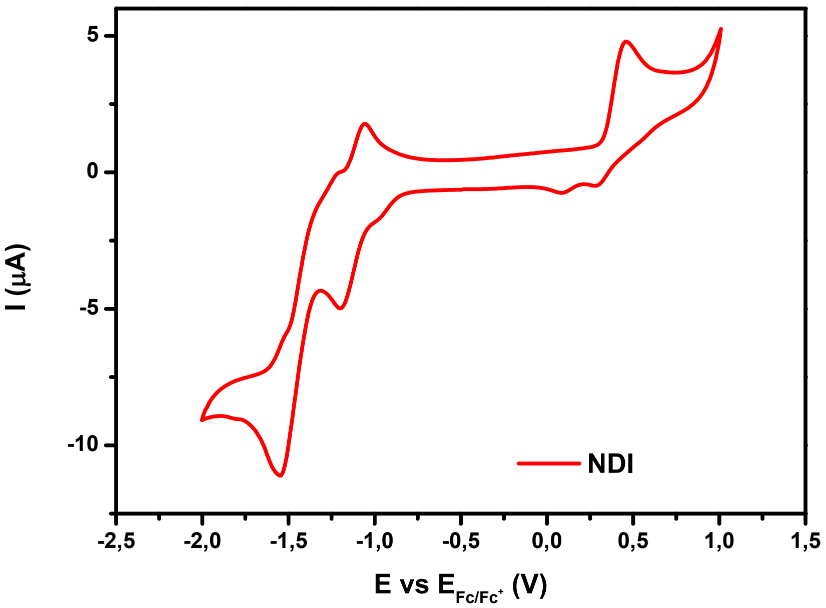

Figure S50. Cyclic voltammetry of **NDI** and 0.1 TBAPF$_6$ in dichloromethane solution.

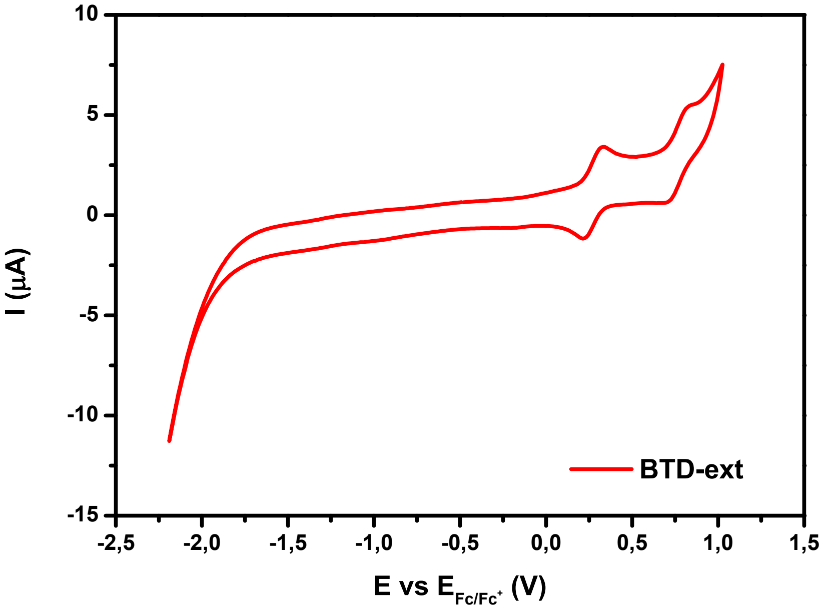

Figure S51. Cyclic voltammetry of **BTD-ext** and 0.1 TBAPF$_6$ in dichloromethane solution.

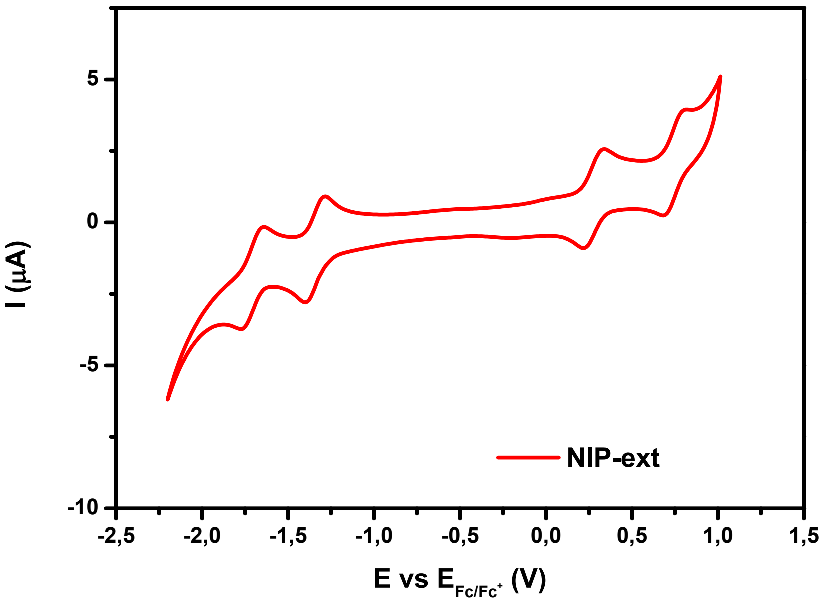

Figure S52. Cyclic voltammetry of **NIP-ext** and 0.1 TBAPF$_6$ in dichloromethane solution.

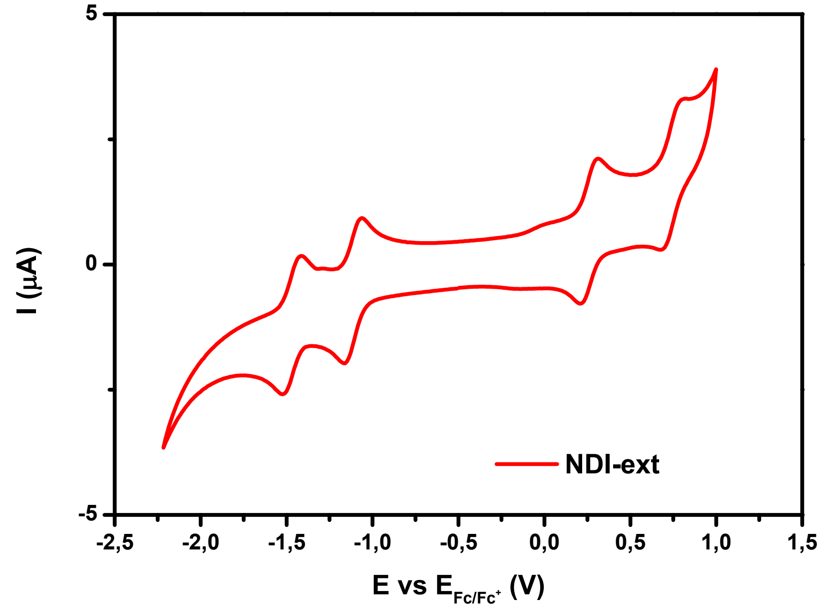

Figure S53. Cyclic voltammetry of **NDI-ext.** and 0.1 TBAPF$_6$ in dichloromethane solution.

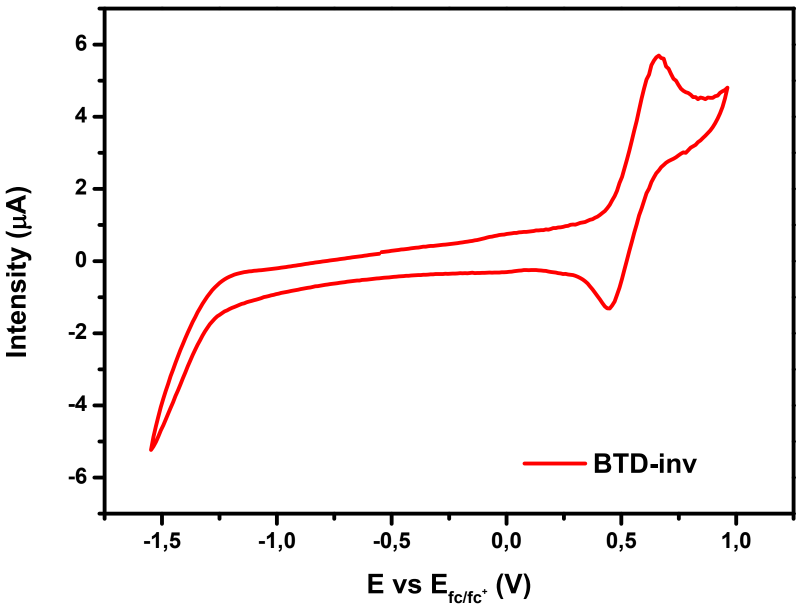

Figure S54. Cyclic voltammetry of **BTD-inv** and 0.1 TBAPF$_6$ in dichloromethane solution.

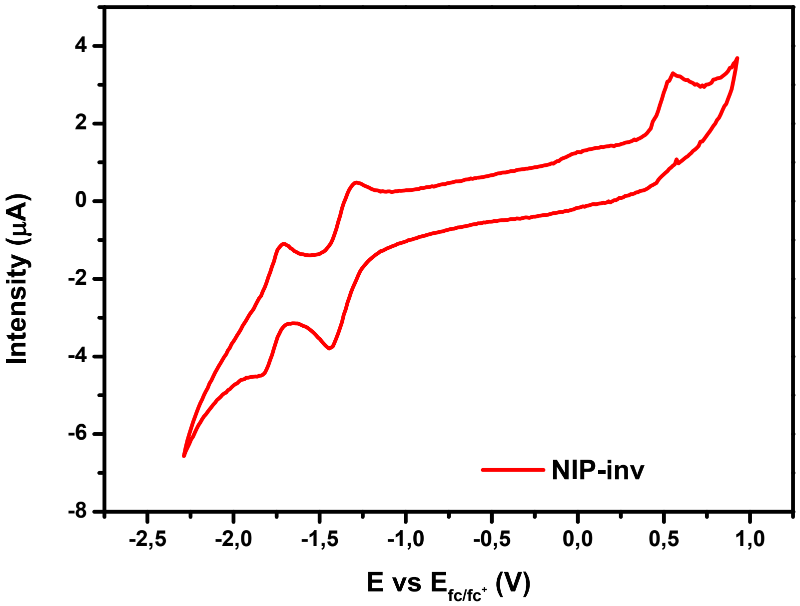

Figure S55. Cyclic voltammetry of **NIP-inv** and 0.1 TBAPF$_6$ in dichloromethane solution.

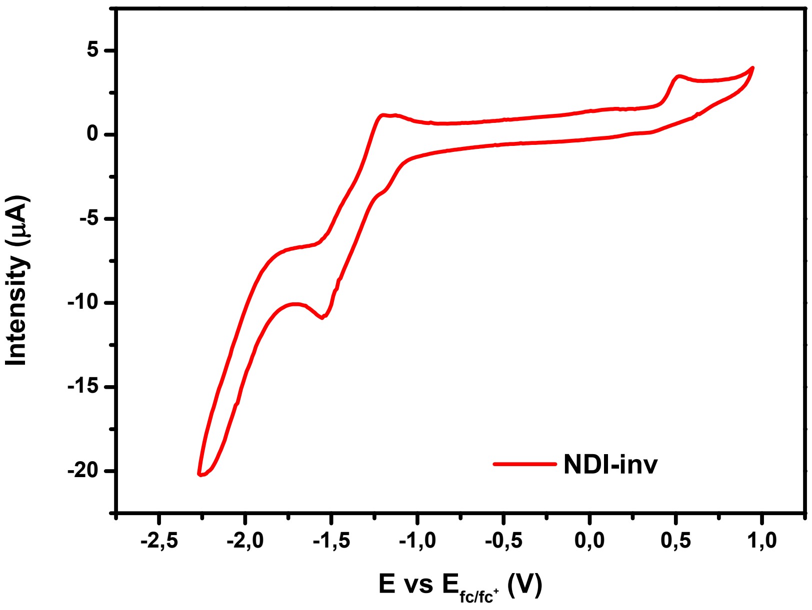

Figure S56. Cyclic voltammetry of **NDI-inv** and 0.1 TBAPF$_6$ in dichloromethane solution.

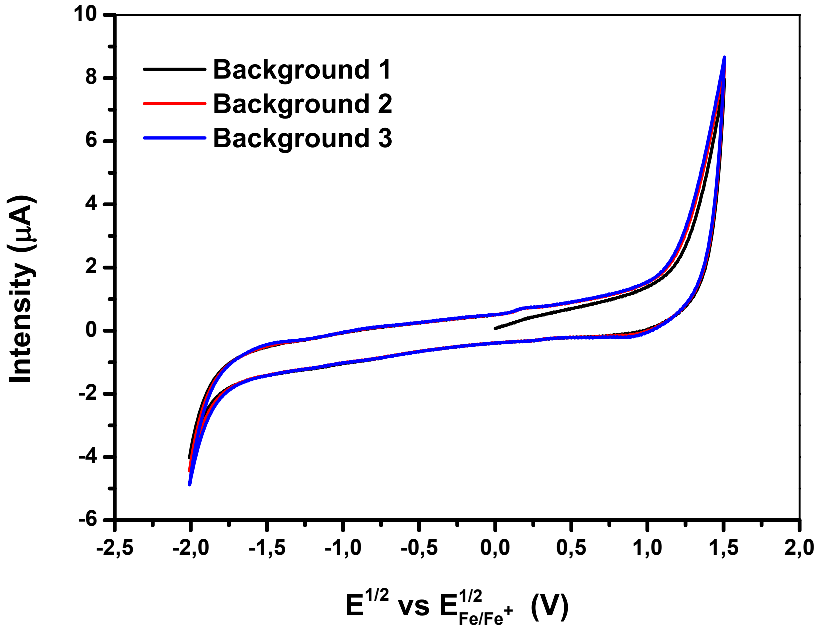

Figure S57. Cyclic voltammetry of Pt working electrode (background) and 0.1 TBAPF$_6$ in dichloromethane solution.

5. Experimental and theoretically spectroelectrochemical measurements

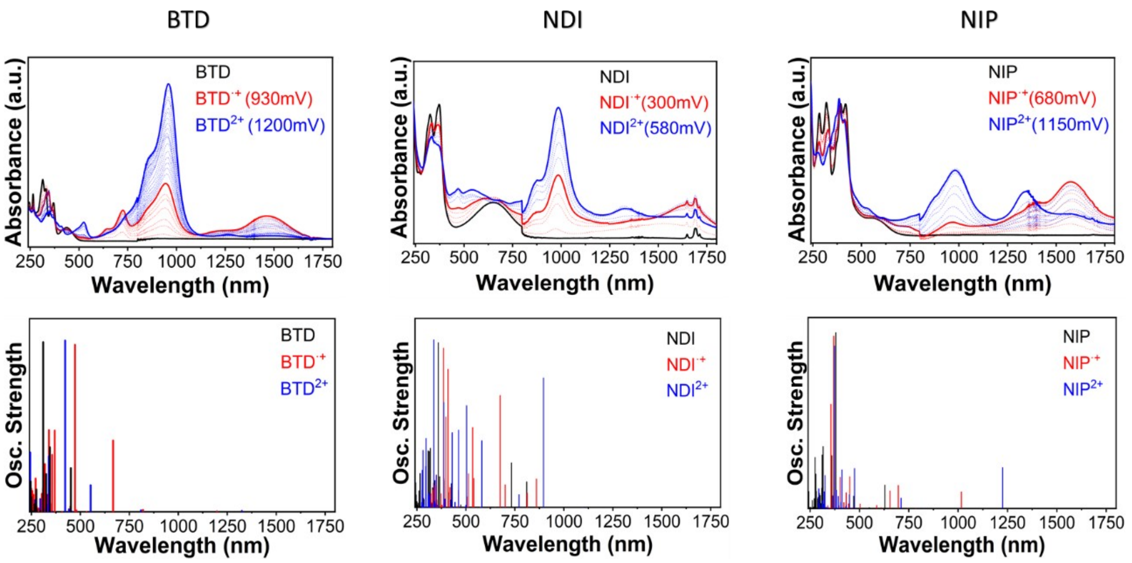

Figure S58. Top, UV/Vis/NIR spectra changes at room temperature upon oxidation of **BTD**, **NDI** and **NIP** within an OTTLE cell in dichloromethane in presence of 0.1M (n-Bu)4NPF6 as the supporting electrolyte. Bottom, TD-DFT/B3LYP calculated vertical transitions energies.

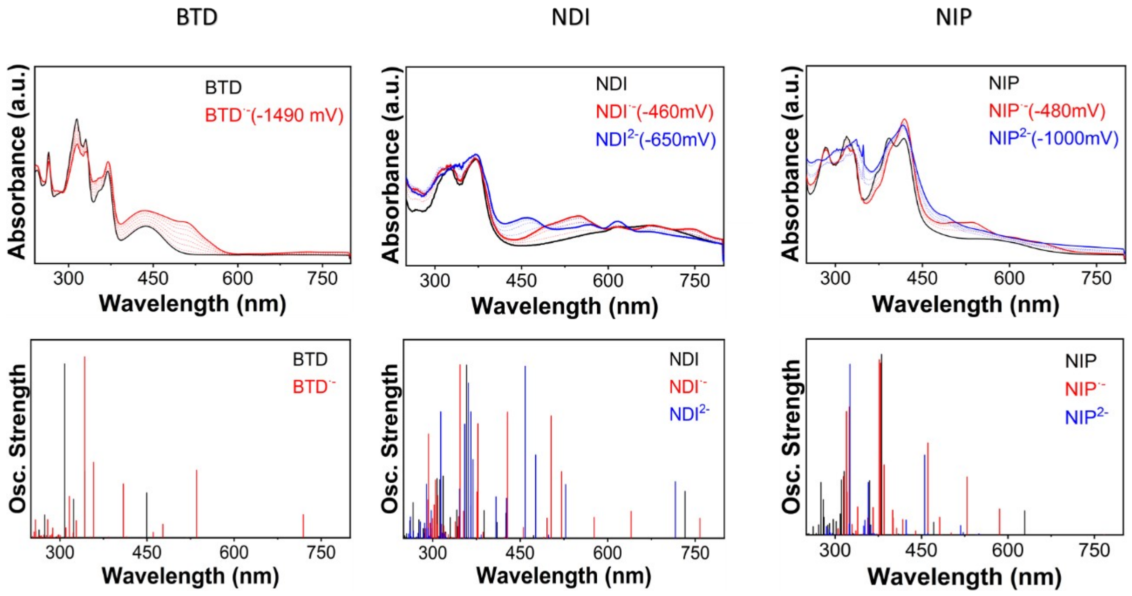

Figure S59. Top, UV/Vis/NIR spectra changes at room temperature upon reduction of **BTD**, **NDI** and **NIP** within an OTTLE cell in dichloromethane in presence of 0.1M (n-Bu)4NPF6 as the supporting electrolyte. Bottom, TD-DFT/B3LYP calculated vertical transitions energies.

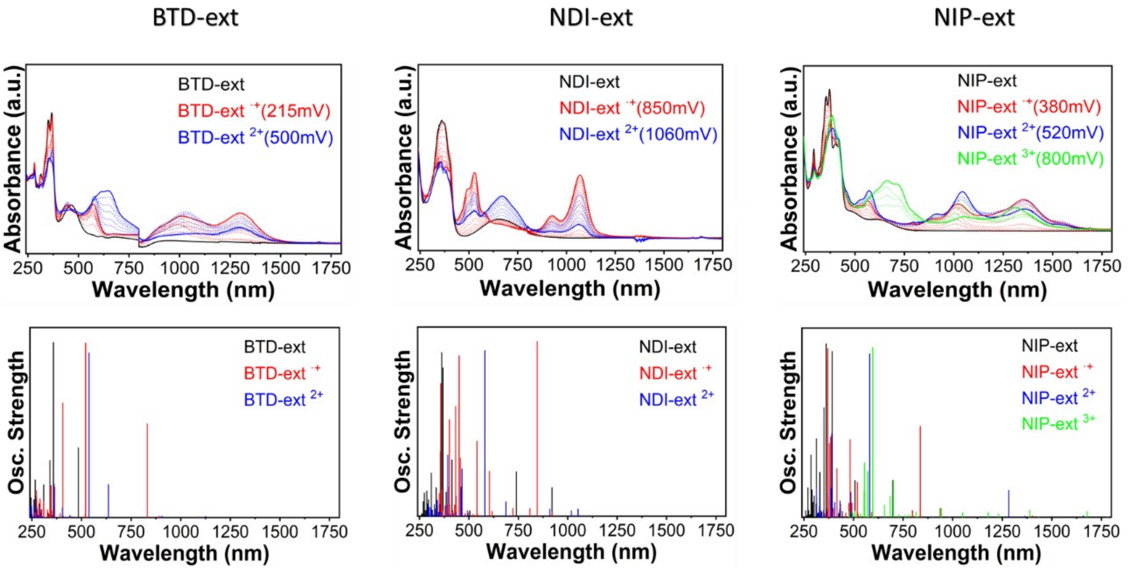

Figure S60. Top, UV/Vis/NIR spectra changes at room temperature upon oxidation of **BTD-ext.**, **NDI-ext.** and **NIP-ext.** within an OTTLE cell in dichloromethane in presence of 0.1M (n-Bu)4NPF6 as the supporting electrolyte. Bottom, TD-DFT/B3LYP calculated vertical transitions energies.

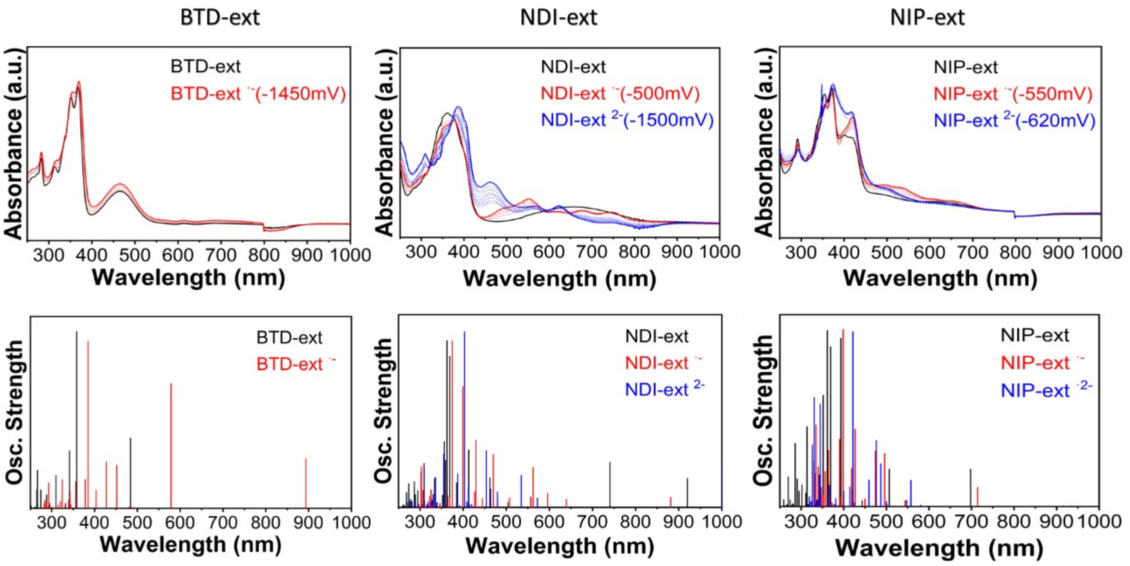

Figure S61. Top, UV/Vis/NIR spectra changes at room temperature upon reduction of **BTD-ext.**, **NDI-ext.** and **NIP-ext.** within an OTTLE cell in dichloromethane in presence of 0.1M (n-Bu)4NPF6 as the supporting electrolyte. Bottom, TD-DFT/B3LYP calculated vertical transitions energies.

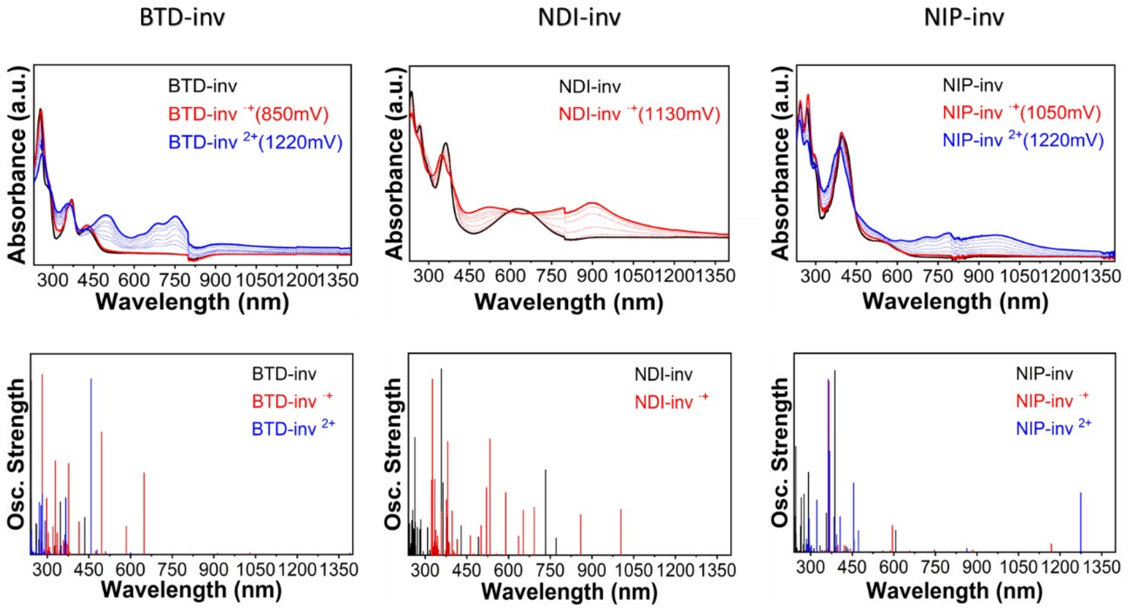

Figure S62. Top, UV/Vis/NIR spectra changes at room temperature upon oxidation of **BTD-inv**, **NDI-inv** and **NIP-inv** within an OTTLE cell in dichloromethane in presence of 0.1M (n-Bu)4NPF6 as the supporting electrolyte. Bottom, TD-DFT/B3LYP calculated vertical transitions energies.

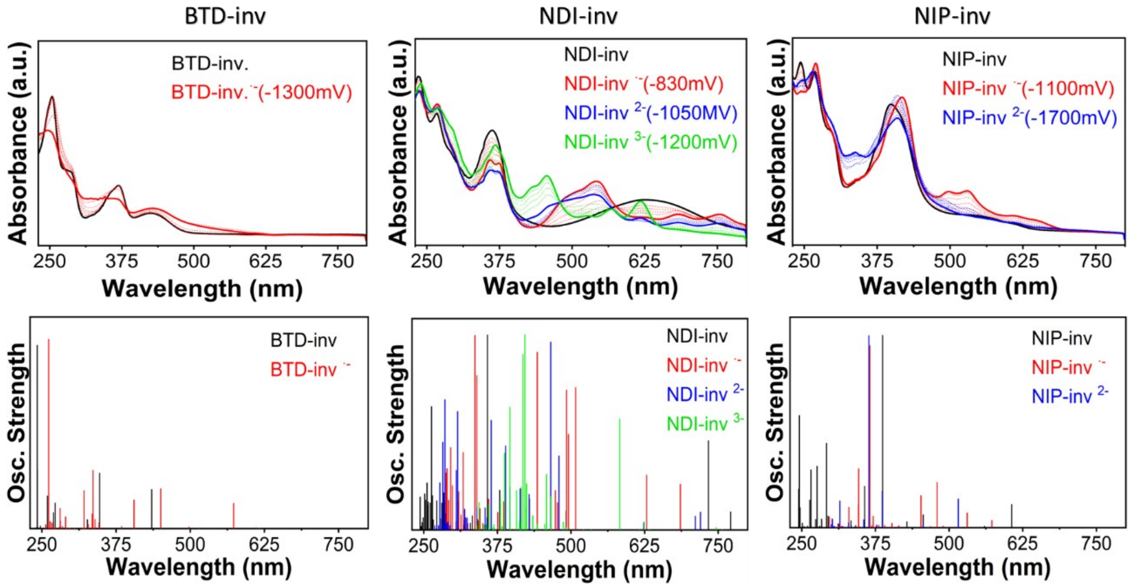

Figure S63. Top, UV/Vis/NIR spectra changes at room temperature upon reduction of **BTD-inv**, **NDI-inv** and **NIP-inv** within an OTTLE cell in dichloromethane in presence of 0.1M (n-Bu)4NPF6 as the supporting electrolyte. Bottom, TD-DFT/B3LYP calculated vertical transitions energies.

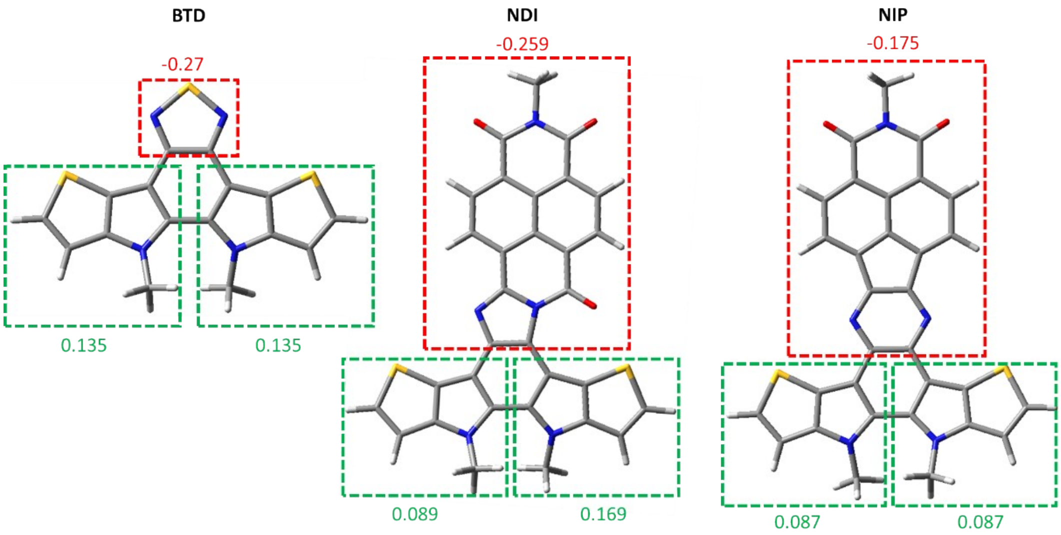

Figure S64. B3LYP/6-31G** charge distributions for **BTD**, **NDI** and **NIP** as neutral species.

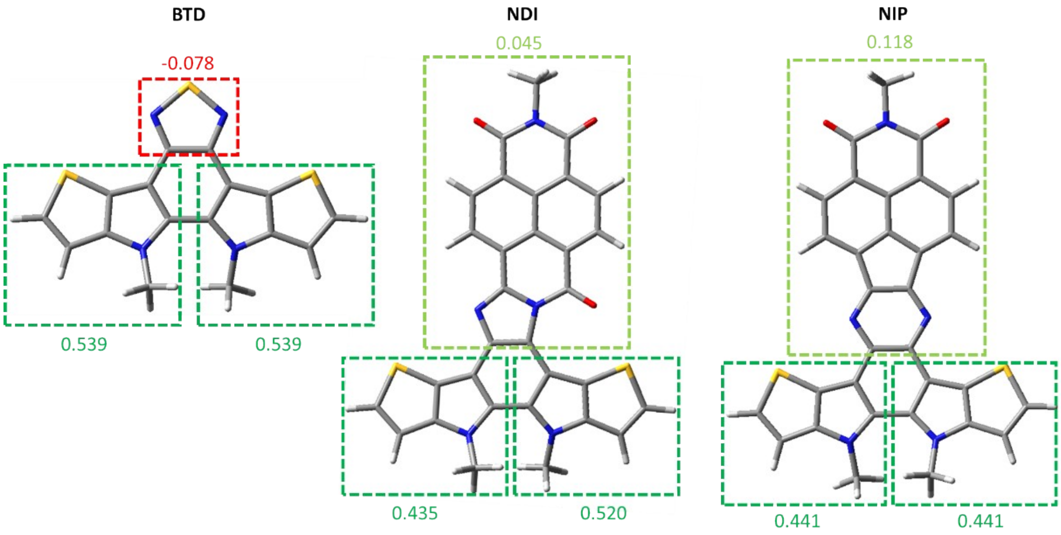

Figure S65. B3LYP/6-31G** charge distributions for **BTD**, **NDI** and **NIP** as cation species.

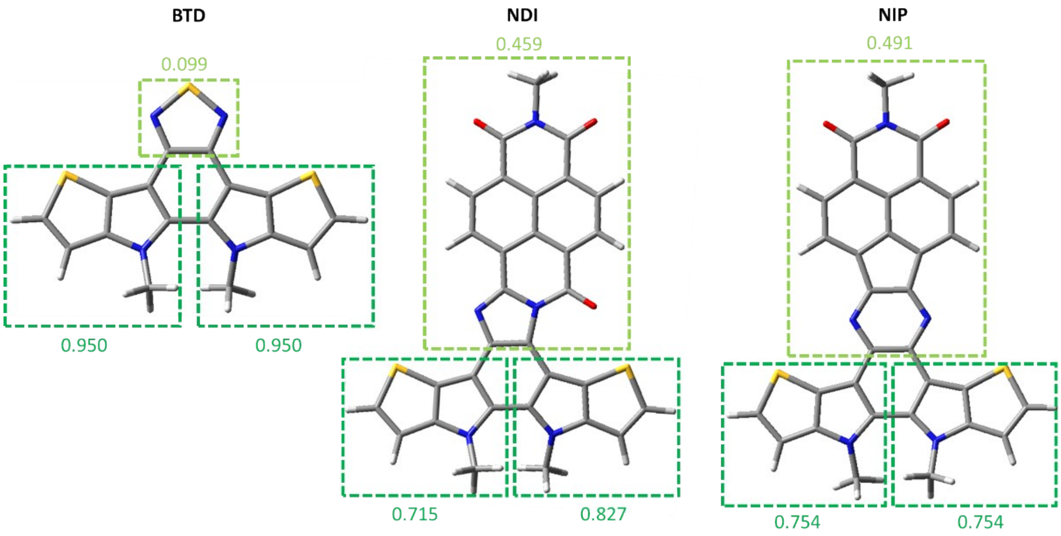

Figure S66. B3LYP/6-31G** charge distributions for **BTD**, **NDI** and **NIP** as dication species.

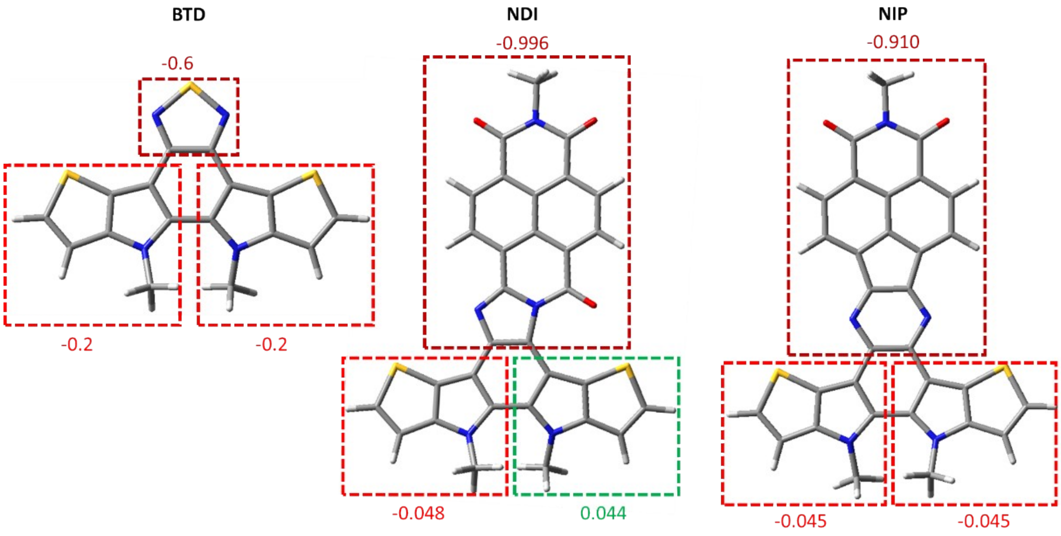

Figure S67. B3LYP/6-31G** charge distributions for **BTD**, **NDI** and **NIP** as anion species.

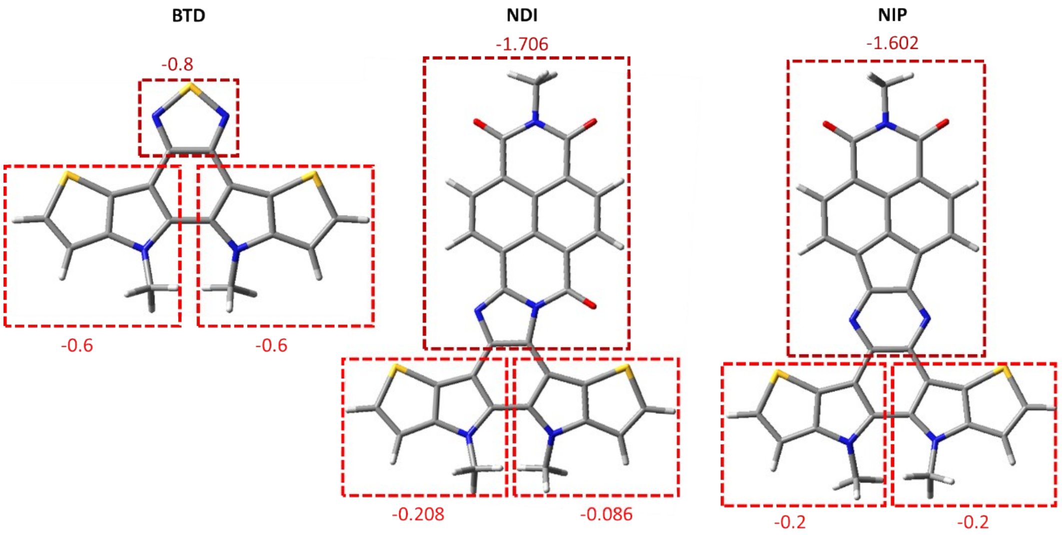

Figure S68. B3LYP/6-31G** charge distributions for **BTD**, **NDI** and **NIP** as dianion species.

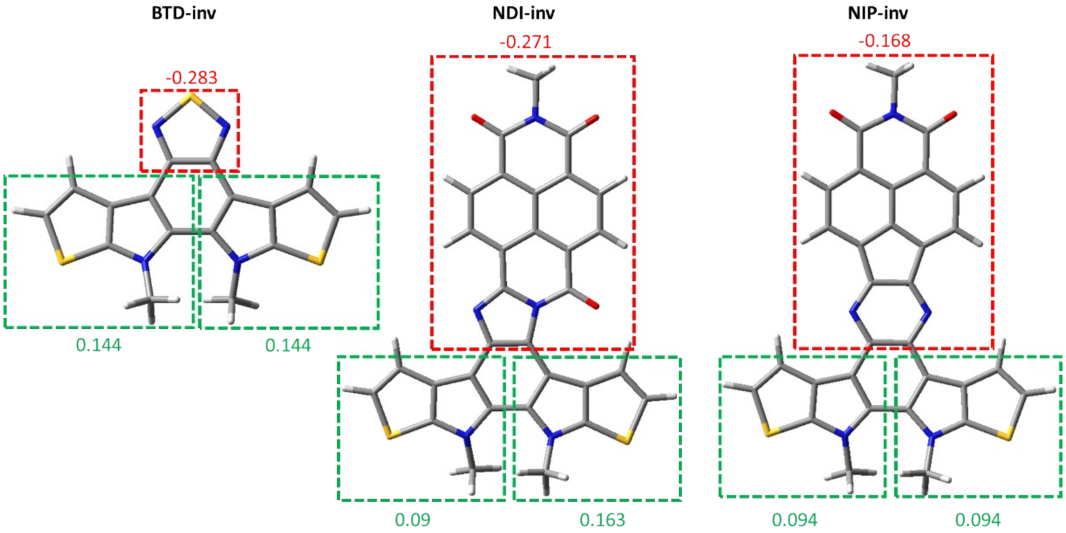

Figure S69. B3LYP/6-31G** charge distributions for **BTD-inv**, **NDI-inv** and **NIP-inv** as neutral species.

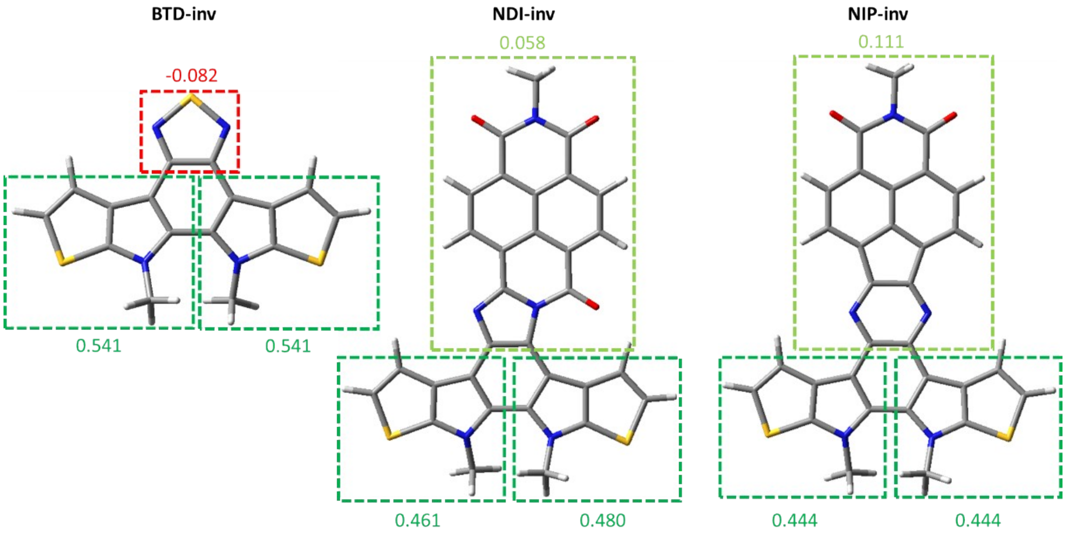

Figure S70. B3LYP/6-31G** charge distributions for **BTD-inv**, **NDI-inv** and **NIP-inv** as cation species.

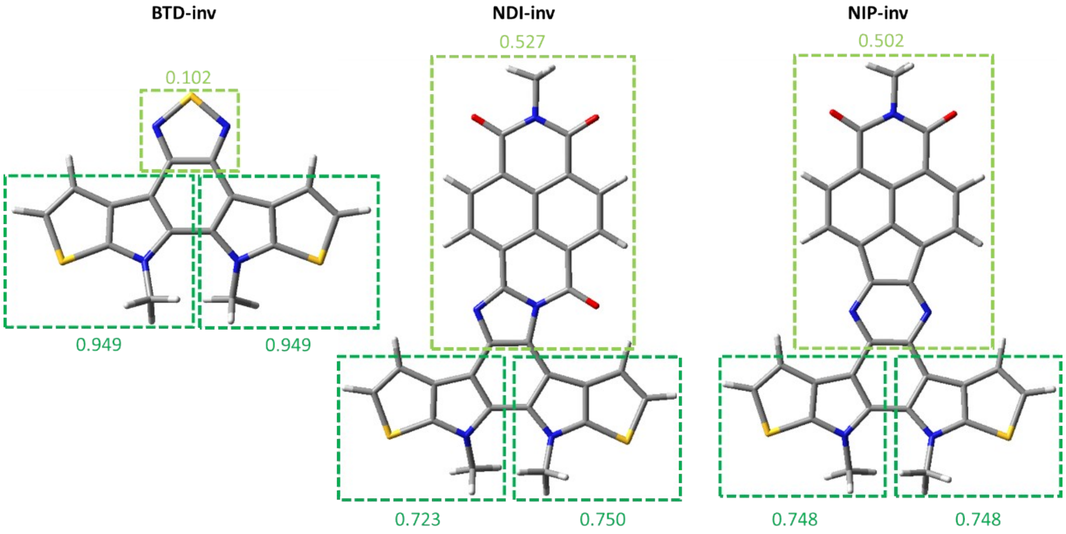

Figure S71. B3LYP/6-31G** charge distributions for **BTD-inv**, **NDI-inv** and **NIP-inv** as dication species.

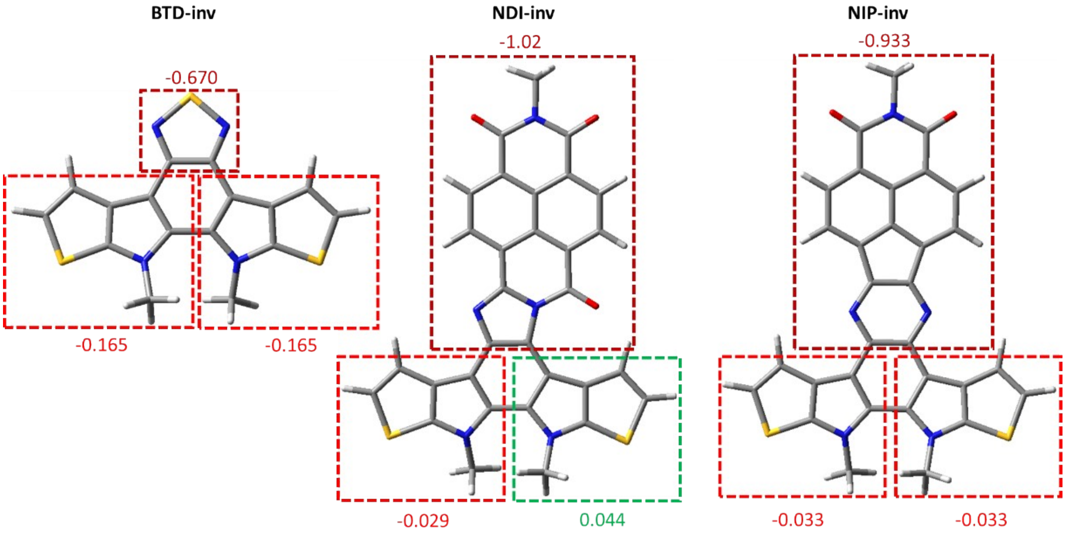

Figure S72. B3LYP/6-31G** charge distributions for **BTD-inv**, **NDI-inv** and **NIP-inv** as anion species.

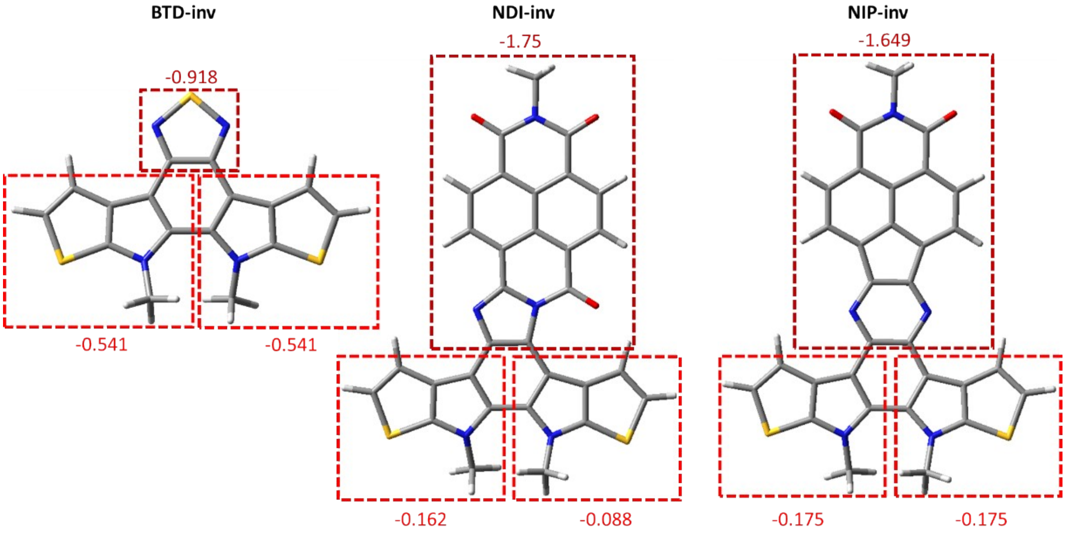

Figure S73. B3LYP/6-31G** charge distributions for **BTD-inv**, **NDI-inv** and **NIP-inv** as dianion species.

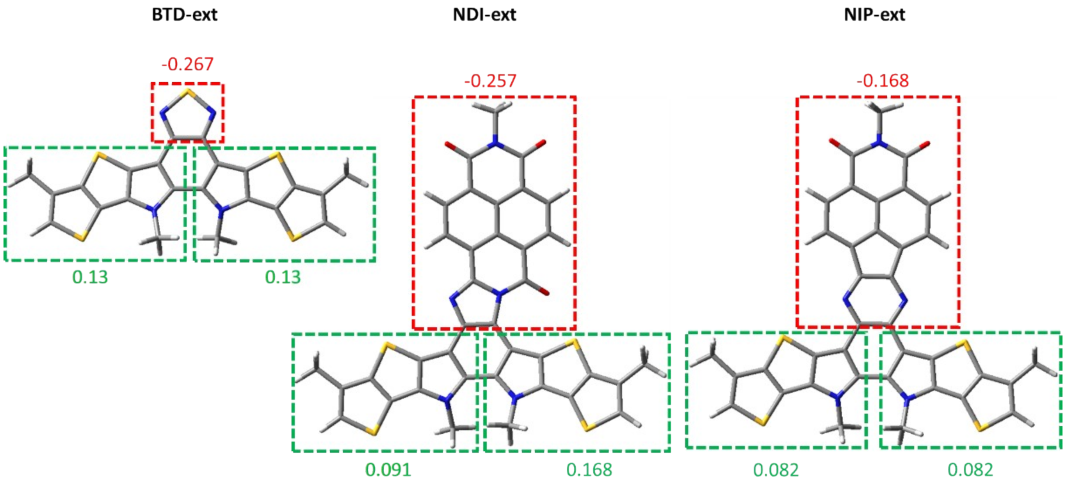

Figure S74. B3LYP/6-31G** charge distributions for **BTD-ext, NDI-ext** and **NIP-ext** as neutral species.

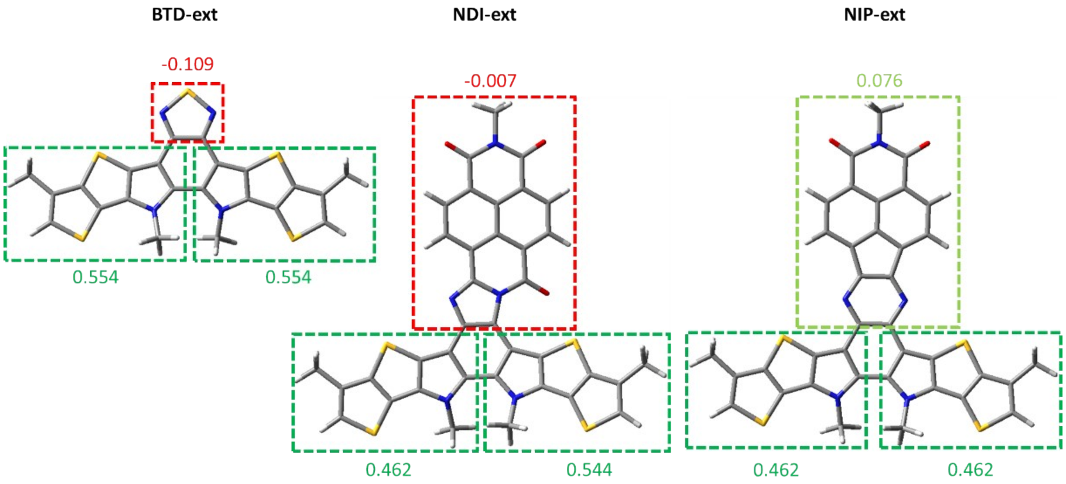

Figure S75. B3LYP/6-31G** charge distributions for **BTD-ext, NDI-ext** and **NIP-ext** as cation species.

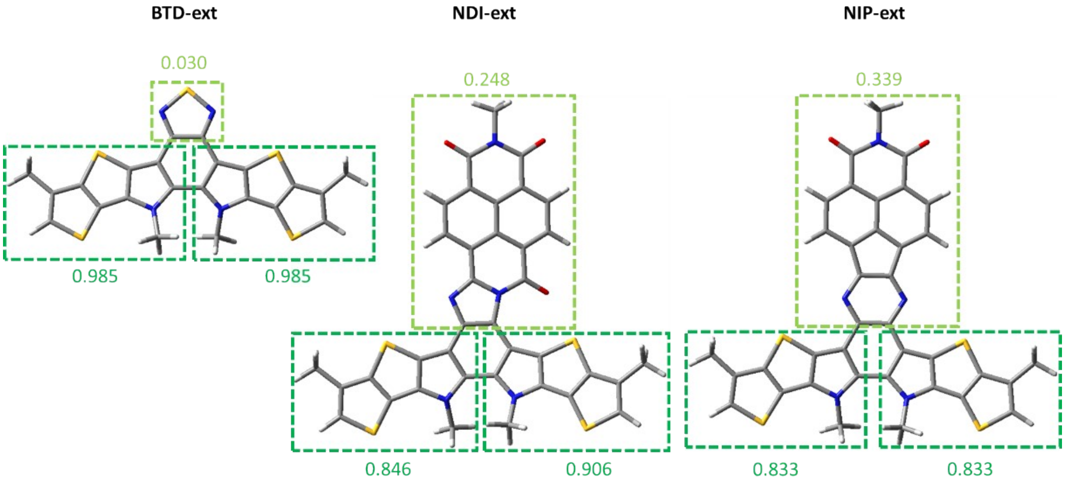

Figure S76. B3LYP/6-31G** charge distributions for **BTD-ext, NDI-ext** and **NIP-ext** as dication species.

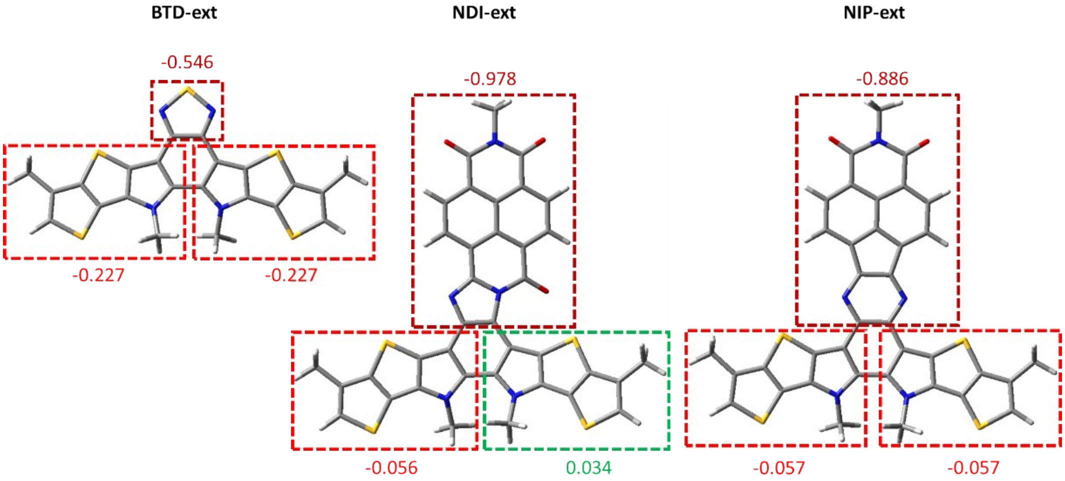

Figure S77. B3LYP/6-31G** charge distributions for **BTD-ext, NDI-ext** and **NIP-ext** as anion species.

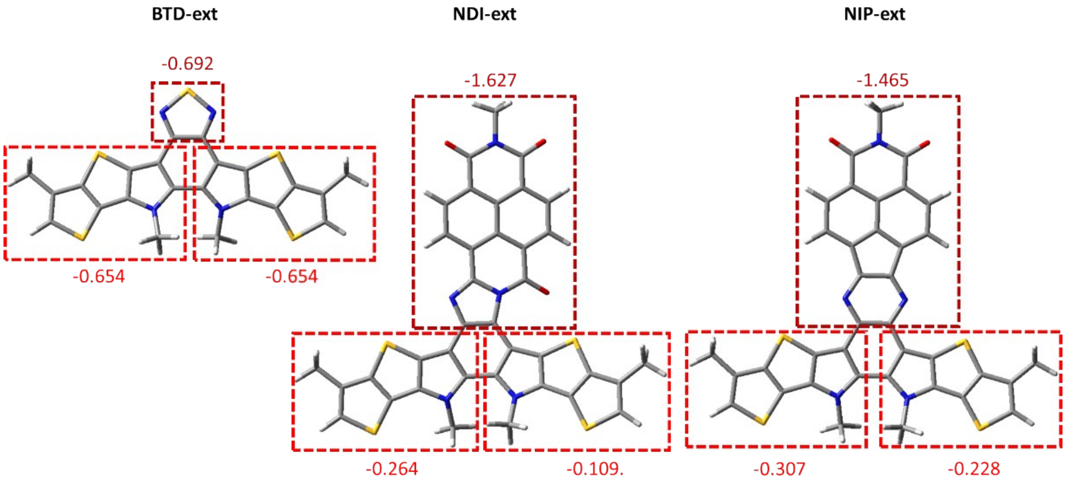

Figure S78. B3LYP/6-31G** charge distributions for **BTD-ext, NDI-ext** and **NIP-ext** as dianion species.

6. FIELD-EFFECT TRANSISTORS CHARACTERIZATION

Table S11. OFET electrical data for deposited films of **NDI**

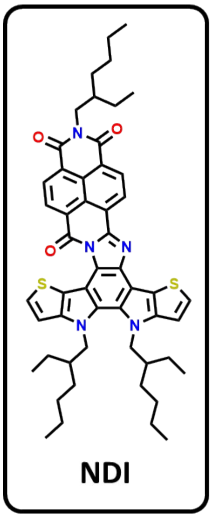

Subst. treatment	temp. (ºC)		μ_h (cm^2 V^{-1} s^{-1})	I_{ON}/I_{OFF}	V_T(V)
OTS	RT	Average	$2\cdot10^{-4}$	$1\cdot10^{+5}$	-41
		Best	$2\cdot10^{-4}$	$8\cdot10^{+4}$	-41
	Annealing 150 3 horas	Average	-	-	-
		Best	-	-	-
	Heater → 80	Average	$1\cdot10^{-4}$	$2\cdot10^{+2}$	-38
		Best	$2\cdot10^{-4}$	$2\cdot10^{+2}$	-40
	Annealing 150 3 horas	Average	$2\cdot10^{-4}$	$2\cdot10^{+4}$	-6
		Best	$\boxed{2\cdot10^{-4}}$	$4\cdot10^{+1}$	-3
HMDS	RT	Average	$9\cdot10^{-5}$	$2\cdot10^{+2}$	-43
		Best	$1\cdot10^{-4}$	$1\cdot10^{-2}$	-42
	Annealing 150 3 horas	Average	$1\cdot10^{-5}$	$6\cdot10^{+3}$	-29
		Best	$2\cdot10^{-5}$	$4\cdot10^{+3}$	-27
	Heater → 80	Average	$7\cdot10^{-5}$	$2\cdot10^{+2}$	-49
		Best	$8\cdot10^{-5}$	$2\cdot10^{+2}$	-48
	Annealing 150 3 horas	Average	$5\cdot10^{-5}$	$5\cdot10^{+4}$	-7
		Best	$8\cdot10^{-5}$	$2\cdot10^{+5}$	-10

Table S12. OFET electrical data for deposited films of **NIP**

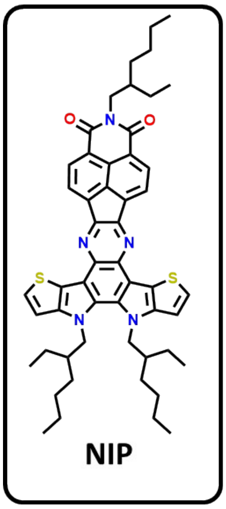

Subst. treatment	temp. (ºC)		μ_h (cm^2 V^{-1} s^{-1})	I_{ON}/I_{OFF}	V_T(V)
OTS	RT	Average	$1\cdot10^{-3}$	$3\cdot10^{+6}$	-29
		Best	$2\cdot10^{-3}$	$6\cdot10^{+5}$	-32
	Annealing 150 3 horas	Average	-	-	-
		Best	-	-	-
	Heater → 80	Average	-	-	-
		Best	-	-	-
	Annealing 150 3 horas	Average	$1\cdot10^{-2}$	$2\cdot10^{+4}$	-20
		Best	$\boxed{1\cdot10^{-2}}$	$3\cdot10^{+4}$	-19
HMDS	RT	Average	-	-	-
		Best	-	-	-
	Annealing 150 3 horas	Average	$9\cdot10^{-4}$	$1\cdot10^{+5}$	-15
		Best	$9\cdot10^{-4}$	$4\cdot10^{+5}$	-21
	Heater → 80	Average	$1\cdot10^{-4}$	$2\cdot10^{+2}$	-50
		Best	$1\cdot10^{-4}$	$2\cdot10^{+2}$	-49
	Annealing 150 3 horas	Average	$2\cdot10^{-3}$	$2\cdot10^{+5}$	-27
		Best	$2\cdot10^{-3}$	$4\cdot10^{+4}$	-24

Table S13. OFET electrical data for deposited films of **NDI-ext.**

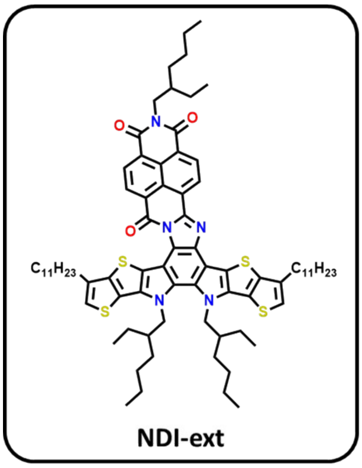

NDI-ext

Subst. treatment	temp. (ºC)		μ_h (cm^2 V^{-1} s^{-1})	I_{ON}/I_{OFF}	V_T(V)
HMDS	RT	Average	$2{\cdot}10^{-6}$	4	10
		Best	$3{\cdot}10^{-6}$	4	2
	Annealing 150 3 horas	Average	-	-	-
		Best	-	-	-
	Heater → 80	Average	$1{\cdot}10^{-6}$	2	52
		Best	$2{\cdot}10^{-6}$	2	35
	Annealing 150 3 horas	Average	-	-	-
		Best	-	-	-

Table S14. OFET electrical data for deposited films of **NIP-ext.**

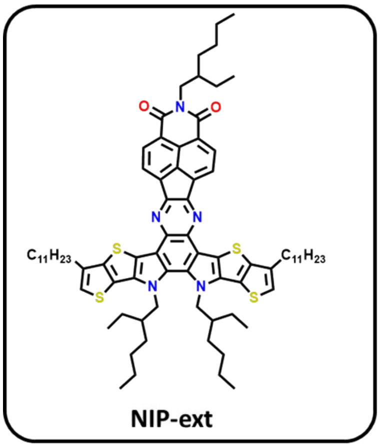

NIP-ext

Subst. treatment	temp. (ºC)		μ_h (cm^2 V^{-1} s^{-1})	I_{ON}/I_{OFF}	V_T(V)
HMDS	RT	Average	$4{\cdot}10^{-6}$	4	2
		Best	$4{\cdot}10^{-6}$	4	12
	Annealing 150 3 horas	Average	-	-	-
		Best	-	-	-
	Heater → 80	Average	$2{\cdot}10^{-6}$	2	7
		Best	$3{\cdot}10^{-6}$	3	43
	Annealing 150 3 horas	Average	-	-	-
		Best	-	-	-

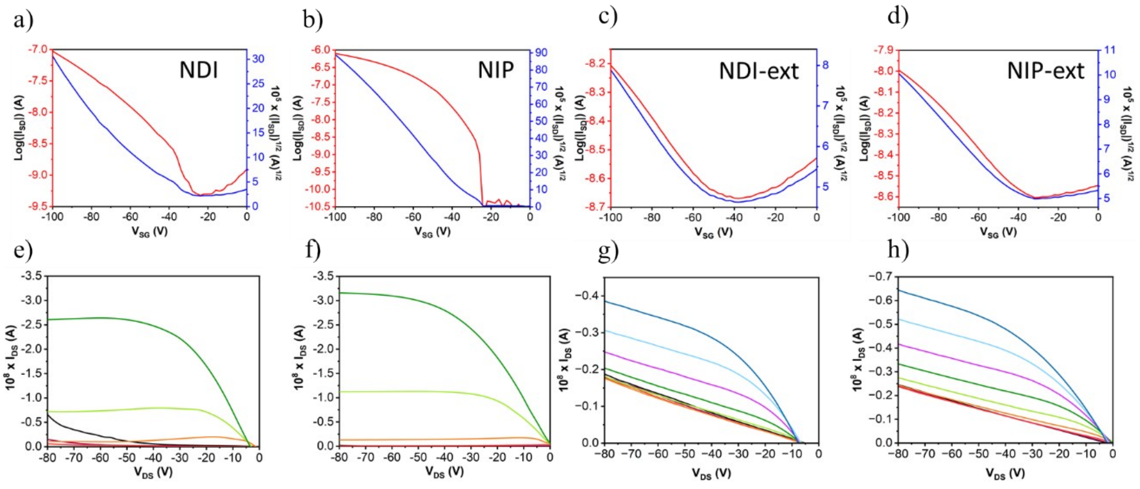

Figure S79. OFET transfer and output characteristic of a), e) for **NDI**, b), f) for **NIP**, c), g) for **NDI-ext** and d), h) for **NIP-ext.**

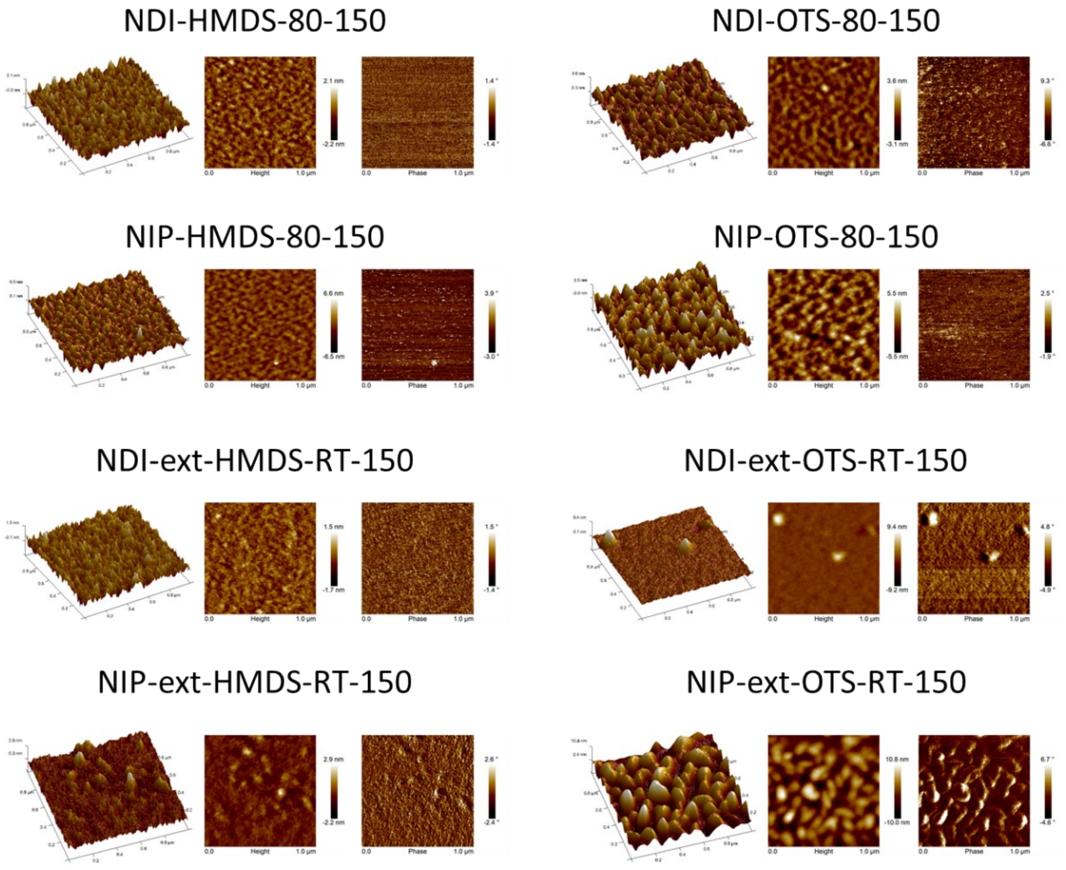

Figure S80. AFM images of thin films of the indicated semiconductors deposited onto OTS-modified substrates and HMDS-modified substrates.

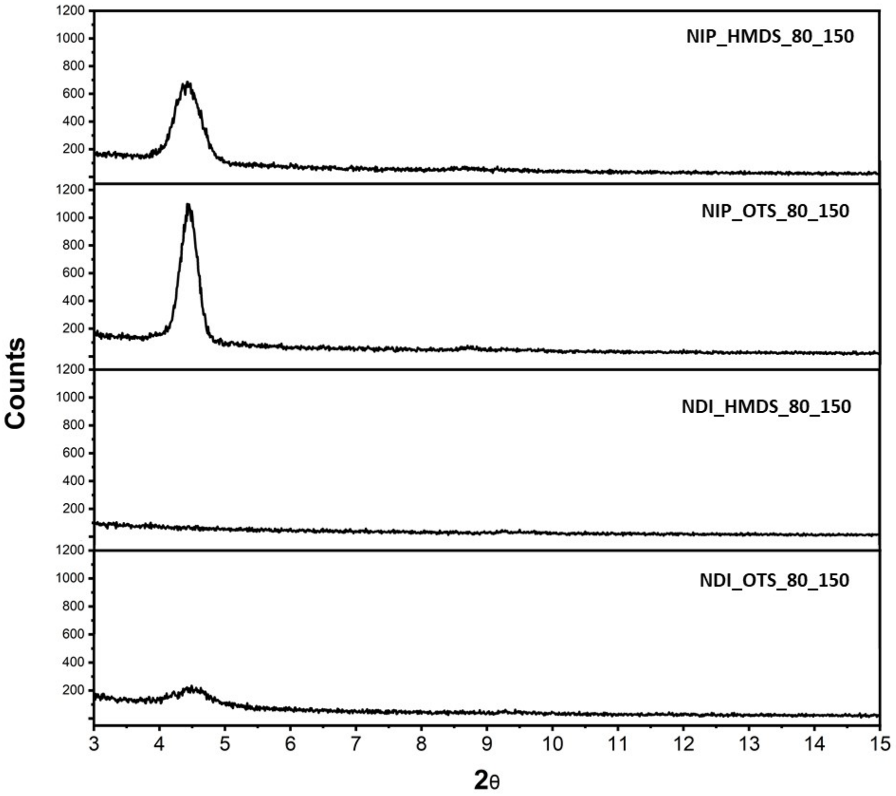

Figure S81. XRD plots for indicated semiconductors onto OTS-modified substrates and HMDS-modified substrates.

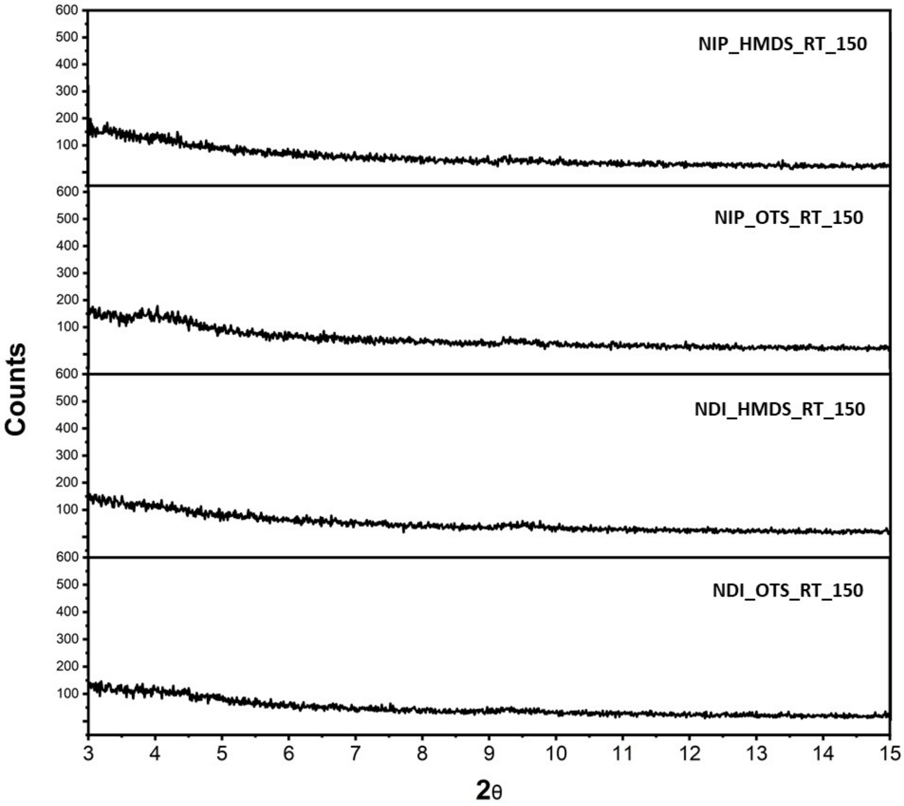

Figure S82. XRD plots for indicated semiconductors onto OTS-modified substrates and HMDS-modified substrate.

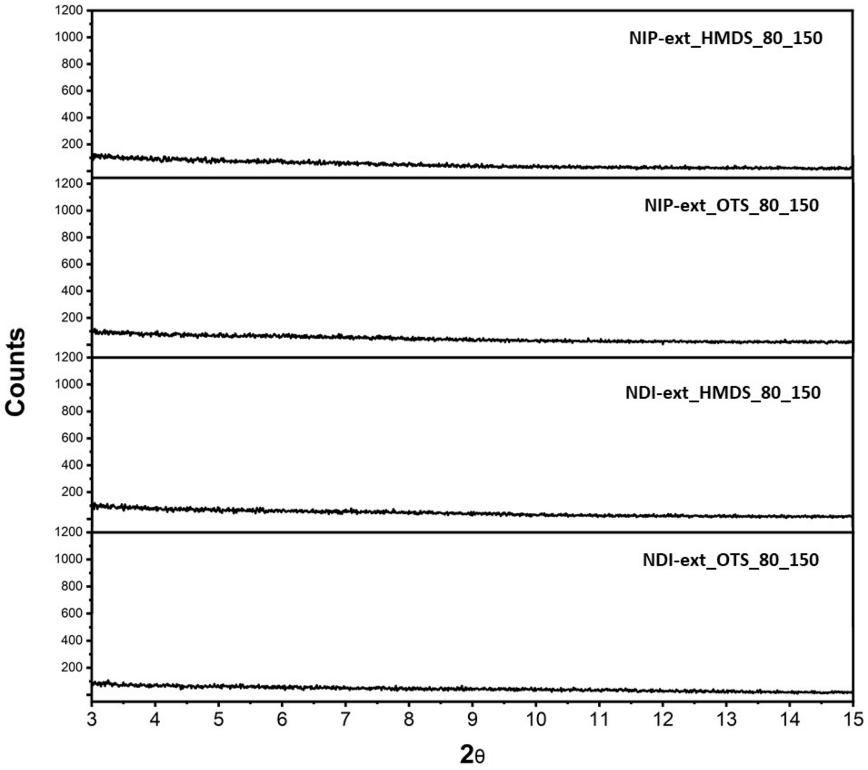

Figure S83. XRD plots for indicated semiconductors onto OTS-modified substrates and HMDS-modified substrate.

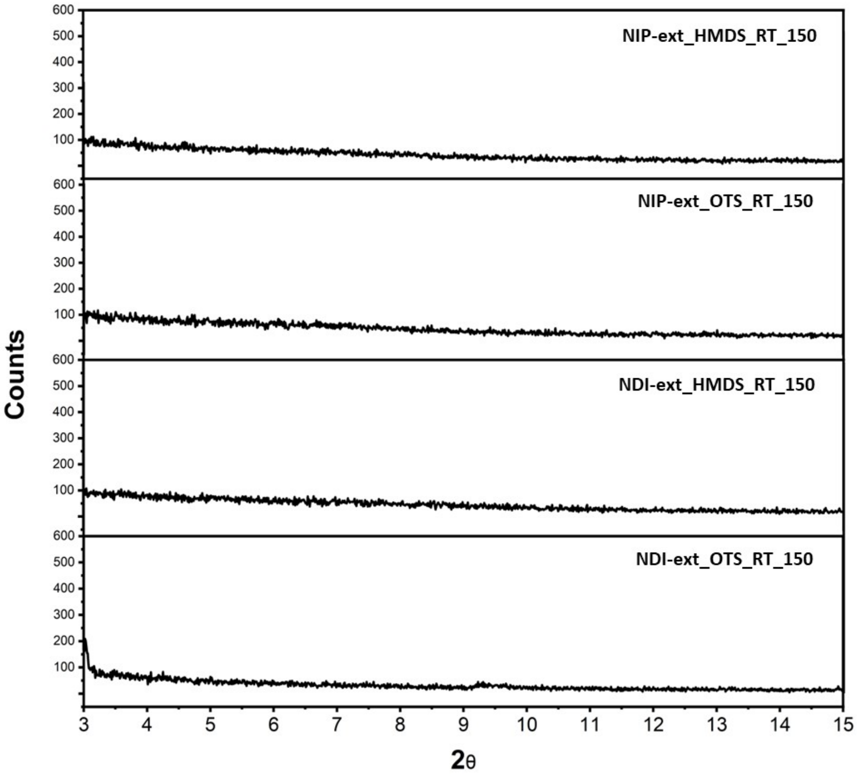

Figure S84. XRD plots for indicated semiconductors onto OTS-modified substrates and HMDS-modified substrate.

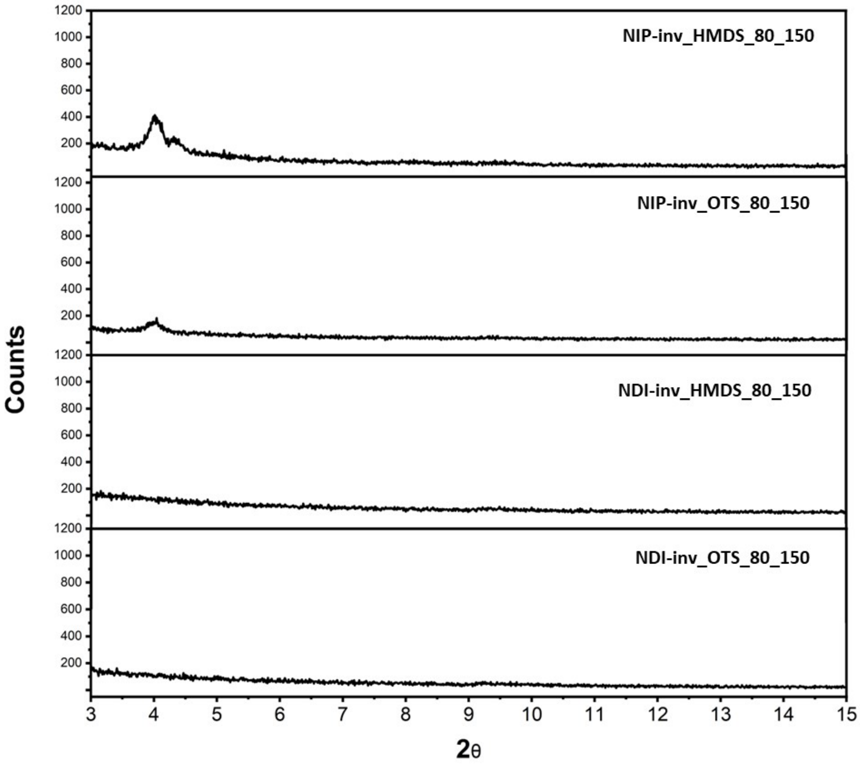

Figure S85. XRD plots for indicated semiconductors onto OTS-modified substrates and HMDS-modified substrate.

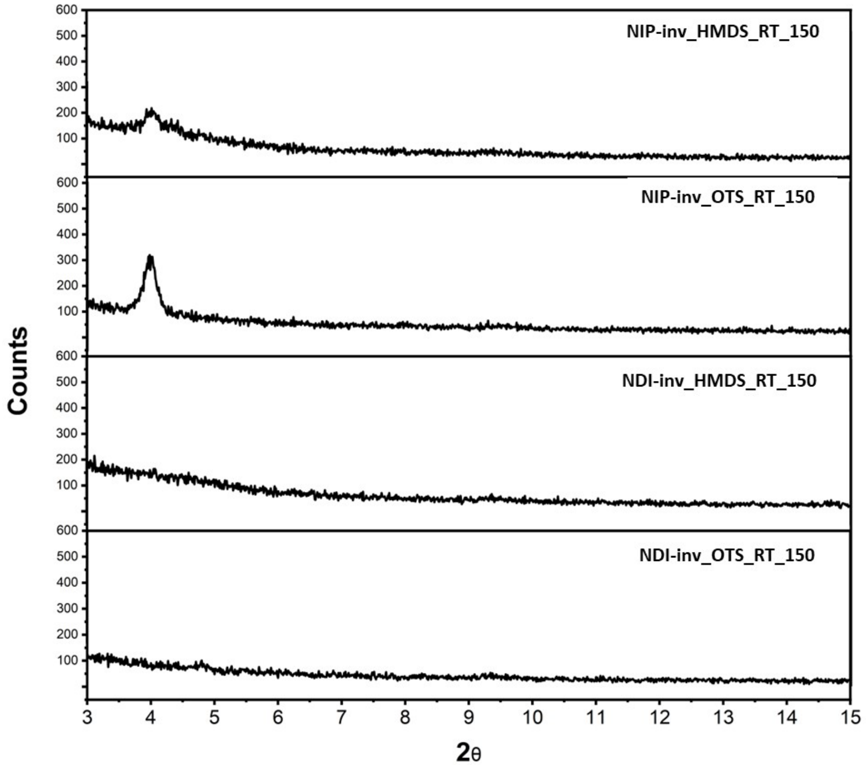

Figure S86. XRD plots for indicated semiconductors onto OTS-modified substrates and HMDS-modified substrate.

7. REFERENCES

1. H. Herrera, P. de Echegaray, M. Urdanpilleta, M. J. Mancheño, E. Mena-Osteritz, P. Bäuerle and J. L. Segura, Linear and star-shaped naphthalimide-fused pyrazinacenes, *Chemical Communications*, 2013, **49**, 713-715.
2. S. R. González, J. Casado, J. T. L. Navarrete, R. Blanco and J. L. Segura, A β-Naphthaleneimide-Modified Terthiophene Exhibiting Charge Transfer and Polarization Through the Short Molecular Axis. Joint Spectroscopic and Theoretical Study, *The Journal of Physical Chemistry A*, 2008, **112**, 6732-6740.
3. S.-i. Kato, T. Furuya, A. Kobayashi, M. Nitani, Y. Ie, Y. Aso, T. Yoshihara, S. Tobita and Y. Nakamura, π-Extended Thiadiazoles Fused with Thienopyrrole or Indole Moieties: Synthesis, Structures, and Properties, *The Journal of Organic Chemistry*, 2012, **77**, 7595-7606.
4. D. Mo, H. Chen, J. Zhou, N. Tang, L. Han, Y. Zhu, P. Chao, H. Lai, Z. Xie and F. He, Alkyl chain engineering of chlorinated acceptors for elevated solar conversion, *Journal of Materials Chemistry A*, 2020, **8**, 8903-8912.
5. J. Yuan, Y. Zhang, L. Zhou, C. Zhang, T.-K. Lau, G. Zhang, X. Lu, H.-L. Yip, S. K. So, S. Beaupré, M. Mainville, P. A. Johnson, M. Leclerc, H. Chen, H. Peng, Y. Li and Y. Zou, Fused Benzothiadiazole: A Building Block for n-Type Organic Acceptor to Achieve High-Performance Organic Solar Cells, *Advanced Materials*, 2019, **31**, 1807577.